Available on CMS information server

CMS AN 2012/XXX

The Compact Muon Solenoid Experiment

Analysis Note

The content of this note is intended for CMS internal use and distribution only

October 31, 2012

Search for Direct Stop Quark Pair Production in the Single Lepton Channel at 8 TeV

L. Bauerdick, K. Burkett, I. Fisk, Y. Gao, O. Gutsche, B. Hooberman, S. Jindariani, J. Linacre, V. Martinez Outschoorn

Fermilab National Accelerator Laboratory, Batavia, USA

C. Campagnari, A. George, F. Golf, D. Kovalskyi, V. Krutelyov

University of California, Santa Barbara, Santa Barbara, USA

G. Cerati, M. D'Alfonso, D. Evans, R. Kelley, I. MacNeill, S. Padhi, Y. Tu, F. Würthwein, V. Welke, A. Yagil, J. Yoo

University of California, San Diego, San Diego, USA

Abstract

This note describes a search for direct stop quark pair production in the single lepton channel using 9.7 fb^{-1} of pp collision data at $\sqrt{s} = 8$ TeV taken with the CMS detector in 2012. A search for an excess of events over the Standard Model prediction is performed in a sample with a single isolated electron or muon, several jets including a b-tagged jet, missing transverse energy, and large transverse mass.

Contents

1 Introduction

This note presents a search for the production of supersymmetric (SUSY) stop quark pairs in events with a single isolated lepton, several jets, missing transverse energy, and large transverse mass. We use a data sample corresponding to an integrated luminosity of 9.7 fb^{-1}. This search is of theoretical interest because of the critical role played by the stop quark in solving the hierarchy problem in SUSY models. This solution requires that the stop quark be light, less than a few hundred GeV and hence within reach for direct pair production. We focus on two decay modes $\tilde{t} \to t\chi_1^0$ and $\tilde{t} \to b\chi_1^+$ which are expected to have large branching fractions if they are kinematically accessible, leading to:

- $pp \to \tilde{t}\bar{\tilde{t}} \to t\bar{t}\chi_1^0\chi_1^0$, and
- $pp \to \tilde{t}\bar{\tilde{t}} \to b\bar{b}\chi_1^+\chi_1^- \to b\bar{b}W^+W^-\chi_1^0\chi_1^0$.

Both of these signatures contain high transverse momentum (p_{T}) jets including two b-jets, and missing transverse energy ($E_{\mathrm{T}}^{\mathrm{miss}}$) due to the invisible χ_1^0 lightest SUSY particles (LSP's). In addition, the presence of two W bosons leads to a large branching fraction to the single lepton final state. Hence we require the presence of exactly one isolated, high p_{T} electron or muon, which provides significant suppression of several backgrounds that are present in the all-hadronic channel. The largest backgrounds for this signature are semi-leptonic $\mathrm{t\bar{t}}$ and W+jets. These backgrounds contain a single leptonically-decaying W boson, and the transverse mass (M_{T}) of the lepton-neutrino system has a kinematic endpoint requiring $M_{\mathrm{T}} < M_W$. For signal stop quark events, the presence of additional LSP's in the final states allows the M_{T} to exceed M_W. Hence we search for an excess of events with large M_{T}. The dominant background in this kinematic region is dilepton $\mathrm{t\bar{t}}$ where one of the leptons is not identified, since the presence of two neutrinos from leptonically-decaying W bosons allows the M_{T} to exceed M_W. Backgrounds are estimated from Monte Carlo (MC) simulation, with careful validation and determination of scale factors (where necessary) and corresponding uncertainties based on data control samples.

The expected stop quark pair production cross section (see Fig. 1) varies between 18 pb for $m_{\tilde{t}} = 200$ GeV and 0.09 pb for $m_{\tilde{t}} = 500$ GeV [1]. The critical challenge of this analysis is due to the fact that for light stop quarks ($m_{\tilde{t}} \approx m_t$), the production cross section is large but the kinematic distributions, in particular M_{T}, are very similar to SM $\mathrm{t\bar{t}}$ production. In this regime it becomes very difficult to distinguish the signal and background. For large stop quark mass the kinematic distributions differ from those in SM $\mathrm{t\bar{t}}$ production, but the cross section decreases rapidly, reducing the signal-to-background ratio.

2 Overview and Strategy for Background Determination

We are searching for a $t\bar{t}\chi^0\chi^0$ or $WbW\bar{b}\chi^0\chi^0$ final state (after top decay in the first mode, the final states are actually the same). So to first order this is "$t\bar{t}$+ extra $E_{\mathrm{T}}^{\mathrm{miss}}$".

We work in the ℓ+ jets final state, where the main background is $t\bar{t}$. We look for $E_{\mathrm{T}}^{\mathrm{miss}}$ inconsistent with $W \to \ell\nu$. We do this by concentrating on the $\ell\nu$ transverse mass (M_T), since except for resolution and W-off-shell effects, $M_T < M_W$ for $W \to \ell\nu$. Thus, the initial analysis is simply a counting experiment in the tail of the M_T distribution.

The event selection is one-and-only-one high p_{T} isolated lepton, four or more jets, and an $E_{\mathrm{T}}^{\mathrm{miss}}$ cut. At least one of the jets has to be b tagged to reduce W+ jets. The event sample is then dominated by $t\bar{t}$, but there are also contributions from W+ jets, single top, dibosons, as well as rare SM processes such as ttW.

The $t\bar{t}$ events in the M_T tail can be broken up into two categories: (i) $t\bar{t} \to \ell$+ jets, and (ii) $t\bar{t} \to \ell^+\ell^-$ where one of the two leptons is not found by the second-lepton-veto (here the second lepton can be a hadronically decaying τ). For a reasonable M_T cut, say $M_T > 150$ GeV, the dilepton background is approximately 70% of the total. This is because in dileptons there are two neutrinos from W decay, thus M_T is not bounded by M_W. This is a very important point: while it is true that we are looking in the tail of M_T, the bulk of the background events end up there not because of some exotic $E_{\mathrm{T}}^{\mathrm{miss}}$ reconstruction failure, but because of well understood physics processes. This means that the background estimate can be taken from Monte Carlo (MC) after carefully accounting for possible data/MC differences.

The search is performed in a number of Signal Regions (SRs) defined by minimum requirements on $E_{\mathrm{T}}^{\mathrm{miss}}$ and M_T. The SRs are defined in Section 4.3.

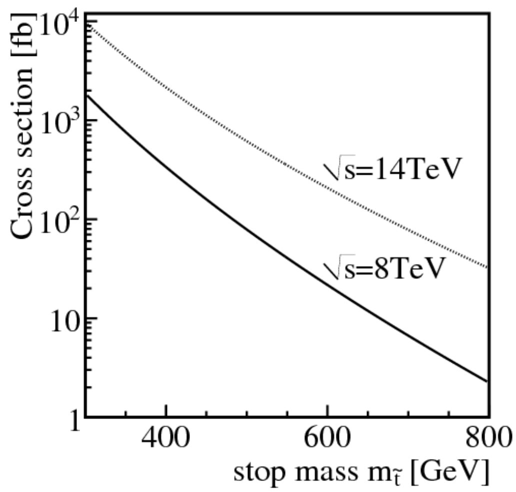

Figure 1: The stop quark pair production cross section as a function of the stop quark mass [2].

In Section 5 we will describe the analysis of various Control Regions (CRs) that are used to test the Monte Carlo model and, if necessary, to extract data/MC scale factors. In this section we give a general description of the procedure. The details of how the final background prediction is assembled are given in Section 8.

One general point is that in order to minimize systematic uncertainties, the MC background predictions are whenever possible normalized to the bulk of the $t\bar{t}$ data, i.e. events passing all of the requirements but with $M_T \approx 80$ GeV. This (mostly) removes uncertainties due to $\sigma(t\bar{t})$, lepton ID, trigger efficiency, luminosity, etc.

2.1 $\ell+$ jets background

The $\ell+$ jets background is dominated by $t\bar{t} \to \ell+$ jets, but also includes some $W+$ jets as well as single top. The MC input used in the background estimation is the ratio of the number of events with M_T in the signal region to the number of events with $M_T \approx 80$ GeV. This ratio is (possibly) corrected by a data/MC scale factor obtained from a study of CRs, as outlined below.

Note that the ratio described above is actually different for $t\bar{t}$/single top and $W+$ jets. This is because in W events there is a significant contribution to the M_T tail from very off-shell Ws. This contribution is much smaller in top events because $M(\ell\nu)$ cannot exceed $M_{top} - M_b$. Therefore the large M_{T} tail in $t\bar{t}$/single top is dominated by jet resolution effects, while for $W+$jets events the large M_{T} tail is dominated by off-shell W production.

For $W+$ jets the ability of the Monte Carlo to model this ratio (R_{wjet}) is validated in a sample of $\ell+$ jets enriched in $W+$ jets by the application of a b-veto. The equivalent ratio for top events (R_{top}) is tested in a sample of well identified $Z \to \ell\ell$ with one lepton added to the $E_{\mathrm{T}}^{\mathrm{miss}}$ calculation. This sample is well suited to testing the resolution effects on the M_T tail, since off-shell effects are eliminated by the Z-mass requirement. However, this test is unfortunately statistically limited and its usefulness is limited to event selections with modest $E_{\mathrm{T}}^{\mathrm{miss}}$ requirements.

Note that the fact that the ratios are different for $t\bar{t}$/single top and $W+$ jets introduces a systematic uncertainty in the background calculation because one needs to know the relative fractions of these two components in the $M_T \approx 80$ GeV lepton + jets sample.

2.2 Dilepton background

To suppress dilepton backgrounds, we veto events with an isolated track of $p_{\mathrm{T}} > 10$ GeV (see Sec. 4.2 for details). Being the common feature for electron, muon, and one-prong tau decays, this veto is highly efficient for rejecting $t\bar{t}$ to dilepton events. The remaining dilepton background can be classified into the following categories:

- lepton is out of acceptance ($|\eta| > 2.5$)
- lepton has $p_{\mathrm{T}} < 10$ GeV, and is inside the acceptance
- lepton has $p_{\mathrm{T}} > 10$ GeV, is inside the acceptance, but survives the additional isolated track veto

The last category includes 1-prong and 3-prong hadronic tau decays, as well as electrons and muons either from direct W decay or via W$\rightarrow \tau \rightarrow \ell$ decay that fail the isolation requirement. We note that at present we do not attempt to veto 3-prong tau decays as they are about 15% of the total dilepton background according to the MC.

The high M_T dilepton background predictions come from MC, but their rate is normalized to the $M_T \approx 80$ GeV peak. In order to perform this normalization in data, the rare background events in the M_T peak are subtracted off. This also introduces a systematic uncertainty.

There are two types of effects that can influence the MC dilepton prediction: physics effects and instrumental effects. We discuss these next, starting from physics.

First of all, many of our $t\bar{t}$ MC samples (e.g. MadGraph) have BR$(W \to \ell\nu) = \frac{1}{9} = 0.1111$. PDG says BR$(W \to \ell\nu) = 0.1080 \pm 0.0009$. This difference matters, so the $t\bar{t}$ MC must be corrected to account for this.

Second, our selection is $\ell + 4$ or more jets. A dilepton event passes the selection only if there are two additional jets from ISR, or one jet from ISR and one jet which is reconstructed from the unidentified lepton, *e.g.*, a three-prong tau. Therefore, all MC dilepton $t\bar{t}$ samples used in the analysis must have their jet multiplicity corrected (if necessary) to agree with what is seen in $t\bar{t}$ data. We use a data control sample of well identified dilepton events with $E_{\mathrm{T}}^{\mathrm{miss}}$ and at least one jet (including at least one b-tag) as a template to "adjust" the N_{jet} distribution of the $t\bar{t} \to$ dileptons MC samples.

The final physics effect has to do with the modeling of $t\bar{t}$ production and decay. Different MC models could in principle result in different BG predictions. Therefore we use several different $t\bar{t}$ MC samples using different generators and different parameters, to test the stability of the dilepton BG prediction. All these predictions, **after** corrections for branching ratio and N_{jet} dependence, are compared to each other. The spread is a measure of the systematic uncertainty associated with the $t\bar{t}$ generator modeling.

The main instrumental effect is associated with the efficiency of the isolated track veto. We use tag-and-probe to compare the isolated track veto performance in $Z + 4$ jets data and MC. Note that the performance of the isolated track veto is not exactly the same on e/μ and on one prong hadronic tau decays. This is because the pions from one-prong taus are often accompanied by π^0's that can then result in extra tracks due to photon conversions. We let the simulation take care of that. Note that JES uncertainties are effectively "calibrated away" by the N_{jet} rescaling described above.

2.3 Other backgrounds

Other backgrounds are tW, ttV, dibosons, tribosons, and Drell Yan. These are small. They are taken from MC with appropriate scale factors for trigger efficiency, and reweighting to match the distribution of reconstructed primary vertices in data.

2.4 Future improvements

Finally, there are possible improvements to this basic analysis strategy that can be added in the future:

- Move from counting experiment to shape analysis. But first, we need to get the counting experiment under control.
- Add an explicit three prong tau veto
- Do something to require that three of the jets in the event be consistent with $t \to Wb, W \to q\bar{q}$. This could help reject some of the dilepton BG in the search for $\widetilde{t} \to t\chi^0$, but is not applicable to the $\widetilde{t} \to b\chi^+$ search.
- Consider the $M(\ell b)$ variable, which is not bounded by M_{top} in $\widetilde{t} \to b\chi^+$

3 Data Samples

The datasets used for this analysis are summarized in Tables 1 (data) and 2 (MC). The total integrated luminosity is 9.7 fb^{-1} after applying the official good run list. The main $\mathrm{t\bar{t}}$ Monte Carlo sample is generated with Powheg since this sample has the largest number of events, though samples with alternative generators such as Madgraph are also used for the derivation of systematic uncertainties in the $\mathrm{t\bar{t}}$ background prediction. The triggers used to select both the signal and control samples are also summarized in Table 3.

Dataset Name
Single Lepton Samples
/SingleElectron/Run2012A-13Jul2012-v1/AOD
/SingleMu/Run2012A-13Jul2012-v1/AOD
/SingleElectron/Run2012B-13Jul2012-v1/AOD
/SingleMu/Run2012B-13Jul2012-v1/AOD
/SingleElectron/Run2012C-PromptReco-v1/AOD
/SingleMu/Run2012C-PromptReco-v1/AOD
/SingleElectron/Run2012C-PromptReco-v2/AOD
/SingleMu/Run2012C-PromptReco-v2/AOD
Dilepton Samples (only used for dilepton control region)
/DoubleElectron/Run2012A-13Jul2012-v1/AOD
/DoubleMu/Run2012A-13Jul2012-v1/AOD
/MuEG/Run2012A-13Jul2012-v1/AOD
/DoubleElectron/Run2012B-13Jul2012-v1/AOD
/DoubleMu/Run2012B-13Jul2012-v1/AOD
/MuEG/Run2012B-13Jul2012-v1/AOD
/DoubleElectron/Run2012C-PromptReco-v1/AOD
/DoubleMu/Run2012C-PromptReco-v1/AOD
/MuEG/Run2012C-PromptReco-v1/AOD
/DoubleElectron/Run2012C-PromptReco-v2/AOD
/DoubleMu/Run2012C-PromptReco-v2/AOD
/MuEG/Run2012C-PromptReco-v2/AOD

Table 1: Summary of data datasets used.

With Pileup: Processed dataset name is (53) Summer12_DR53X-PU_S10_START53_V7A-v*/AODSIM (52) Summer12-START52_V9_FSIM-v*/AODSIM		
Description	Primary Dataset Name	cross-section [pb]
$t\bar{t}$	/TT_CT10_TuneZ2Star_8TeV-powheg-tauola (53)	225.2
W $\rightarrow \ell\nu$	/WJetsToLNu_TuneZ2Star_8TeV-madgraph-tauola (53)	37509
W $\rightarrow \ell\nu$+3 jets	/W3JetsToLNu_TuneZ2Star_8TeV-madgraph-tauola (53)	640
W $\rightarrow \ell\nu+\geq$ 4 jets	/W4JetsToLNu_TuneZ2Star_8TeV-madgraph-tauola (53)	264
WW	/WWJetsTo2L2Nu_TuneZ2star_8TeV-madgraph-tauola (53)	5.8
WZ	/WZJetsTo3LNu_TuneZ2_8TeV-madgraph-tauola (53)	1.1
	/WZJetsTo2L2Q_TuneZ2star_8TeV-madgraph-tauola (53	1.1
ZZ	/ZZJetsTo2L2Nu_TuneZ2star_8TeV-madgraph-tauola (53)	0.4
	/ZZJetsTo4L_TuneZ2star_8TeV-madgraph-tauola (53)	0.2
	/ZZJetsTo2L2Q_TuneZ2star_8TeV-madgraph-tauola (53	2.4
t (s-chan)	/T_TuneZ2Star_s-channel_8TeV-powheg-tauola (53)	3.9
$\bar{t}$ (s-chan)	/Tbar_TuneZ2Star_s-channel_8TeV-powheg-tauola (53)	1.8
t (t-chan)	/T_TuneZ2Star_t-channel_8TeV-powheg-tauola (53)	55.5
$\bar{t}$ (t-chan)	/Tbar_TuneZ2Star_t-channel_8TeV-powheg-tauola (53)	30.0
tW	/T_TuneZ2Star_tW-channel-DR_8TeV-powheg-tauola (53)	11.2
$\bar{t}W$	/Tbar_TuneZ2Star_tW-channel-DR_8TeV-powheg-tauola (53)	11.2
$Z/\gamma^* \rightarrow \ell\ell$	/DYJetsToLL_TuneZ2Star_M-50_8TeV-madgraph-tarball (53)	3532.8
$Z/\gamma^* \rightarrow \ell\ell+\geq$ 4 jets	/DY4JetsToLL_TuneZ2Star_M-50_8TeV-madgraph-tarball (53)	27.6
$t\bar{t}W$	/TTW_TuneZ2Star_8TeV-madgraph (53)	0.23
$t\bar{t}Z$	/TTZ_TuneZ2Star_8TeV-madgraph (53)	0.21
$t\bar{t}\gamma$	/TTGJets_TuneZ2Star_8TeV-madgraph (53)	0.65
WWW	/WWW_TuneZ2Star_8TeV-madgraph (53)	0.082
WWZ	/WWZNoGstar_TuneZ2Star_8TeV-madgraph (53)	0.063
WZZ	/WZZNoGstar_TuneZ2Star_8TeV-madgraph (53)	0.019
ZZZ	/ZZZNoGstar_TuneZ2Star_8TeV-madgraph (53)	0.019
$\tilde{t}\bar{\tilde{t}} \rightarrow t\bar{t}\chi_1^0\chi_1^0$	/SMS-T2tt_FineBin_Mstop-225to1200_mLSP-0to1000_8TeV-Pythia6Z (52)	scan
$\tilde{t}\bar{\tilde{t}} \rightarrow b\bar{b}\chi_1^+\chi_1^-$	/SMS-T2bw_FineBin_Mstop-100to600_mLSP-0to500_8TeV-Pythia6Z (52)	scan
$t\bar{t}$	/TTJets_MassiveBinDECAY_TuneZ2Star_8TeV-madgraph-tauola (53)	225.2
$t\bar{t}$ ($Q^2 \times 2$)	/TTjets_TuneZ2Star_scaleup_8TeV-madgraph-tauola (53)	225.2
$t\bar{t}$ ($Q^2 \times 0.5$)	/TTjets_TuneZ2Star_scaledown_8TeV-madgraph-tauola (53)	225.2
$t\bar{t}$ ($x_q > 40$ GeV)	/TTjets_TuneZ2Star_matchingup_8TeV-madgraph-tauola (53)	225.2
$t\bar{t}$ ($x_q > 10$ GeV)	/TTjets_TuneZ2Star_matchingdown_8TeV-madgraph-tauola (53)	225.2
$t\bar{t}$ ($m_{\rm top} = 178.5$ GeV)	/TTJets_TuneZ2Star_mass178_5_8TeV-madgraph-tauola (53)	225.2
$t\bar{t}$ ($m_{\rm top} = 166.5$ GeV)	/TTJets_TuneZ2Star_mass166_5_8TeV-madgraph-tauola (53)	225.2

Table 2: Summary of Monte Carlo datasets used.

Triggers
Single Muon Sample
HLT_IsoMu24_v*
HLT_IsoMu24_eta2p1_v*
Single Electron Sample
HLT_Ele27_WP80_v*
Dilepton Sample (only used for dilepton control regions)
HLT_Mu17_Mu8_v*
HLT_Mu17_Ele8_CaloIdT_CaloIsoVL_TrkIdVL_TrkIsoVL_v*
HLT_Mu8_Ele17_CaloIdT_CaloIsoVL_TrkIdVL_TrkIsoVL*
HLT_Ele17_CaloIdT_CaloIsoVL_TrkIdVL_TrkIsoVL_Ele8_CaloIdT_CaloIsoVL_TrkIdVL_TrkIsoVL_v*

Table 3: Summary of triggers used.

4 Event Selection

Here we define the selections of leptons, jets, and $E_{\mathrm{T}}^{\mathrm{miss}}$. We also describe our measurements of the lepton and trigger efficiency. The analysis uses several different Control Regions (CRs) in addition to the Signal Regions (SRs). All of these different regions are defined in this section. This section also includes some information on the basic MC corrections that we apply.

4.1 Single Lepton Selection

The single lepton selection is based on the following criteria, starting from the requirements described on https://twiki.cern.ch/twiki/bin/viewauth/CMS/SUSYstop#SINGLE_LEPTON_CHANNEL (revision r20)

- satisfy the trigger requirement (see Table 3). Note that the analysis triggers are inclusive single lepton triggers. Dilepton triggers are used only for the dilepton control region.
- select events with one high p_{T} electron or muon, requiring
  - $p_{\mathrm{T}} > 30$ GeV/c and $|\eta| < 1.4442(2.1)$ for electrons (muons). The restriction to the barrel for electrons is motivated by an observed excess of events with large M_{T} with endcap electrons in the b-veto control region, and does not significantly reduce the signal acceptance since the leptons tend to be central.
  - muon ID criteria is based on the 2012 POG recommended tight working point
  - electron ID critera is based on the 2012 POG recommended medium working point
  - PF-based isolation ($\Delta R < 0.3$) relative isolation < 0.15 and absolute isolation < 5 GeV. PU corrections are performed with the $\Delta\beta$ scheme for muons and effective-area fastjet rho scheme for electrons (as recommended by the relevant POGs).
  - $|p_{\mathrm{T}}(\mathrm{PF_{lep}}) - \mathrm{p_T}(\mathrm{RECO_{lep}})| < 10$ GeV
  - $E/p_{\mathrm{in}} < 4$ (electrons only)
  - We remove electron events with $E_{\mathrm{T}}^{\mathrm{miss}} > 50$ GeV and $M_T > 100$ GeV with at least one crystal in the supercluster with laser correction >2.[1]
- require at least 4 PF jets in the event with $p_{\mathrm{T}} > 30$ GeV within $|\eta| < 2.5$ out of which at least 1 satisfies the CSV medium working point b-tagging requirement
- require moderate $E_{\mathrm{T}}^{\mathrm{miss}} > 50$ GeV (type1-corrected pfmet with ϕ corrections applied as described in Sec. 4.7.1).
- Isolated track veto, see Section 4.2

4.2 Isolated track veto

The isolated track veto is intended to remove top dilepton events. Looking for an isolated track is an effective way of identifying $W \to e$, $W \to \mu$, $W \to \tau \to \ell$, and $W \to \tau \to h^{\pm} + n\pi^{0}$. The requirements on the track are

- $P_T > 10$ GeV
- Relative track isolation $< 10\%$ computed from charged PF candidates with $d_Z < 0.05$ cm from the primary vertex.

4.3 Signal Region Selection

The signal regions (SRs) are selected to improve the sensitivity for the single lepton requirements and cover a range of scalar top scenarios. The M_{T} and $E_{\mathrm{T}}^{\mathrm{miss}}$ variables are used to define the signal regions and the requirements are listed in Table 4.

---

1) This is an ad-hoc removal based on run-event numbers, since the problem was found very recently and the filter was not available when we processed the events.

Signal Region	Minimum M_{T} [GeV]	Minimum $E_{\mathrm{T}}^{\mathrm{miss}}$ [GeV]
SRA	150	100
SRB	120	150
SRC	120	200
SRD	120	250
SRE	120	300
SRF	120	350
SRG	120	400

Table 4: Signal region definitions based on M_{T} and $E_{\mathrm{T}}^{\mathrm{miss}}$ requirements. These requirements are applied in addition to the baseline single lepton selection.

Table 5 shows the expected number of SM background yields for the SRs. A few stop signal yields for four values of the parameters are also shown for comparison. The signal regions with looser requirements are sensitive to lower stop masses $\mathrm{M}(\tilde{t})$, while those with tighter requirements are more sensitive to higher $\mathrm{M}(\tilde{t})$. Kinematic distributions for a few sample signal points can be found in Appendix E.

Sample	SRA	SRB	SRC	SRD	SRE	SRF	SRG
$\mathrm{t\bar{t}} \to \ell\ell$	619 ± 9	366 ± 7	127 ± 4	44 ± 2	17 ± 1	7 ± 1	4 ± 1
$\mathrm{t\bar{t}} \to \ell +$ jets & single top (1ℓ)	95 ± 3	67 ± 3	15 ± 1	6 ± 1	2 ± 1	1 ± 1	1 ± 0
W+jets	29 ± 2	15 ± 2	6 ± 1	3 ± 1	1 ± 0	0 ± 0	0 ± 0
Rare	59 ± 3	38 ± 3	16 ± 2	8 ± 1	4 ± 1	2 ± 0	1 ± 0
Total	802 ± 10	486 ± 8	164 ± 5	62 ± 3	23 ± 2	10 ± 1	6 ± 1
Yield UL (optimistic)	147 (10%)	94 (10%)	47 (15%)	25 (20%)	14 (25%)	8.6 (30%)	7.5 (50%)
Yield UL (pessimistic)	200 (15%)	152 (20%)	64 (25%)	30 (30%)	15 (35%)	9.7 (50%)	8.2 (100%)
T2tt m(stop) = 250 m(χ^0) = 0	315 ± 18	193 ± 14	53 ± 8	13 ± 4	2 ± 2	0 ± 0	0 ± 0
T2tt m(stop) = 300 m(χ^0) = 50	296 ± 11	236 ± 10	88 ± 6	28 ± 3	10 ± 2	2 ± 1	0 ± 0
T2tt m(stop) = 300 m(χ^0) = 100	128 ± 7	93 ± 6	29 ± 3	10 ± 2	5 ± 1	2 ± 1	1 ± 1
T2tt m(stop) = 350 m(χ^0) = 0	224 ± 6	206 ± 6	119 ± 4	52 ± 3	20 ± 2	8 ± 1	3 ± 1
T2tt m(stop) = 450 m(χ^0) = 0	71 ± 2	71 ± 2	53 ± 1	36 ± 1	21 ± 1	11 ± 1	5 ± 0

Table 5: Expected SM background contributions and signal yields for a few sample points, including both muon and electron channels. This is "dead reckoning" MC with no correction. It is meant only as a general guide. The uncertainties are statistical only. The signal yield expected upper limits are also shown for two values of the total background systematic uncertainty, indicated in parentheses.

4.4 Control Region Selection

Control regions (CRs) are used to validate the background estimation procedure and derive systematic uncertainties for some contributions. The CRs are selected to have similar kinematics to the SRs, but have a different requirement in terms of number of b-tags and number of leptons, thus enhancing them in different SM contributions. The four CRs used in this analysis are summarized in Table 6.

Selection Criteria	exactly 1 lepton	exactly 2 leptons	1 lepton + isolated track
0 b-tags	CR1) W+Jets dominated: Validate W+Jets M_{T} tail	CR2) apply Z-mass constraint $\to$ Z+Jets dominated: Validate $\mathrm{t\bar{t}} \to \ell +$ jets M_{T} tail comparing data vs. MC "pseudo-M_{T}"	CR3) not used
≥ 1 b-tags	SIGNAL REGION	CR4) Apply Z-mass veto $\to \mathrm{t\bar{t}} \to \ell\ell$ dominated: Validate "physics" modelling of $\mathrm{t\bar{t}} \to \ell\ell$	CR5) $\mathrm{t\bar{t}} \to \ell\ell$, $\mathrm{t\bar{t}} \to \ell\tau$ and $\mathrm{t\bar{t}} \to \ell$fake dominated: Validate τ and fake lepton modeling/ detector effects in $\mathrm{t\bar{t}} \to \ell\ell$

Table 6: Summary of signal and control regions.

4.5 Definition of M_T peak region

This region is defined as $50 < M_T < 80$ GeV.

4.6 Default $\mathrm{t\bar{t}}$ MC sample

Our default $\mathrm{t\bar{t}}$ MC sample is Powheg.

4.7 MC Corrections

All MC samples are corrected for trigger efficiency. In the case of single lepton selections, we apply the p_{T} and η-dependent scale factors that we measure ourselves, see Section 4.9. In the case of dilepton selections that require the dilepton triggers, we apply overall scale factors of 0.95, 0.88, and 0.92 for ee, $\mu\mu$, and $e\mu$ respectively [3].

The leptonic branching fraction used in some of the $\mathrm{t\bar{t}}$ MC samples differs from the value listed in the PDG $(10.80 \pm 0.09)\%$. Table 7 summarizes the branching fractions used in the generation of the various $\mathrm{t\bar{t}}$ MC samples. For $\mathrm{t\bar{t}}$ samples with the incorrect leptonic branching fraction, event weights are applied based on the number of true leptons and the ratio of the corrected and incorrect branching fractions.

$\mathrm{t\bar{t}}$ Sample - Event Generator	Leptonic Branching Fraction
Madgraph	0.111
MC@NLO	0.111
Pythia	0.108
Powheg	0.108

Table 7: Leptonic branching fractions for the various $\mathrm{t\bar{t}}$ samples used in the analysis. The $\mathrm{t\bar{t}}$ MC samples produced with Madgraph and MC@NLO has a branching fraction that is almost 3% higher than the PDG value.

All $\mathrm{t\bar{t}}$ dilepton samples are corrected (when needed and appropriate) in order to have the correct jet multiplicity distribution. This correction procedure is described in Section 5.3.1.

4.7.1 Corrections to Jets and $E_{\mathrm{T}}^{\mathrm{miss}}$

The official recommendations from the Jet/MET group are used for the data and MC samples. In particular, the jet energy corrections (JEC) are updated using the official recipe. L1FastL2L3Residual (L1FastL2L3) corrections are applied for data (MC), based on the global tags GR_R_52_V9 (START52_V9B) for data (MC). In addition, these jet energy corrections are propagated to the $E_{\mathrm{T}}^{\mathrm{miss}}$ calculation, following the official prescription for deriving the Type I corrections.

Events with anomalous "rho" pile-up corrections are excluded from the sample since these can correspond to events with unphysically large $E_{\mathrm{T}}^{\mathrm{miss}}$ and M_{T}. In addition, the recommended MET filters are applied. A correction to remove the ϕ modulation in $E_{\mathrm{T}}^{\mathrm{miss}}$ is also applied to the data.

4.8 Lepton Selection Efficiency Measurements

In this section we measure the identification and isolation efficiencies for muons and electrons in data and MC using tag-and-probe studies. The tag is required to pass the full offline analysis selection and have $p_{\mathrm{T}} > 30$ GeV, $|\eta| < 2.1$, and be matched to the single lepton trigger, HLT_IsoMu24(_eta2p1) for muons and HLT_Ele27_WP80 for electrons. The probe is required to have $|\eta| < 2.1$ and $p_{\mathrm{T}} > 20$ GeV. To measure the identification efficiency we require the probe to pass the isolation requirement, to measure the isolation efficiency we require the probe to pass the identification requirement.

The tag-probe pair is required to have opposite-sign and an invariant mass in the range 76–106 GeV. In order to suppress lepton pairs from sources other than Z boson decays, we require the event to have $E_{\mathrm{T}}^{\mathrm{miss}} < 30$ GeV and no b-tagged jets (CSV loose working point).

The muon efficiencies are summarized in Table 8 for inclusive events (i.e. no jet requirements). These efficiencies are displayed in Fig. 2 for several different jet multiplicity requirements. We currently observe good agreement for muons with p_{T} up to about 300 GeV. For high p_{T} muons we observe a source of background in the data with large impact parameters, which we suppress by requiring muon $d_0 < 0.02$ cm and $d_Z < 0.5$ cm. The electron efficiencies are summarized in Table 9 for inclusive events (i.e. no jet requirements). These efficiencies are displayed in Fig. 3 for several different jet multiplicity requirements. In general we observe good agreement between the data and MC identification and isolation efficiencies.

We do not correct the MC for differences in lepton efficiency. In the background calculation, we do not take any systematics due to lepton selection efficiency uncertainties. This is because all backgrounds except the rare MC background are normalized to the M_T peak, thus the lepton identification uncertainty cancels out. For the rare MC these uncertainties are negligible compared to the assumed cross-section uncertainty (Section 6).

Table 8: Summary of the data and MC muon identification and isolation efficiencies measured with tag-and-probe studies.

MC ID p_T range [GeV]	$\|\eta\| < 0.8$	$0.8 < \|\eta\| < 1.5$	$1.5 < \|\eta\| < 2.1$
20 - 30	0.9672 ± 0.0005	0.9640 ± 0.0006	0.9471 ± 0.0008
30 - 40	0.9684 ± 0.0002	0.9657 ± 0.0003	0.9446 ± 0.0004
40 - 50	0.9704 ± 0.0002	0.9687 ± 0.0002	0.9432 ± 0.0004
50 - 60	0.9684 ± 0.0005	0.9640 ± 0.0005	0.9414 ± 0.0009
60 - 80	0.9678 ± 0.0009	0.9640 ± 0.0010	0.9354 ± 0.0018
80 - 100	0.9709 ± 0.0021	0.9642 ± 0.0027	0.9234 ± 0.0051
100 - 150	0.9679 ± 0.0029	0.9654 ± 0.0035	0.9261 ± 0.0069
150 - 200	0.9643 ± 0.0069	0.9568 ± 0.0088	0.9045 ± 0.0198
200 - 300	0.9647 ± 0.0116	0.9388 ± 0.0171	0.8906 ± 0.0390
300 - 10000	1.0000 ± 0.0000	1.0000 ± 0.0000	1.0000 ± 0.0000
MC ISO p_T range [GeV]	$\|\eta\| < 0.8$	$0.8 < \|\eta\| < 1.5$	$1.5 < \|\eta\| < 2.1$
20 - 30	0.8966 ± 0.0007	0.9153 ± 0.0008	0.9298 ± 0.0009
30 - 40	0.9610 ± 0.0002	0.9632 ± 0.0003	0.9707 ± 0.0003
40 - 50	0.9876 ± 0.0001	0.9897 ± 0.0001	0.9912 ± 0.0002
50 - 60	0.9921 ± 0.0002	0.9927 ± 0.0003	0.9939 ± 0.0003
60 - 80	0.9927 ± 0.0004	0.9937 ± 0.0004	0.9947 ± 0.0005
80 - 100	0.9920 ± 0.0012	0.9921 ± 0.0013	0.9932 ± 0.0016
100 - 150	0.9898 ± 0.0017	0.9923 ± 0.0017	0.9933 ± 0.0022
150 - 200	0.9901 ± 0.0037	0.9922 ± 0.0039	0.9950 ± 0.0050
200 - 300	0.9919 ± 0.0057	1.0000 ± 0.0000	0.9828 ± 0.0171
300 - 10000	1.0000 ± 0.0000	1.0000 ± 0.0000	1.0000 ± 0.0000
DATA ID p_T range [GeV]	$\|\eta\| < 0.8$	$0.8 < \|\eta\| < 1.5$	$1.5 < \|\eta\| < 2.1$
20 - 30	0.9530 ± 0.0005	0.9517 ± 0.0006	0.9369 ± 0.0008
30 - 40	0.9556 ± 0.0003	0.9519 ± 0.0003	0.9362 ± 0.0005
40 - 50	0.9584 ± 0.0002	0.9558 ± 0.0003	0.9355 ± 0.0004
50 - 60	0.9540 ± 0.0005	0.9487 ± 0.0006	0.9314 ± 0.0010
60 - 80	0.9536 ± 0.0010	0.9466 ± 0.0012	0.9307 ± 0.0019
80 - 100	0.9505 ± 0.0028	0.9414 ± 0.0035	0.9289 ± 0.0053
100 - 150	0.9472 ± 0.0038	0.9454 ± 0.0045	0.9149 ± 0.0079
150 - 200	0.9628 ± 0.0073	0.9675 ± 0.0089	0.8950 ± 0.0217
200 - 300	0.9463 ± 0.0157	0.9290 ± 0.0206	0.8889 ± 0.0468
300 - 10000	0.9412 ± 0.0404	1.0000 ± 0.0000	0.4000 ± 0.2191
DATA ISO p_T range [GeV]	$\|\eta\| < 0.8$	$0.8 < \|\eta\| < 1.5$	$1.5 < \|\eta\| < 2.1$
20 - 30	0.8939 ± 0.0007	0.9144 ± 0.0008	0.9361 ± 0.0008
30 - 40	0.9598 ± 0.0002	0.9646 ± 0.0003	0.9744 ± 0.0003
40 - 50	0.9870 ± 0.0001	0.9901 ± 0.0001	0.9920 ± 0.0002
50 - 60	0.9912 ± 0.0002	0.9933 ± 0.0002	0.9953 ± 0.0003
60 - 80	0.9920 ± 0.0004	0.9934 ± 0.0005	0.9956 ± 0.0005
80 - 100	0.9926 ± 0.0011	0.9933 ± 0.0013	0.9955 ± 0.0014
100 - 150	0.9913 ± 0.0016	0.9949 ± 0.0015	0.9965 ± 0.0017
150 - 200	0.9969 ± 0.0022	0.9974 ± 0.0026	0.9944 ± 0.0055
200 - 300	1.0000 ± 0.0000	1.0000 ± 0.0000	1.0000 ± 0.0000
300 - 10000	1.0000 ± 0.0000	1.0000 ± 0.0000	1.0000 ± 0.0000
Scale Factor ID p_T range [GeV]	$\|\eta\| < 0.8$	$0.8 < \|\eta\| < 1.5$	$1.5 < \|\eta\| < 2.1$
20 - 30	0.9853 ± 0.0007	0.9872 ± 0.0009	0.9893 ± 0.0012
30 - 40	0.9868 ± 0.0003	0.9857 ± 0.0005	0.9911 ± 0.0007
40 - 50	0.9877 ± 0.0003	0.9866 ± 0.0004	0.9918 ± 0.0006
50 - 60	0.9851 ± 0.0007	0.9841 ± 0.0009	0.9894 ± 0.0014
60 - 80	0.9853 ± 0.0014	0.9820 ± 0.0017	0.9949 ± 0.0028
80 - 100	0.9790 ± 0.0036	0.9763 ± 0.0046	1.0059 ± 0.0080
100 - 150	0.9786 ± 0.0049	0.9793 ± 0.0059	0.9879 ± 0.0113
150 - 200	0.9984 ± 0.0104	1.0112 ± 0.0131	0.9894 ± 0.0323
200 - 300	0.9810 ± 0.0201	0.9896 ± 0.0284	0.9981 ± 0.0684
300 - 10000	0.9412 ± 0.0404	1.0000 ± 0.0000	0.4000 ± 0.2191
Scale Factor ISO p_T range [GeV]	$\|\eta\| < 0.8$	$0.8 < \|\eta\| < 1.5$	$1.5 < \|\eta\| < 2.1$
20 - 30	0.9970 ± 0.0012	0.9989 ± 0.0012	1.0068 ± 0.0013
30 - 40	0.9987 ± 0.0004	1.0014 ± 0.0004	1.0038 ± 0.0005
40 - 50	0.9994 ± 0.0002	1.0004 ± 0.0002	1.0008 ± 0.0002
50 - 60	0.9991 ± 0.0003	1.0006 ± 0.0003	1.0013 ± 0.0004
60 - 80	0.9993 ± 0.0006	0.9997 ± 0.0006	1.0009 ± 0.0008
80 - 100	1.0006 ± 0.0016	1.0012 ± 0.0018	1.0023 ± 0.0022
100 - 150	1.0015 ± 0.0023	1.0027 ± 0.0023	1.0032 ± 0.0028
150 - 200	1.0068 ± 0.0044	1.0053 ± 0.0047	0.9994 ± 0.0075
200 - 300	1.0081 ± 0.0058	1.0000 ± 0.0000	1.0175 ± 0.0177
300 - 10000	1.0000 ± 0.0000	1.0000 ± 0.0000	1.0000 ± 0.0000

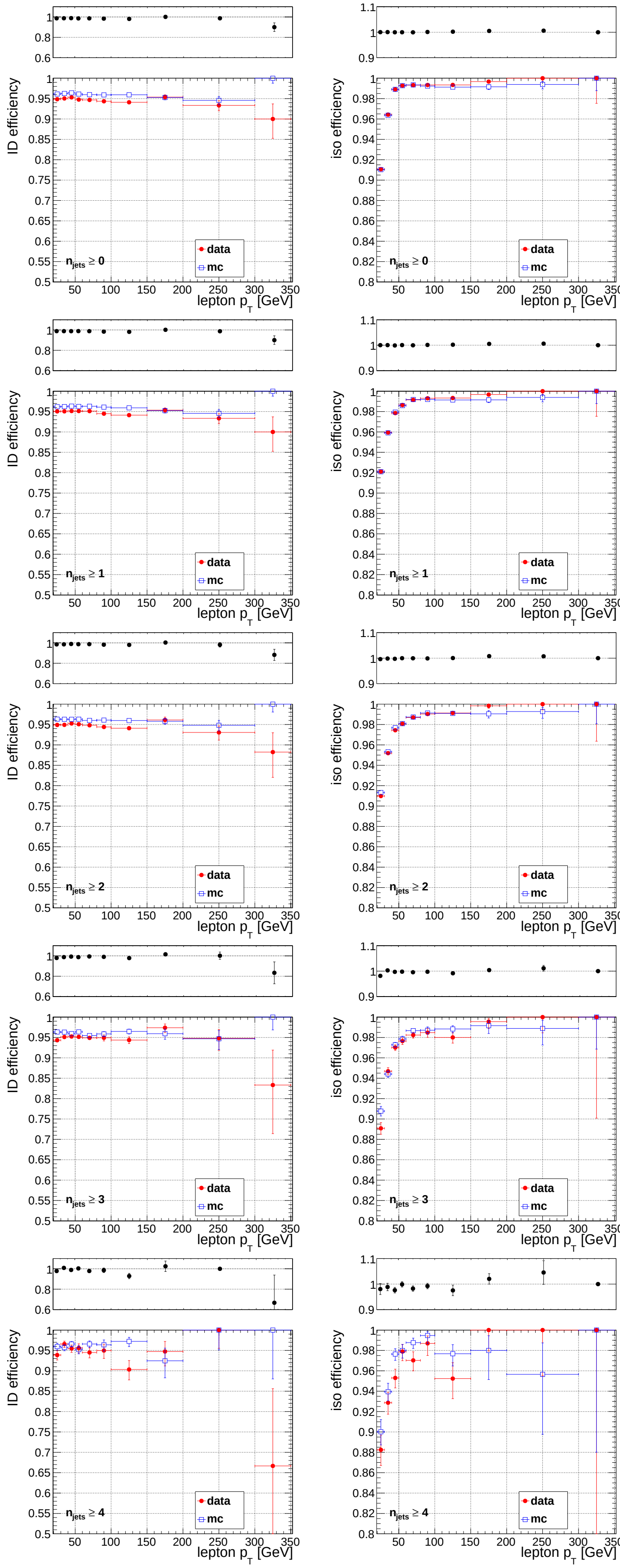

Figure 2: Comparison of the muon identification and isolation efficiencies in data and MC for various jet multiplicity requirements.

Table 9: Summary of the data and MC electron identification and isolation efficiencies measured with tag-and-probe studies.

MC ID p_T range [GeV]	$\|\eta\| < 1.5$	$1.5 < \|\eta\| < 2.1$
20 - 30	0.8156 $\pm$ 0.0008	0.6565 $\pm$ 0.0019
30 - 40	0.8670 $\pm$ 0.0004	0.7450 $\pm$ 0.0010
40 - 50	0.8922 $\pm$ 0.0003	0.7847 $\pm$ 0.0008
50 - 60	0.9023 $\pm$ 0.0006	0.7956 $\pm$ 0.0018
60 - 80	0.9097 $\pm$ 0.0011	0.8166 $\pm$ 0.0034
80 - 100	0.9203 $\pm$ 0.0028	0.8196 $\pm$ 0.0090
100 - 150	0.9162 $\pm$ 0.0037	0.8378 $\pm$ 0.0117
150 - 200	0.9106 $\pm$ 0.0087	0.8111 $\pm$ 0.0292
200 - 300	0.9304 $\pm$ 0.0119	0.9153 $\pm$ 0.0363
300 - 10000	0.8684 $\pm$ 0.0388	0.8000 $\pm$ 0.1789
MC ISO p_T range [GeV]	$\|\eta\| < 1.5$	$1.5 < \|\eta\| < 2.1$
20 - 30	0.9245 $\pm$ 0.0006	0.9466 $\pm$ 0.0011
30 - 40	0.9682 $\pm$ 0.0002	0.9741 $\pm$ 0.0004
40 - 50	0.9876 $\pm$ 0.0001	0.9883 $\pm$ 0.0002
50 - 60	0.9909 $\pm$ 0.0002	0.9912 $\pm$ 0.0005
60 - 80	0.9916 $\pm$ 0.0004	0.9930 $\pm$ 0.0008
80 - 100	0.9915 $\pm$ 0.0010	0.9908 $\pm$ 0.0025
100 - 150	0.9929 $\pm$ 0.0012	0.9894 $\pm$ 0.0035
150 - 200	0.9919 $\pm$ 0.0029	0.9932 $\pm$ 0.0068
200 - 300	0.9953 $\pm$ 0.0033	1.0000 $\pm$ 0.0000
300 - 10000	1.0000 $\pm$ 0.0000	1.0000 $\pm$ 0.0000
DATA ID p_T range [GeV]	$\|\eta\| < 1.5$	$1.5 < \|\eta\| < 2.1$
20 - 30	0.8145 $\pm$ 0.0008	0.6528 $\pm$ 0.0018
30 - 40	0.8676 $\pm$ 0.0004	0.7462 $\pm$ 0.0010
40 - 50	0.8955 $\pm$ 0.0003	0.7922 $\pm$ 0.0008
50 - 60	0.9049 $\pm$ 0.0006	0.8072 $\pm$ 0.0018
60 - 80	0.9110 $\pm$ 0.0011	0.8212 $\pm$ 0.0035
80 - 100	0.9156 $\pm$ 0.0028	0.8358 $\pm$ 0.0091
100 - 150	0.9257 $\pm$ 0.0036	0.8507 $\pm$ 0.0116
150 - 200	0.9186 $\pm$ 0.0084	0.8929 $\pm$ 0.0292
200 - 300	0.9106 $\pm$ 0.0149	0.7576 $\pm$ 0.0746
300 - 10000	0.9400 $\pm$ 0.0336	1.0000 $\pm$ 0.0000
DATA ISO p_T range [GeV]	$\|\eta\| < 1.5$	$1.5 < \|\eta\| < 2.1$
20 - 30	0.9201 $\pm$ 0.0006	0.9419 $\pm$ 0.0011
30 - 40	0.9667 $\pm$ 0.0002	0.9734 $\pm$ 0.0004
40 - 50	0.9872 $\pm$ 0.0001	0.9892 $\pm$ 0.0002
50 - 60	0.9904 $\pm$ 0.0002	0.9922 $\pm$ 0.0004
60 - 80	0.9923 $\pm$ 0.0004	0.9916 $\pm$ 0.0009
80 - 100	0.9914 $\pm$ 0.0010	0.9921 $\pm$ 0.0024
100 - 150	0.9945 $\pm$ 0.0011	1.0000 $\pm$ 0.0000
150 - 200	0.9908 $\pm$ 0.0031	1.0000 $\pm$ 0.0000
200 - 300	0.9941 $\pm$ 0.0042	1.0000 $\pm$ 0.0000
300 - 10000	0.9792 $\pm$ 0.0206	1.0000 $\pm$ 0.0000
Scale Factor ID p_T range [GeV]	$\|\eta\| < 1.5$	$1.5 < \|\eta\| < 2.1$
20 - 30	0.9987 $\pm$ 0.0014	0.9944 $\pm$ 0.0040
30 - 40	1.0007 $\pm$ 0.0006	1.0015 $\pm$ 0.0019
40 - 50	1.0036 $\pm$ 0.0005	1.0096 $\pm$ 0.0015
50 - 60	1.0029 $\pm$ 0.0010	1.0146 $\pm$ 0.0031
60 - 80	1.0014 $\pm$ 0.0018	1.0057 $\pm$ 0.0060
80 - 100	0.9949 $\pm$ 0.0043	1.0197 $\pm$ 0.0158
100 - 150	1.0104 $\pm$ 0.0057	1.0154 $\pm$ 0.0198
150 - 200	1.0087 $\pm$ 0.0134	1.1008 $\pm$ 0.0535
200 - 300	0.9786 $\pm$ 0.0203	0.8277 $\pm$ 0.0879
300 - 10000	1.0824 $\pm$ 0.0619	1.2500 $\pm$ 0.2795
Scale Factor ISO p_T range [GeV]	$\|\eta\| < 1.5$	$1.5 < \|\eta\| < 2.1$
20 - 30	0.9952 $\pm$ 0.0009	0.9950 $\pm$ 0.0016
30 - 40	0.9984 $\pm$ 0.0003	0.9992 $\pm$ 0.0006
40 - 50	0.9996 $\pm$ 0.0002	1.0009 $\pm$ 0.0003
50 - 60	0.9995 $\pm$ 0.0003	1.0009 $\pm$ 0.0006
60 - 80	1.0006 $\pm$ 0.0005	0.9985 $\pm$ 0.0012
80 - 100	0.9999 $\pm$ 0.0014	1.0013 $\pm$ 0.0035
100 - 150	1.0016 $\pm$ 0.0016	1.0108 $\pm$ 0.0036
150 - 200	0.9989 $\pm$ 0.0042	1.0068 $\pm$ 0.0069
200 - 300	0.9987 $\pm$ 0.0053	1.0000 $\pm$ 0.0000
300 - 10000	0.9792 $\pm$ 0.0206	1.0000 $\pm$ 0.0000

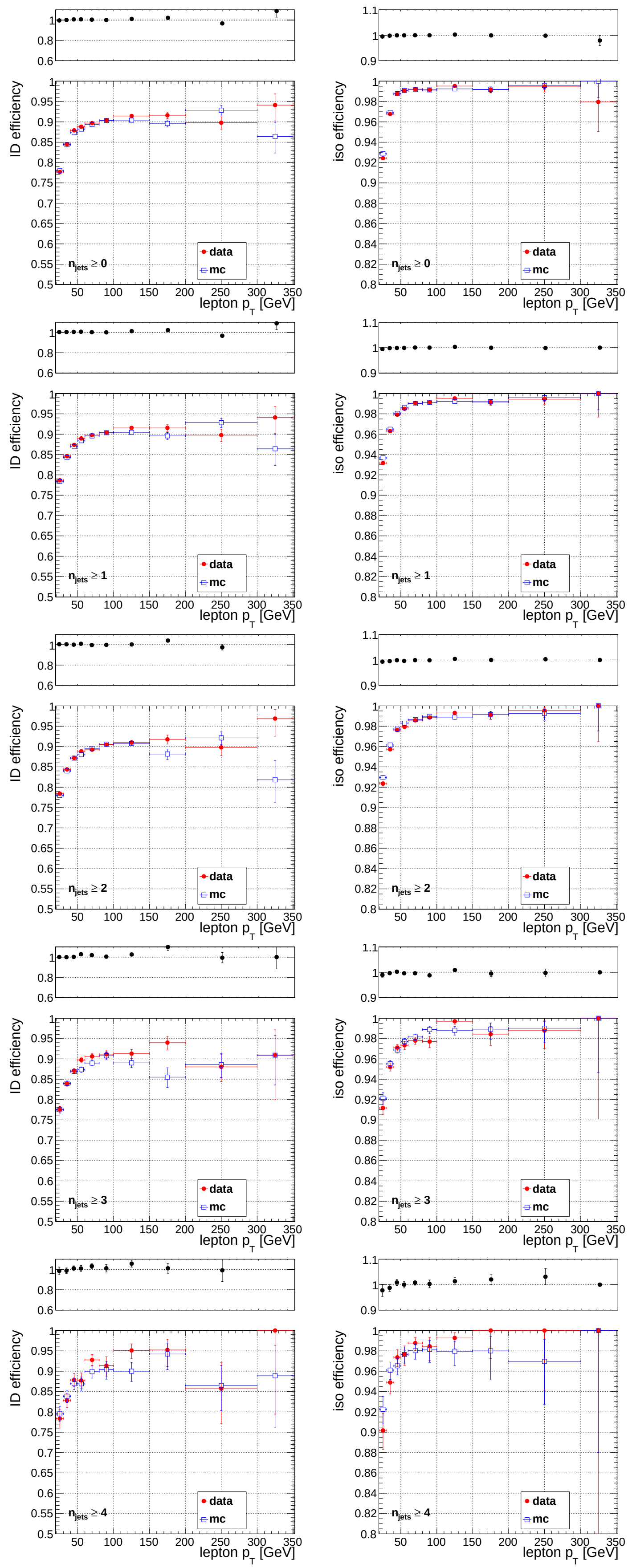

Figure 3: Comparison of the electron identification and isolation efficiencies in data and MC for various jet multiplicity requirements.

4.9 Trigger Efficiency Measurements

In this section we measure the efficiencies of the single lepton triggers, HLT_IsoMu24(_eta2p1) for muons and HLT_Ele27_WP80 for electrons, using a tag-and-probe approach. The tag is required to pass the full offline analysis selection and have $p_T > 30$ GeV, $|\eta| < 2.1$, and be matched to the single lepton trigger. The probe is also required to pass the full offline analysis selection and have $|\eta| < 2.1$, but the p_T requirement is relaxed to 20 GeV in order to measure the p_T turn-on curve. The tag-probe pair is required to have opposite-sign and an invariant mass in the range 76–106 GeV.

The measured trigger efficiencies are displayed in Fig. 4 and summarized in Table 10 (muons) and Table 11 (electrons). These trigger efficiencies are applied to the MC when used to predict data yields selected by single lepton triggers.

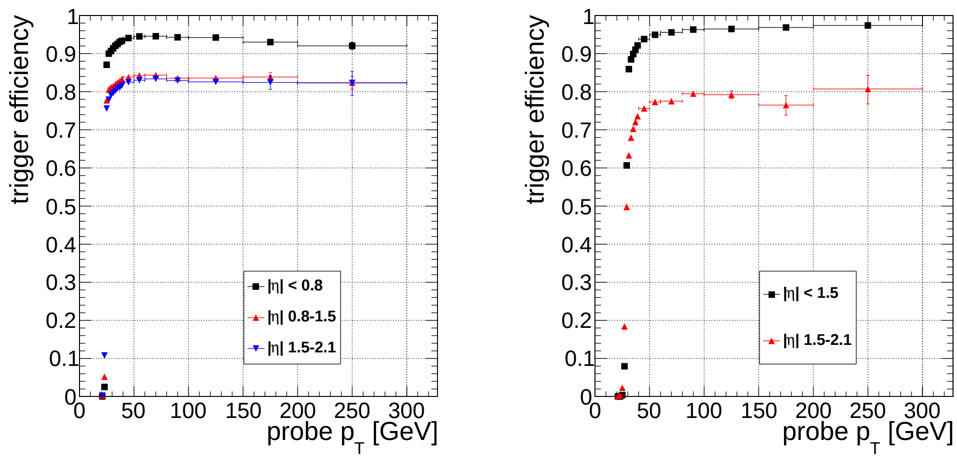

Figure 4: Efficiency for the single muon trigger HLT_IsoMu24(_eta2p1) (left) and single electron trigger HLT_Ele27_WP80 (right) as a function of lepton p_T, for several bins in lepton $|\eta|$.

Table 10: Summary of the single muon trigger efficiency HLT_IsoMu24(_eta2p1). Uncertainties are statistical.

p_{T} range [GeV]	$\|\eta\| < 0.8$	$0.8 < \|\eta\| < 1.5$	$1.5 < \|\eta\| < 2.1$
20 - 22	0.00 ± 0.000	0.00 ± 0.000	0.00 ± 0.000
22 - 24	0.03 ± 0.001	0.05 ± 0.001	0.11 ± 0.002
24 - 26	0.87 ± 0.002	0.78 ± 0.002	0.76 ± 0.003
26 - 28	0.90 ± 0.001	0.81 ± 0.002	0.78 ± 0.002
28 - 30	0.91 ± 0.001	0.81 ± 0.002	0.79 ± 0.002
30 - 32	0.91 ± 0.001	0.81 ± 0.001	0.80 ± 0.002
32 - 34	0.92 ± 0.001	0.82 ± 0.001	0.80 ± 0.002
34 - 36	0.93 ± 0.001	0.82 ± 0.001	0.81 ± 0.001
36 - 38	0.93 ± 0.001	0.83 ± 0.001	0.81 ± 0.001
38 - 40	0.93 ± 0.001	0.83 ± 0.001	0.82 ± 0.001
40 - 50	0.94 ± 0.000	0.84 ± 0.000	0.82 ± 0.001
50 - 60	0.95 ± 0.000	0.84 ± 0.001	0.83 ± 0.001
60 - 80	0.95 ± 0.001	0.84 ± 0.002	0.83 ± 0.002
80 - 100	0.94 ± 0.002	0.84 ± 0.004	0.83 ± 0.006
100 - 150	0.94 ± 0.003	0.84 ± 0.005	0.83 ± 0.008
150 - 200	0.93 ± 0.006	0.84 ± 0.011	0.82 ± 0.018
>200	0.92 ± 0.010	0.82 ± 0.017	0.82 ± 0.031

Table 11: Summary of the single electron trigger efficiency HLT_Ele27_WP80. Uncertainties are statistical.

p_{T} range [GeV]	$\|\eta\| < 1.5$	$1.5 < \|\eta\| < 2.1$
20 - 22	0.00 ± 0.000	0.00 ± 0.000
22 - 24	0.00 ± 0.000	0.00 ± 0.001
24 - 26	0.00 ± 0.000	0.02 ± 0.001
26 - 28	0.08 ± 0.001	0.18 ± 0.003
28 - 30	0.61 ± 0.002	0.50 ± 0.004
30 - 32	0.86 ± 0.001	0.63 ± 0.003
32 - 34	0.88 ± 0.001	0.68 ± 0.003
34 - 36	0.90 ± 0.001	0.70 ± 0.002
36 - 38	0.91 ± 0.001	0.72 ± 0.002
38 - 40	0.92 ± 0.001	0.74 ± 0.002
40 - 50	0.94 ± 0.000	0.76 ± 0.001
50 - 60	0.95 ± 0.000	0.77 ± 0.002
60 - 80	0.96 ± 0.001	0.78 ± 0.003
80 - 100	0.96 ± 0.002	0.80 ± 0.008
100 - 150	0.96 ± 0.002	0.79 ± 0.010
150 - 200	0.97 ± 0.004	0.76 ± 0.026
>200	0.97 ± 0.005	0.81 ± 0.038

5 Control Region Studies

The CR studies described in this Section are key to validating the background predictions. The CRs are defined in Section 4.4.

CR1 and CR2 are designed to test the M_T tail in $W+$ jets and $t\bar{t}$ respectively. Note that, as explained in Section 2.1, these tails are different in the two samples because the off-shell effects are much more pronounced for $W+$ jets (the s- and t-channel single top have the same M_T tail as $t\bar{t}$). To put things in perspective, keep in mind that these backgrounds are only about 15% of the total, see Table 5.

CR4 and CR5 address the dominant $t\bar{t}$ dilepton background. In CR4 we test the M_T tail in well identified dilepton events. In CR5 we test the same quantity, but in events where the second lepton is identified as an isolated track. Clearly CR4 and CR5 overlap.

5.1 W+Jets MC Modelling Validation from CR1

The estimate of the uncertainty on this background is based on CR1, defined by applying the full signal selection, including the isolated track veto, but requiring 0 b-tags (CSV medium working point as described in Sec. 4). The sample is dominanted by W+jets and is thus used to validate the MC modelling of this background.

In Table 12 we show the amount that we need to scale the W+jets MC by in order to have agreement between data and Monte Carlo in the M_T peak region, defined as $50 < M_T < 80$ GeV, for the different signal regions. (Recall, the signal regions have different $E_{\mathrm{T}}^{\mathrm{miss}}$ requirements). These scale factors are not terribly important, but it is reassuring that they are not too different from 1.

Sample	CR1PRESEL	CR1A	CR1B	CR1C	CR1D	CR1E	CR1F	CR1G
μ M_{T}-SF	0.92 ± 0.02	0.97 ± 0.03	0.90 ± 0.04	0.91 ± 0.06	0.93 ± 0.09	0.98 ± 0.13	0.94 ± 0.18	0.96 ± 0.25
e M_{T}-SF	0.94 ± 0.02	0.90 ± 0.04	0.84 ± 0.05	0.80 ± 0.07	0.83 ± 0.10	0.77 ± 0.13	0.86 ± 0.20	0.87 ± 0.29

Table 12: M_{T} peak Data/MC scale factors applied to W+jets samples. No scaling is made for backgrounds from other processes. CR1PRESEL refers to a sample with $E_{\mathrm{T}}^{\mathrm{miss}} > 50$ GeV. The uncertainties are statistical only.

Next, in Fig 45, 6, and 7, we show plots of $E_{\mathrm{T}}^{\mathrm{miss}}$ and then M_T for different $E_{\mathrm{T}}^{\mathrm{miss}}$ requirements corresponding to those defining our signal regions. It is clear that there are more events in the M_T tail than predicted from MC. This implies that we need to rescale the MC W+jets background in the tail region.

The rescaling is explored in Table 13, where we compare the data and MC yields in the M_T signal regions and in a looser control region. Note that the MC is normalized in the M_T peak region by rescaling the W+jets component according to Table 12.

We also derive data/MC scale factors. As shown in Table 13, these are derived in two different ways, separately for muons and electrons and then combined, as follows:

- For the first three sets of scale factors, above the triple horizontal line, we calculate the scale factor as the amount by which we would need to rescale **all** MC (W+jets , $t\bar{t}$, single top, rare) in order to have data-MC agreement in the M_T tail.
- For the next three set of scale factors, below the triple horizontal line, we calculate the scale factor as the amount by which we would need to scale W+jets keeping all other components fixed in order to have data-MC agreement in the tail.

The true W+jets scale factor is somewhere in between these two extremes. We also note that there is no statistically significant difference between the electron and muon samples. We use these data to extract a data/MC scale factor for W+jets which will be used to rescale the W+jets MC tail. This scale factor is listed in the last line of the Table, and is called SFR_{wjets}. It is calculated as follows.

- Separately for each signal region
- As the average of the two methods described above

Sample	CR1PRESEL	CR1A	CR1B	CR1C	CR1D	CR1E	CR1F	CR1G
μ MC	480 ± 22	173 ± 5	114 ± 4	40 ± 2	16 ± 1	8 ± 1	4 ± 1	2 ± 1
μ Data	629	238	139	45	12	8	3	2
μ Data/MC	1.31 ± 0.08	1.37 ± 0.10	1.22 ± 0.11	1.12 ± 0.18	0.75 ± 0.23	0.99 ± 0.37	0.75 ± 0.45	0.96 ± 0.72
e MC	330 ± 8	118 ± 4	79 ± 3	29 ± 2	13 ± 1	5 ± 1	3 ± 1	2 ± 0
e Data	473	174	100	36	16	5	5	2
e Data/MC	1.43 ± 0.07	1.47 ± 0.12	1.27 ± 0.14	1.23 ± 0.22	1.26 ± 0.34	1.07 ± 0.51	1.80 ± 0.91	1.26 ± 0.97
μ+e MC	810 ± 23	291 ± 7	192 ± 5	69 ± 3	29 ± 2	13 ± 1	7 ± 1	4 ± 1
μ+e Data	1102	412	239	81	28	13	8	4
μ+e Data/MC	1.36 ± 0.08	1.42 ± 0.13	1.24 ± 0.15	1.17 ± 0.23	0.97 ± 0.31	1.02 ± 0.51	1.18 ± 0.69	1.09 ± 0.96
μ W MC	300 ± 23	84 ± 5	52 ± 4	20 ± 2	9 ± 2	5 ± 1	3 ± 1	1 ± 1
μ W Data	449 ± 26	149 ± 16	78 ± 12	25 ± 7	5 ± 4	5 ± 3	2 ± 2	1 ± 1
μ W Data/MC	1.50 ± 0.14	1.77 ± 0.21	1.49 ± 0.26	1.25 ± 0.38	0.56 ± 0.39	0.98 ± 0.62	0.60 ± 0.73	0.94 ± 1.14
e W MC	192 ± 8	55 ± 4	36 ± 3	14 ± 2	6 ± 1	3 ± 1	2 ± 1	1 ± 0
e W Data	335 ± 22	111 ± 13	58 ± 10	20 ± 6	10 ± 4	3 ± 2	4 ± 2	1 ± 1
e W Data/MC	1.74 ± 0.14	2.02 ± 0.29	1.58 ± 0.32	1.49 ± 0.50	1.50 ± 0.70	1.10 ± 0.80	2.27 ± 1.55	1.51 ± 1.96
μ+e W MC	493 ± 24	139 ± 6	89 ± 5	33 ± 3	16 ± 2	8 ± 1	4 ± 1	2 ± 1
μ+e W Data	785 ± 59	260 ± 37	135 ± 28	45 ± 16	15 ± 9	8 ± 7	6 ± 5	3 ± 3
μ+e W Data/MC	1.59 ± 0.14	1.87 ± 0.28	1.53 ± 0.33	1.35 ± 0.50	0.95 ± 0.58	1.03 ± 0.83	1.29 ± 1.13	1.16 ± 1.65
SFR_{wjet}	1.48 ± 0.26	1.64 ± 0.38	1.38 ± 0.30	1.26 ± 0.39	0.96 ± 0.45	1.02 ± 0.67	1.23 ± 0.92	1.12 ± 1.31

Table 13: Yields in M_{T} tail comparing the MC prediction (after applying SFs) to data. CR1PRESEL refers to a sample with $E_{\mathrm{T}}^{\mathrm{miss}} > 50$ GeV and $M_{\mathrm{T}} > 150$ GeV. See text for details.

- Including the statistical uncertainty
- Adding in quadrature to the uncertainty one-half of the deviation from 1.0

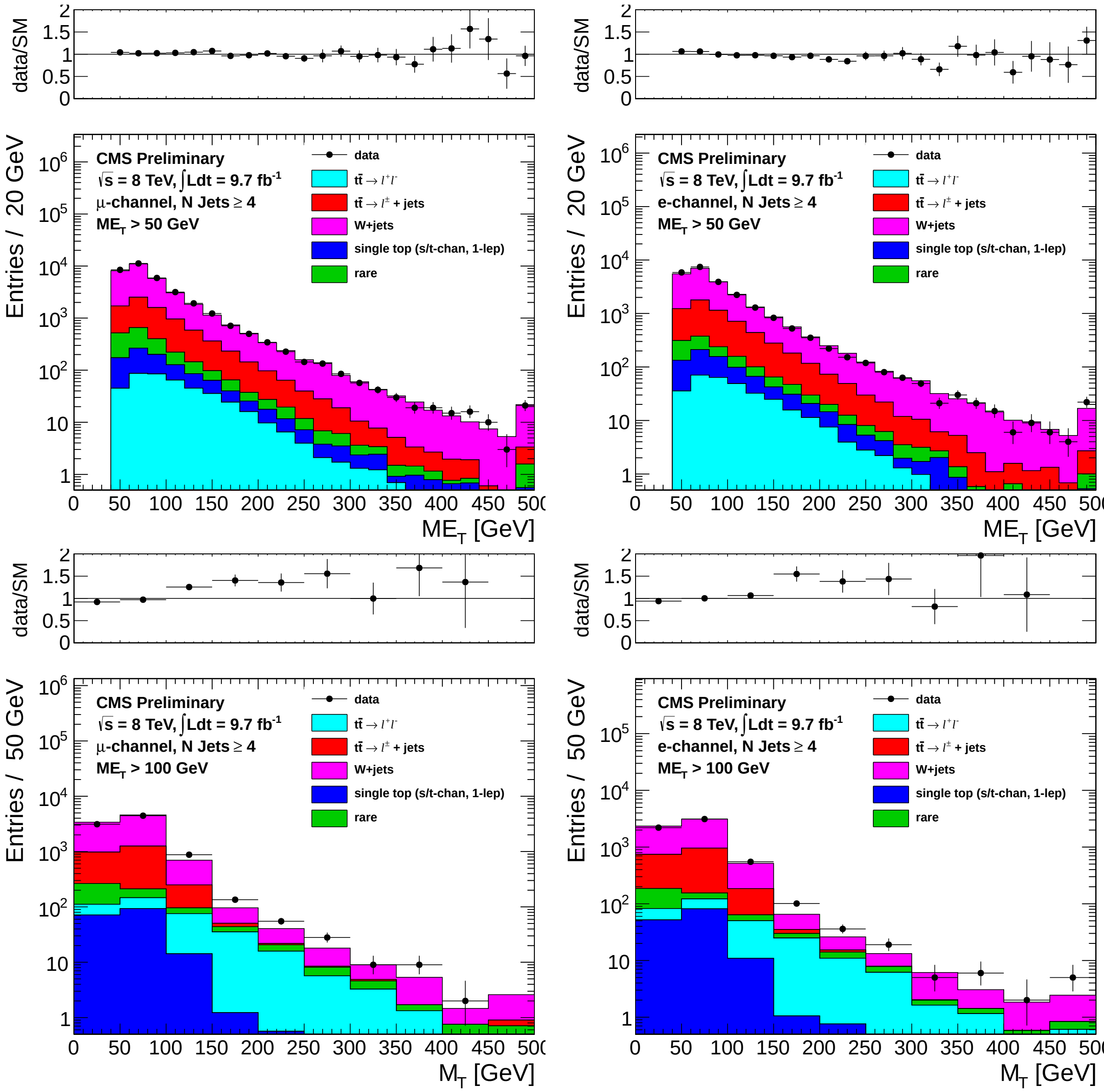

Figure 5: Comparison of the $E_{\mathrm{T}}^{\mathrm{miss}}$ (top) and M_{T} for $E_{\mathrm{T}}^{\mathrm{miss}} > 100$ (bottom) distributions in data vs. MC for events with a leading muon (left) and leading electron (right) satisfying the requirements of CR1.

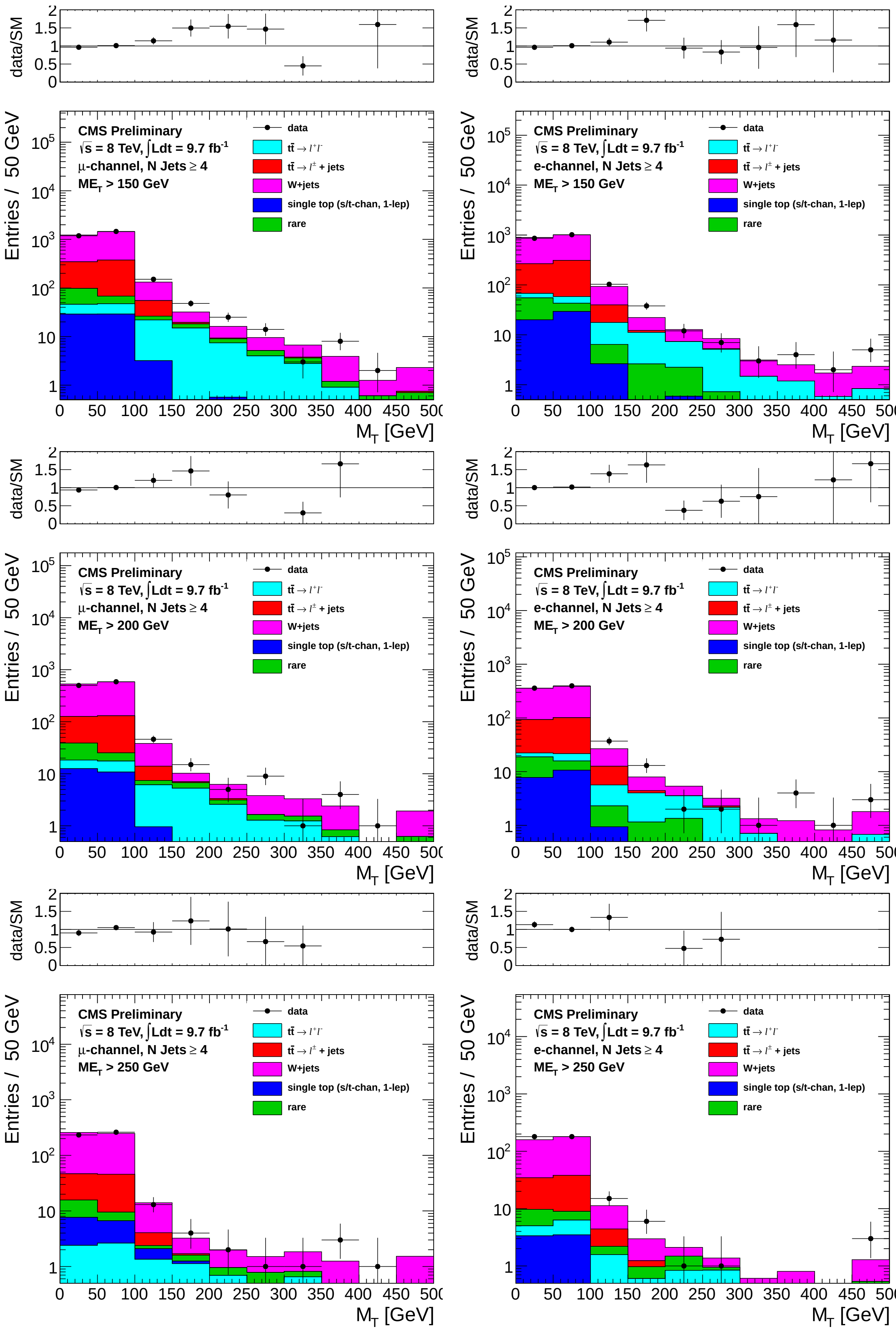

Figure 6: Comparison of the M_T distribution in data vs. MC for events with a leading muon (left) and leading electron (right) satisfying the requirements of CR1. The E_T^{miss} requirements used are 150 GeV (top), 200 GeV (middle) and 250 GeV (bottom).

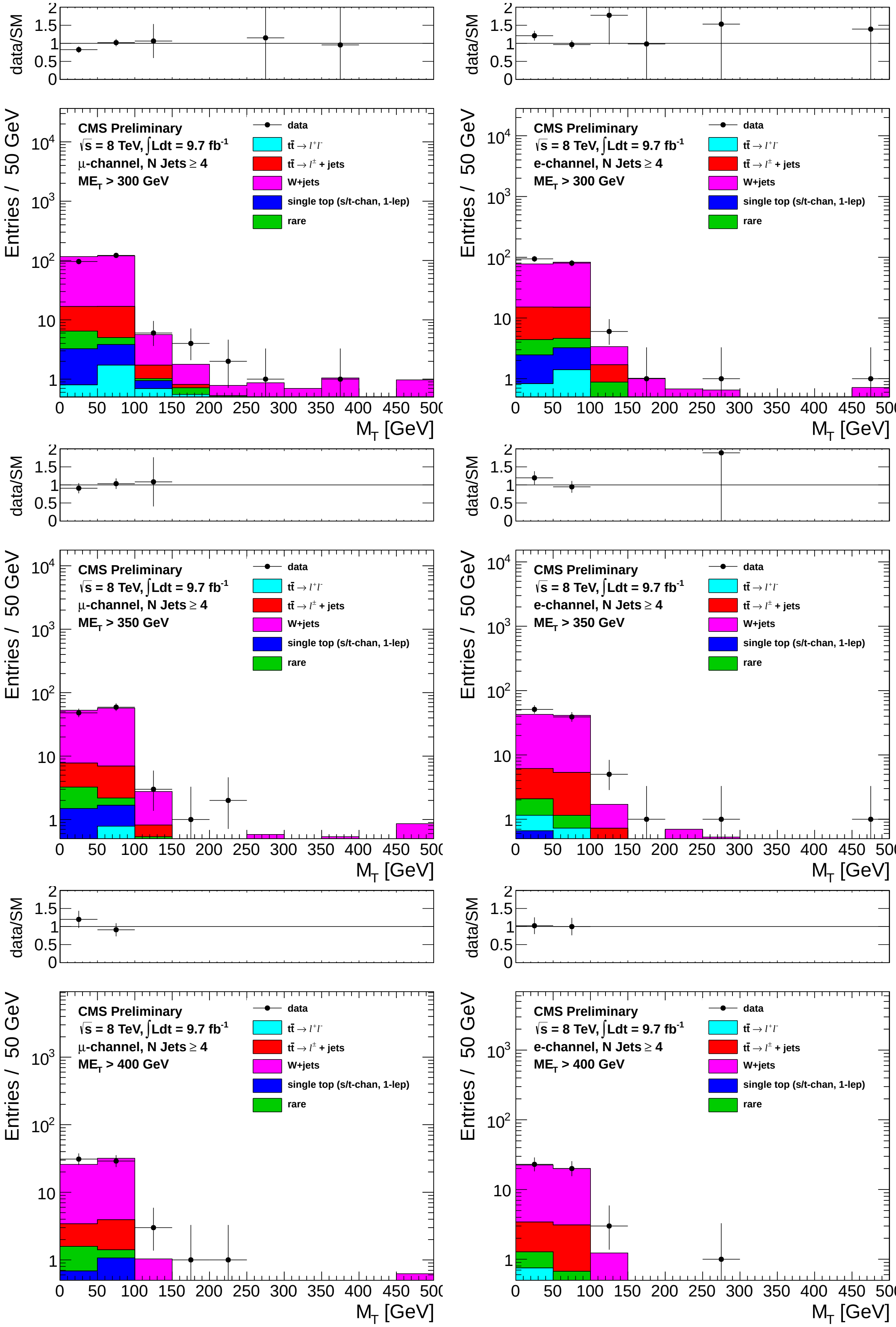

Figure 7: Comparison of the M_T distribution in data vs. MC for events with a leading muon (left) and leading electron (right) satisfying the requirements of CR1. The $E_\mathrm{T}^\mathrm{miss}$ requirements used are 300 GeV (top), 350 GeV (middle) and 400 GeV (bottom).

5.2 Single Lepton Top MC Modelling Validation from CR2

The M_{T} tail for single-lepton top events ($\mathrm{t\bar{t}} \to \ell + \mathrm{jets}$ and single top) is dominated by jet resolution effects. The W cannot be far off-shell because $M_{\mathrm{W}} < M_{\mathrm{top}}$. The modeling of the M_{T} tail from jet resolution effects can be studied using Z+jets data and MC samples. However, as we will show below, this test is statistically limited and can only be performed for the $E_{\mathrm{T}}^{\mathrm{miss}}$ requirements corresponding to SRA and SRB.

Z events are selected by requiring exactly 2 good leptons (satisfying ID and isolation requirements) and requiring the $M_{\ell\ell}$ to be in the range $81 - 101$ GeV. Events with additional isolated tracks are vetoed, as in Section 4.2. To reduce $\mathrm{t\bar{t}}$ backgrounds, events with a CSVM tag are removed. The positive lepton is treated as a neutrino and so is added to the MET: $E_{\mathrm{T}}^{\mathrm{miss}} \to p_{\mathrm{T}}(\ell^{+}) + E_{\mathrm{T}}^{\mathrm{miss}}$, and the M_{T} is recalculated with the negative lepton: $M_{\mathrm{T}}(\ell^{-},\ E_{\mathrm{T}}^{\mathrm{miss}})$. The resulting "pseudo-$M_{\mathrm{T}}$" is dominated by jet resolution effects, since no off-shell Z production enters the sample due to the $M_{\ell\ell}$ requirement. This section describes how well the MC predicts the tail of "pseudo-M_{T}".

The underlying distributions are shown in Fig. 46. We then perform the exact same type of Data/MC comparison and analysis as described for CR1 in Section D.3. For CR1 we collected the data/MC tail information in Table 13; the equivalent for CR2 is Table 14 (for CR2 the statistics are not sufficient to split electrons and muons). The last line of Table 14 gives the data/MC scale factors for the $\mathrm{t\bar{t}}$ lepton + jets M_T tail (SFR_{top}). This is calculated in the same way as SFR_{wjets} of Table 13. Just as in CR1, there is an excess of data in the tails, as reflected in the values of SFR_{top}. There are insufficient events to derive scale factors for $E_{\mathrm{T}}^{\mathrm{miss}} > 150$ GeV. As a result, the scale factors derived from CR2 are not used for the central prediction of the single-lepton top background. They serve as a valuable cross check of the predictions described in Section 7. The single lepton top predictions obtained for SRA and SRB using the SFR_{top} values described here are consistent with the default predictions.

Sample	CR2PRESEL0	CR2PRESEL1	CR2A	CR2B
MC	32 ± 2	28 ± 2	10 ± 1	10 ± 1
Data	50	45	17	17
Data/MC	1.56 ± 0.24	1.63 ± 0.27	1.68 ± 0.45	1.74 ± 0.48
DY MC	25 ± 2	20 ± 2	5 ± 1	5 ± 1
DY Data	42 ± 7	38 ± 7	12 ± 4	12 ± 4
DY Data/MC	1.73 ± 0.32	1.85 ± 0.37	2.37 ± 0.96	2.58 ± 1.16
SFR_{top}	1.64 ± 0.40	1.74 ± 0.46	2.02 ± 0.68	2.16 ± 0.75

Table 14: Yields in M_{T} tail comparing the Z+jets MC prediction (after applying SFs) to data without subtracting the non-Z+jets components (top table) and with subtracting the non-Z+jets components (bottom table). CR2PRESEL refers to a sample with $E_{\mathrm{T}}^{\mathrm{miss}} > 50$ GeV and $M_{\mathrm{T}} > 150$ GeV.

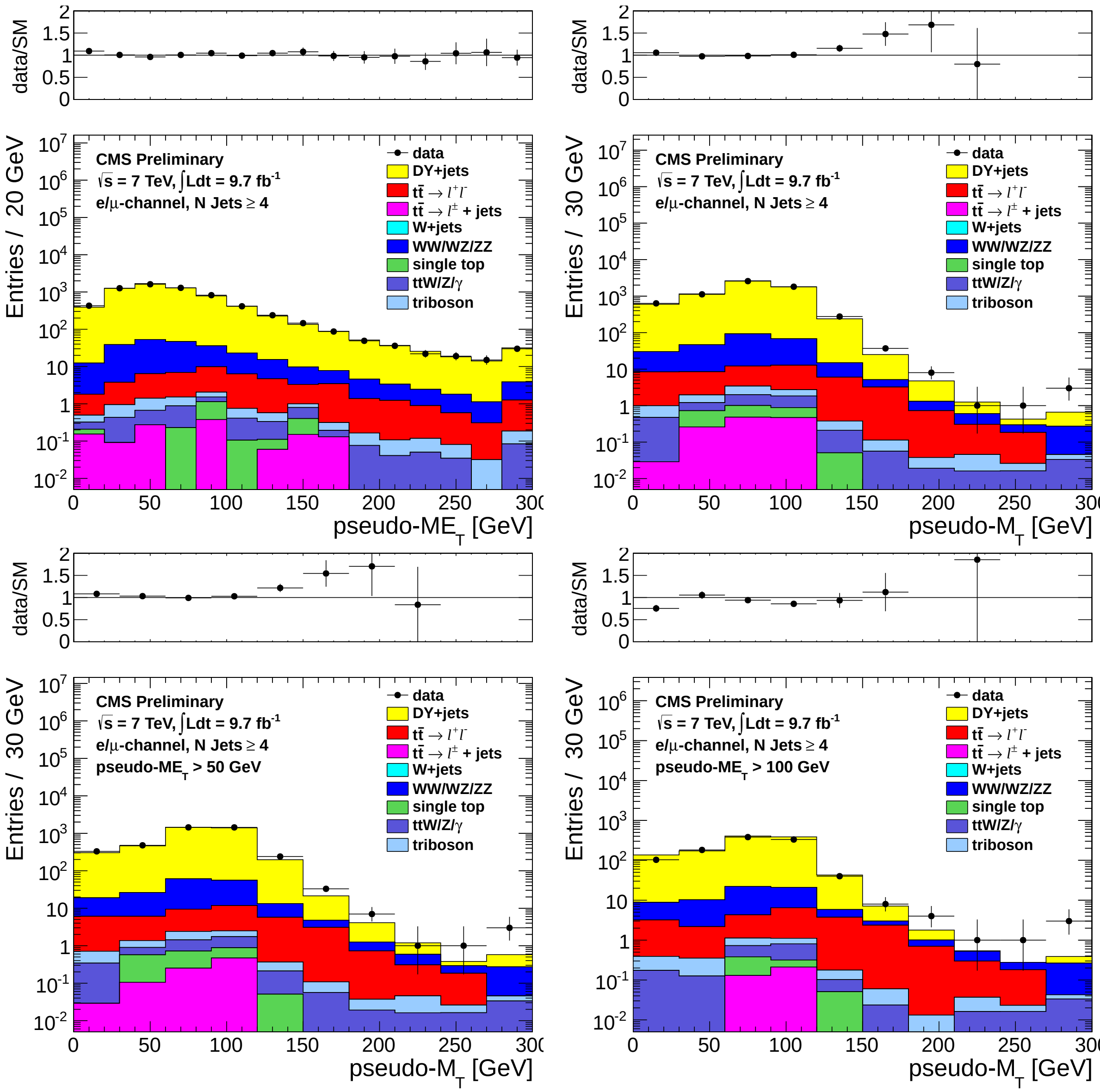

Figure 8: Comparison of the pseudo-$E_{\mathrm{T}}^{\mathrm{miss}}$ (top, left), pseudo-M_{T} (top, right and bottom) distributions in data vs. MC for events satisfying the requirements of CR2, combining both the muon and electron channels. The pseudo-M_{T} distributions are shown before any additional requirements (top, right) and after requiring pseudo-$E_{\mathrm{T}}^{\mathrm{miss}}$>50 GeV (bottom, left) and pseudo-$E_{\mathrm{T}}^{\mathrm{miss}}$> 100 GeV (bottom, right).

5.3 Dilepton studies in CR4

5.3.1 Modeling of Additional Hard Jets in Top Dilepton Events

Dilepton $t\bar{t}$ events have 2 jets from the top decays, so additional jets from radiation or higher order contributions are required to enter the signal sample. In this Section we develop an algorithm to be applied to all $t\bar{t} \to \ell\ell$ MC samples to ensure that the distribution of extra jets is properly modelled.

The modeling of additional jets in $t\bar{t}$ events is checked in a $t\bar{t} \to \ell\ell$ control sample, selected by requiring

- exactly 2 electrons or muons with p_T> 20 GeV
- $E_T^{miss} > 50$ GeV
- ≥ 1 b-tagged jet
- Z-veto ($|m_{\ell\ell} - 91| > 15$ GeV)

Figure 9 shows a comparison of the jet multiplicity distribution in data and MC for this two-lepton control sample. After requiring at least 1 b-tagged jet, most of the events have 2 jets, as expected from the dominant process $t\bar{t} \to \ell\ell$. There is also a significant fraction of events with additional jets. The 3-jet sample is mainly comprised of $t\bar{t}$ events with 1 additional emission and similarly the $\geq$ 4-jet sample contains primarily $t\bar{t}+ \geq 2$ jet events.

It should be noted that in the case of $t\bar{t} \to \ell\ell$ events with a single reconstructed lepton, the other lepton may be mis-reconstructed as a jet. For example, a hadronic tau may be misidentified as a jet (since no τ identification is used). In this case only 1 additional jet from radiation may suffice for a $t\bar{t} \to \ell\ell$ event to enter the signal sample. As a result, both the samples with $t\bar{t} + 1$ jet and $t\bar{t}+ \geq 2$ jets are relevant for estimating the top dilepton background in the signal region.

Table 15 shows scale factors (K_3 and K_4) used to correct the fraction of events with additional jets in MC to the observed fraction in data. These scale factors are calculated from Fig. 9 as follows:

- N_2 = data yield minus non-dilepton $t\bar{t}$ MC yield for N_{jets} =1 or 2.
- N_3 = data yield minus non-dilepton $t\bar{t}$ MC yield for $N_{jets} = 3$
- N_4 = data yield minus non-dilepton $t\bar{t}$ MC yield for $N_{jets} \geq 4$
- M_2 = dilepton $t\bar{t}$ MC yield for $N_{jets} = 1$ or 2
- M_3 = dilepton $t\bar{t}$ MC yield for $N_{jets} = 3$
- M_4 = dilepton $t\bar{t}$ MC yield for $N_{jets} \geq 4$

then

- $SF_2 = N_2/M_2$
- $SF_3 = N_3/M_3$
- $SF_4 = N_4/M_4$
- $K_3 = SF_3/SF_2$
- $K_4 = SF_4/SF_2$

This insures that $K_3M_3/(M_2 + K_3M_3 + K_4M_4) = N_3/(N_2 + N_3 + N_4)$ and similarly for the ≥ 4 jet bin.

Table 15 also shows the values of K_3 and K_4 for different values of the E_T^{miss} cut in the control sample definition. This demonstrates that there is no statistically significant dependence of K_3 and K_4 on the E_T^{miss} cut.

The factors K_3 and K_4 (derived with the 100 GeV E_T^{miss} cut) are applied to the $t\bar{t} \to \ell\ell$ MC throughout the entire analysis, i.e. whenever $t\bar{t} \to \ell\ell$ MC is used to estimate or subtract a yield or distribution.

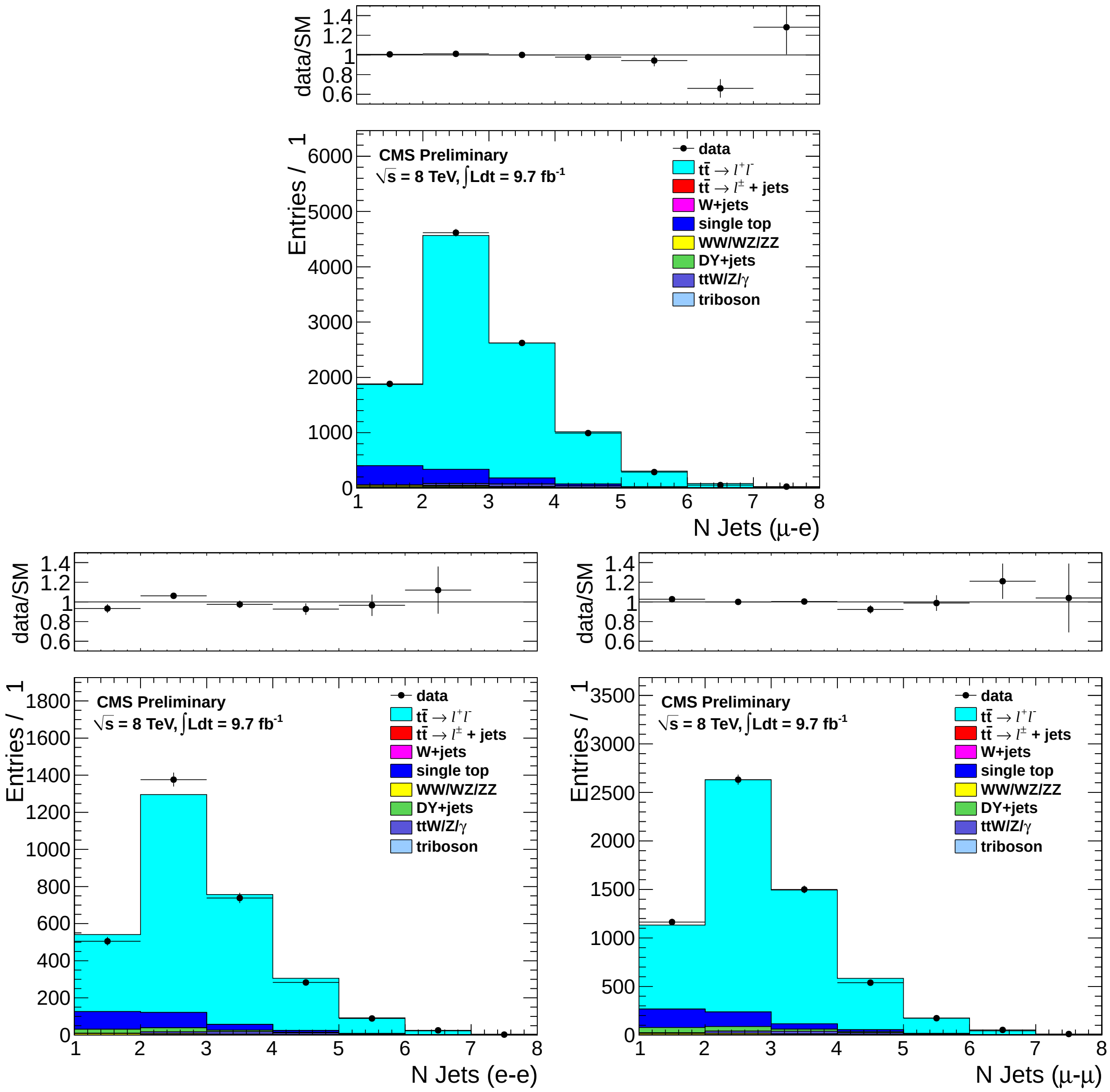

Figure 9: Comparison of the jet multiplicity distribution in data and MC for dilepton events in the e-μ (top), e-e (bottom left) and μ-μ (bottom right) channels.

To be explicit, whenever Powheg is used, the Powheg K_3 and K_4 are used; whenever default MadGraph is used, the MadGraph K_3 and K_4 are used, etc. In order to do so, it is first necessary to count the number of additional jets from radiation and exclude leptons misidentified as jets. A jet is considered a misidentified lepton if it is matched to a generator-level second lepton with sufficient energy to satisfy the jet p_{T} requirement ($p_{\mathrm{T}} > 30$ GeV). Then $t\bar{t} \rightarrow \ell\ell$ events that need two radiation jets to enter our selection are scaled by K_4, while those that only need one radiation jet are scaled by K_3.

	$E_{\mathrm{T}}^{\mathrm{miss}}$ cut for data/MC scale factors					
Sample	50 GeV	100 GeV	150 GeV	200 GeV	250 GeV	300 GeV
N jets = 3	$K_3 = 0.98 \pm 0.02$	$K_3 = 1.01 \pm 0.03$	$K_3 = 1.00 \pm 0.08$	$K_3 = 1.03 \pm 0.18$	$K_3 = 1.29 \pm 0.51$	$K_3 = 1.58 \pm 1.23$
N jets ≥ 4	$K_4 = 0.94 \pm 0.02$	$K_4 = 0.93 \pm 0.04$	$K_4 = 1.00 \pm 0.08$	$K_4 = 1.07 \pm 0.18$	$K_4 = 1.30 \pm 0.48$	$K_4 = 1.65 \pm 1.19$

Table 15: Data/MC scale factors used to account for differences in the fraction of events with additional hard jets from radiation in $\mathrm{t\bar{t}} \to \ell\ell$ events. The N jets = 3 scale factor, K_3, is sensitive to $\mathrm{t\bar{t}} + 1$ extra jet from radiation, while the N jets ≥ 4 scale factor, K_4, is sensitive to $\mathrm{t\bar{t}}+ \geq 2$ extra jets from radiation. The values derived with the 100 GeV $E_{\mathrm{T}}^{\mathrm{miss}}$ cut are applied to the $\mathrm{t\bar{t}} \to \ell\ell$ MC throughout the analysis.

5.3.2 Validation of the "Physics" Modelling of the $\mathrm{t\bar{t}} \to \ell\ell$ MC in CR4

As mentioned above, $t\bar{t} \to$ dileptons where one of the leptons is somehow lost constitutes the main background. The object of this test is to validate the M_T distribution of this background by looking at the M_T distribution of well identified dilepton events. We construct a transverse mass variable from the leading lepton and the $E_{\mathrm{T}}^{\mathrm{miss}}$. We distinguish between events with leading electrons and leading muons.

The $t\bar{t}$ MC is corrected using the K_3 and K_4 factors from Section 5.3.1. It is also normalized to the total data yield separately for the $E_{\mathrm{T}}^{\mathrm{miss}}$ requirements of the various signal regions. These normalization factors are listed in Table 16 and are close to unity.

The underlying $E_{\mathrm{T}}^{\mathrm{miss}}$ and M_T distributions are shown in Figures 43 and 11. The data-MC agreement is quite good. Quantitatively, this is also shown in Table 17. This is a **very** important Table. It shows that for well identified $\mathrm{t\bar{t}} \to \ell\ell$, the MC can predict the M_T tail. Since the main background is also $\mathrm{t\bar{t}} \to \ell\ell$ except with one "missed" lepton, this is a key test.

Sample	CR4PRESEL	CR4A	CR4B	CR4C	CR4D	CR4E	CR4F
μ Data/MC-SF	1.01 ± 0.03	0.96 ± 0.04	0.99 ± 0.07	1.05 ± 0.13	0.91 ± 0.20	1.10 ± 0.34	1.50 ± 0.67
e Data/MC-SF	0.99 ± 0.03	0.99 ± 0.05	0.91 ± 0.08	0.84 ± 0.13	0.70 ± 0.18	0.73 ± 0.29	0.63 ± 0.38

Table 16: Data/MC scale factors for total yields, applied to compare the shapes of the distributions. The uncertainties are statistical only.

Sample	CR4PRESEL	CR4A	CR4B	CR4C	CR4D	CR4E	CR4F
μ MC	256 ± 14	152 ± 11	91 ± 9	26 ± 5	6 ± 2	4 ± 2	2 ± 1
μ Data	251	156	98	27	8	6	4
μ Data/MC SF	0.98 ± 0.08	1.02 ± 0.11	1.08 ± 0.16	1.04 ± 0.28	1.29 ± 0.65	1.35 ± 0.80	2.10 ± 1.72
e MC	227 ± 13	139 ± 11	73 ± 8	21 ± 4	5 ± 2	2 ± 1	1 ± 1
e Data	219	136	72	19	2	1	1
e Data/MC SF	0.96 ± 0.09	0.98 ± 0.11	0.99 ± 0.16	0.92 ± 0.29	0.41 ± 0.33	0.53 ± 0.62	0.76 ± 0.96
μ+e MC	483 ± 19	291 ± 16	164 ± 13	47 ± 7	11 ± 3	6 ± 2	3 ± 2
μ+e Data	470	292	170	46	10	7	5
μ+e Data/MC SF	0.97 ± 0.06	1.00 ± 0.08	1.04 ± 0.11	0.99 ± 0.20	0.90 ± 0.37	1.11 ± 0.57	1.55 ± 1.04

Table 17: Yields in M_{T} tail comparing the MC prediction (after applying SFs) to data. The uncertainties are statistical only.

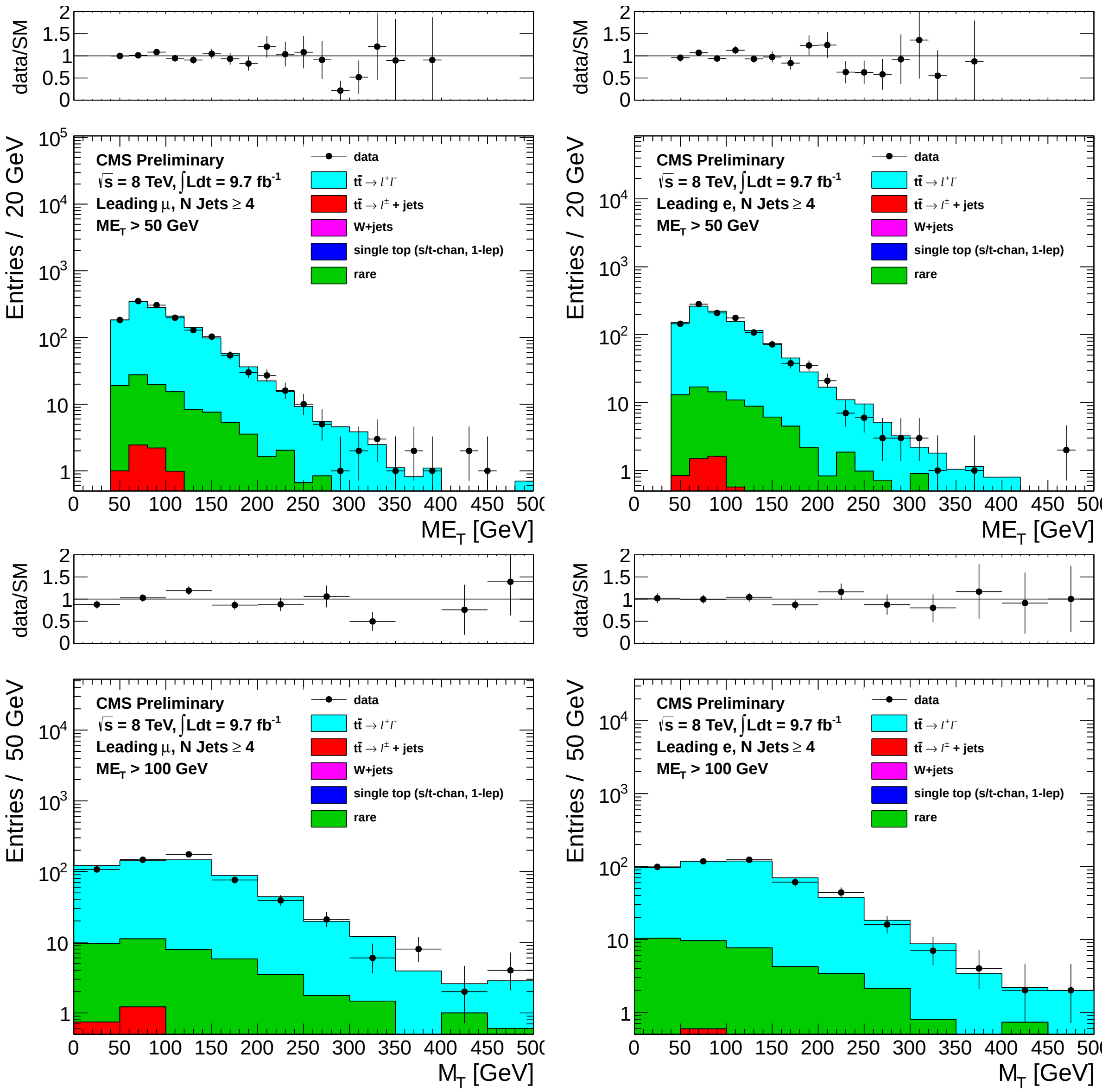

Figure 10: Comparison of the $E_{\mathrm{T}}^{\mathrm{miss}}$ (top) and M_{T} for $E_{\mathrm{T}}^{\mathrm{miss}} > 100$ (bottom) distributions in data vs. MC for events with a leading muon (left) and leading electron (right) satisfying the requirements of CR4.

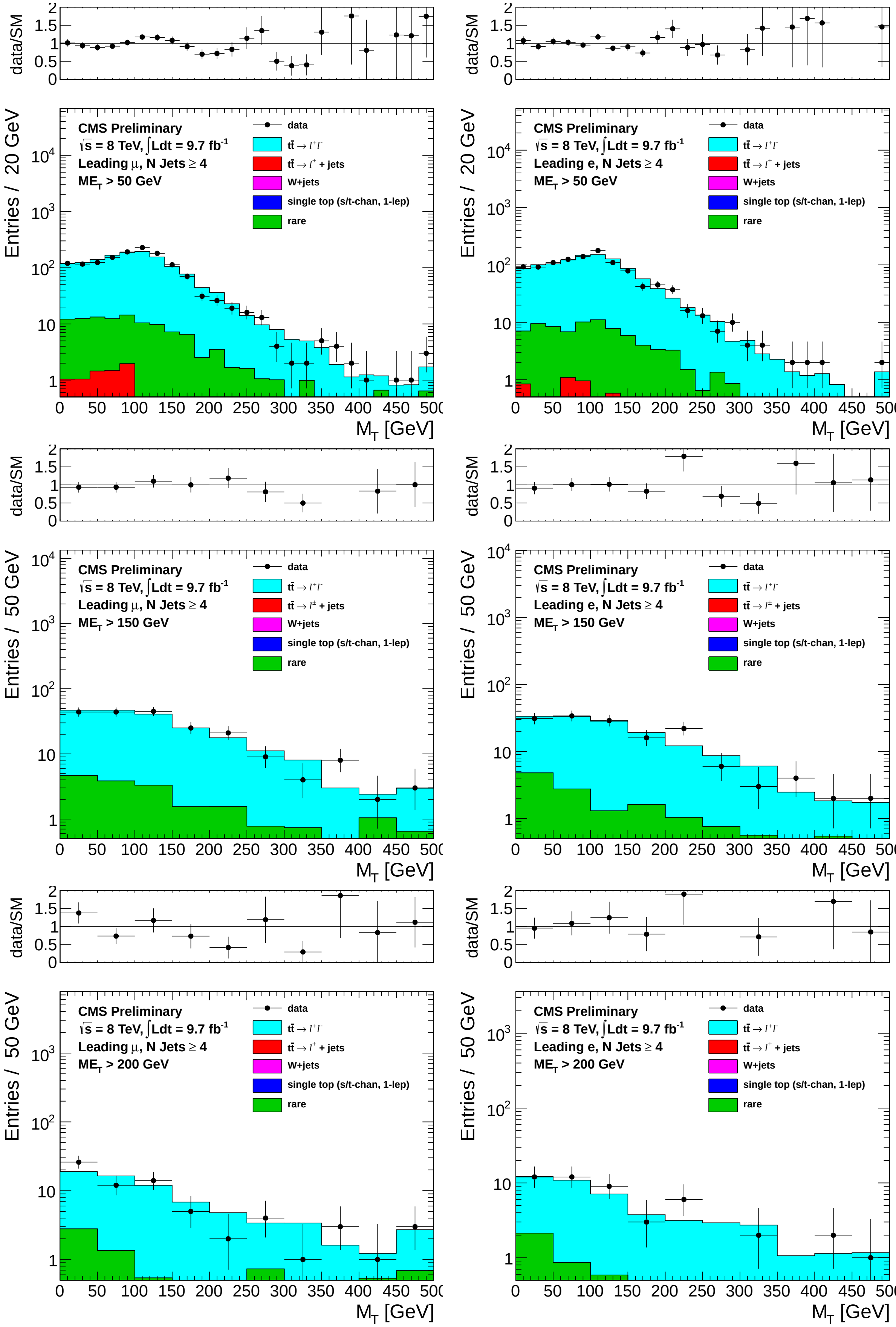

Figure 11: Comparison of the M_T distribution in data vs. MC for events with a leading muon (left) and leading electron (right) satisfying the requirements of CR4. The $E_T^{\rm miss}$ requirements used are 50 GeV (top), 200 GeV (middle) and 250 GeV (bottom).

5.4 Test of control region with isolated track in CR5

This CR consists of events that pass all cuts but fail the isolated track veto cut. These events (especially in the tail of M_T) are predominantly $t\bar{t}$ dileptons. Thus the test in this control region is similar to that performed in CR4 and described in Section 5.3.2. There is some non-trivial complementarity because CR5 also includes events with taus and events with electrons or muons below the threshold of the CR4 selection. Also, this test is somewhat sensitive to the simulation of the track isolation requirement, since the number of dilepton events in CR5 depends on the (in)efficiency of that cut.

In CR5 there is also a significant component of $t\bar{t} \to \ell+$ jets, where one of the jets fluctuates to an isolated track. This component dominates at low M_T and is not necessarily well reproduced quantitatively by the simulation. This makes the normalization of the top MC a little bit tricky. We define a "pre-veto" sample as the sample of events that pass all cuts without any isolated track requirements. This sample is dominated by $t\bar{t} \to \ell+$ jets. We normalize the dilepton component of the top MC to that sample. This is done by normalizing the total $\mathrm{t\bar{t}}$ MC to the M_T peak region, $50 < M_T < 80$ GeV in this sample.

Next we define a "post-veto" sample as the events that have an isolated track (note that we use the term "post-veto" to refer to the application of the isolated track cut of the sample, which in this case is an isolated track requirement). The $t\bar{t} \to \ell+$ jets component is normalized in this sample, again by normalizing to the M_T peak region. These normalization factors are summarized in Table 18.

The post-veto $\mathrm{t\bar{t}} \to \ell\ell$ is taken from MC, but with scale factor obtained by the normalization of the "pre-veto" sample.

The underlying $E_{\mathrm{T}}^{\mathrm{miss}}$ and M_T distributions are shown in Figures 44 and 13. The data-MC agreement is quite good. Quantitatively, this is also shown in Table 19. This is the second key test of the $\mathrm{t\bar{t}} \to \ell\ell$ modeling

Sample	CR5PRESEL	CR5A	CR5B	CR5C	CR5D	CR5E	CR5F	CR5G
μ pre-veto M_{T}-SF	1.05 ± 0.01	1.02 ± 0.02	0.95 ± 0.03	0.90 ± 0.05	0.98 ± 0.08	0.97 ± 0.13	0.85 ± 0.18	0.92 ± 0.31
μ post-veto M_{T}-SF	1.25 ± 0.04	1.17 ± 0.07	1.05 ± 0.12	0.85 ± 0.19	0.84 ± 0.30	1.07 ± 0.54	1.38 ± 1.14	0.68 ± 2.05
e pre-veto M_{T}-SF	1.01 ± 0.01	0.95 ± 0.02	0.95 ± 0.03	0.94 ± 0.06	0.85 ± 0.09	0.84 ± 0.13	1.05 ± 0.23	1.04 ± 0.33
e post-veto M_{T}-SF	1.21 ± 0.04	1.12 ± 0.07	1.25 ± 0.14	1.17 ± 0.27	2.01 ± 0.64	1.71 ± 0.99	2.79 ± 2.04	0.81 ± 1.58

Table 18: M_{T} peak Data/MC scale factors. The pre-veto SFs are applied to the $\mathrm{t\bar{t}} \to \ell\ell$ sample, while the post-veto SFs are applied to the single lepton samples. The raw MC is used for backgrounds from rare processes. The uncertainties are statistical only.

Sample	CR5PRESEL	CR5A	CR5B	CR5C	CR5D	CR5E	CR5F	CR5G
μ MC	490 ± 9	299 ± 7	155 ± 6	49 ± 3	19 ± 2	7 ± 1	3 ± 1	2 ± 1
μ Data	514	311	167	57	12	4	2	1
μ Data/MC SF	1.05 ± 0.05	1.04 ± 0.06	1.08 ± 0.09	1.17 ± 0.17	0.64 ± 0.20	0.54 ± 0.29	0.66 ± 0.49	0.58 ± 0.62
e MC	405 ± 8	239 ± 7	130 ± 5	43 ± 3	16 ± 2	8 ± 1	6 ± 2	3 ± 1
e Data	427	248	120	38	14	4	3	2
e Data/MC SF	1.06 ± 0.06	1.04 ± 0.07	0.93 ± 0.09	0.89 ± 0.16	0.86 ± 0.25	0.52 ± 0.28	0.54 ± 0.35	0.76 ± 0.60
μ+e MC	894 ± 12	538 ± 10	284 ± 8	92 ± 4	35 ± 3	15 ± 2	9 ± 2	4 ± 1
μ+e Data	941	559	287	95	26	8	5	3
μ+e Data/MC SF	1.05 ± 0.04	1.04 ± 0.05	1.01 ± 0.07	1.04 ± 0.12	0.74 ± 0.16	0.53 ± 0.20	0.58 ± 0.29	0.69 ± 0.43

Table 19: Yields in M_{T} tail comparing the MC prediction (after applying SFs) to data. The uncertainties are statistical only.

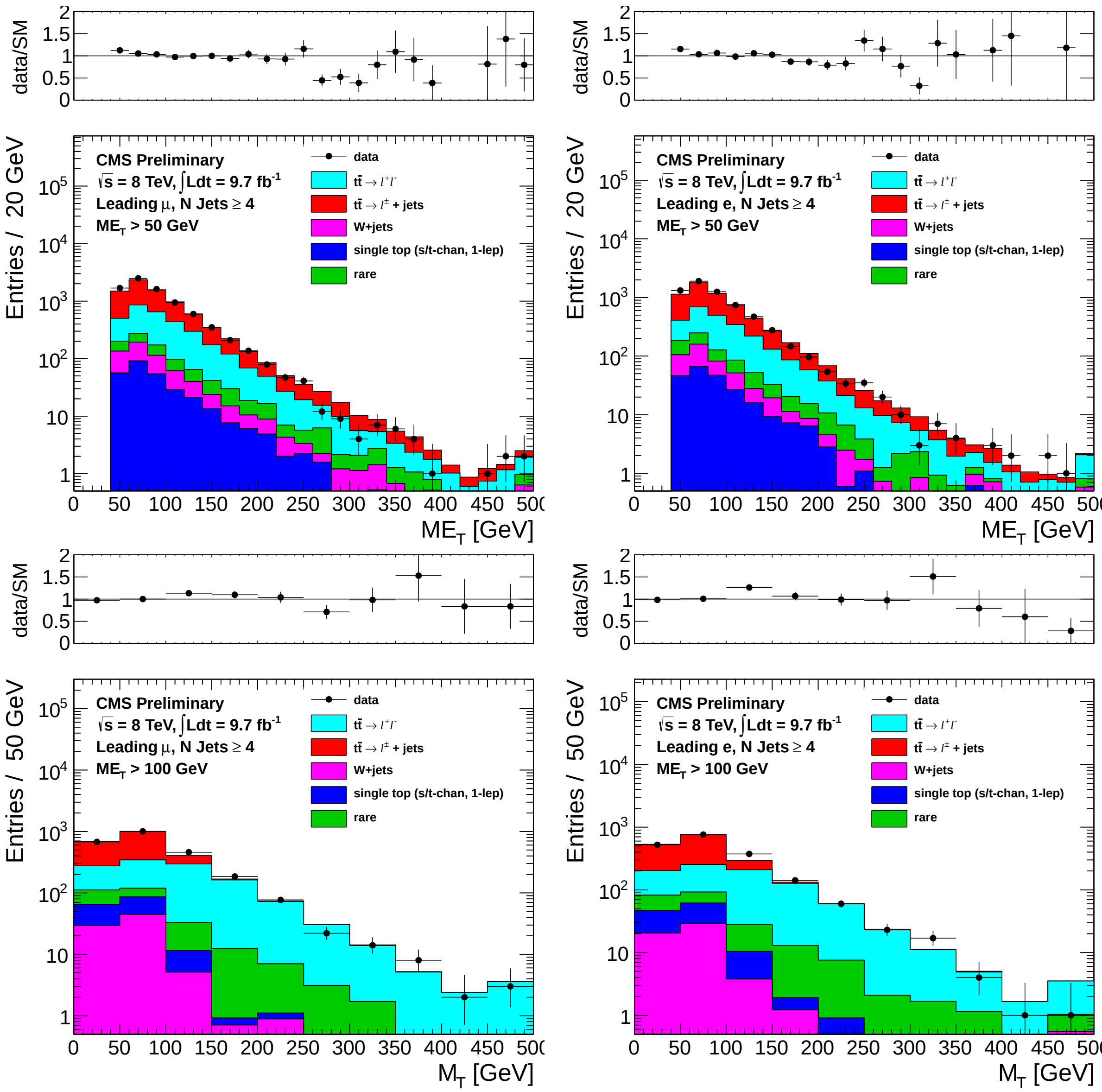

Figure 12: Comparison of the $E_{\mathrm{T}}^{\mathrm{miss}}$ (top) and M_{T} for $E_{\mathrm{T}}^{\mathrm{miss}} > 100$ (bottom) distributions in data vs. MC for events with a leading muon (left) and leading electron (right) satisfying the requirements of CR5.

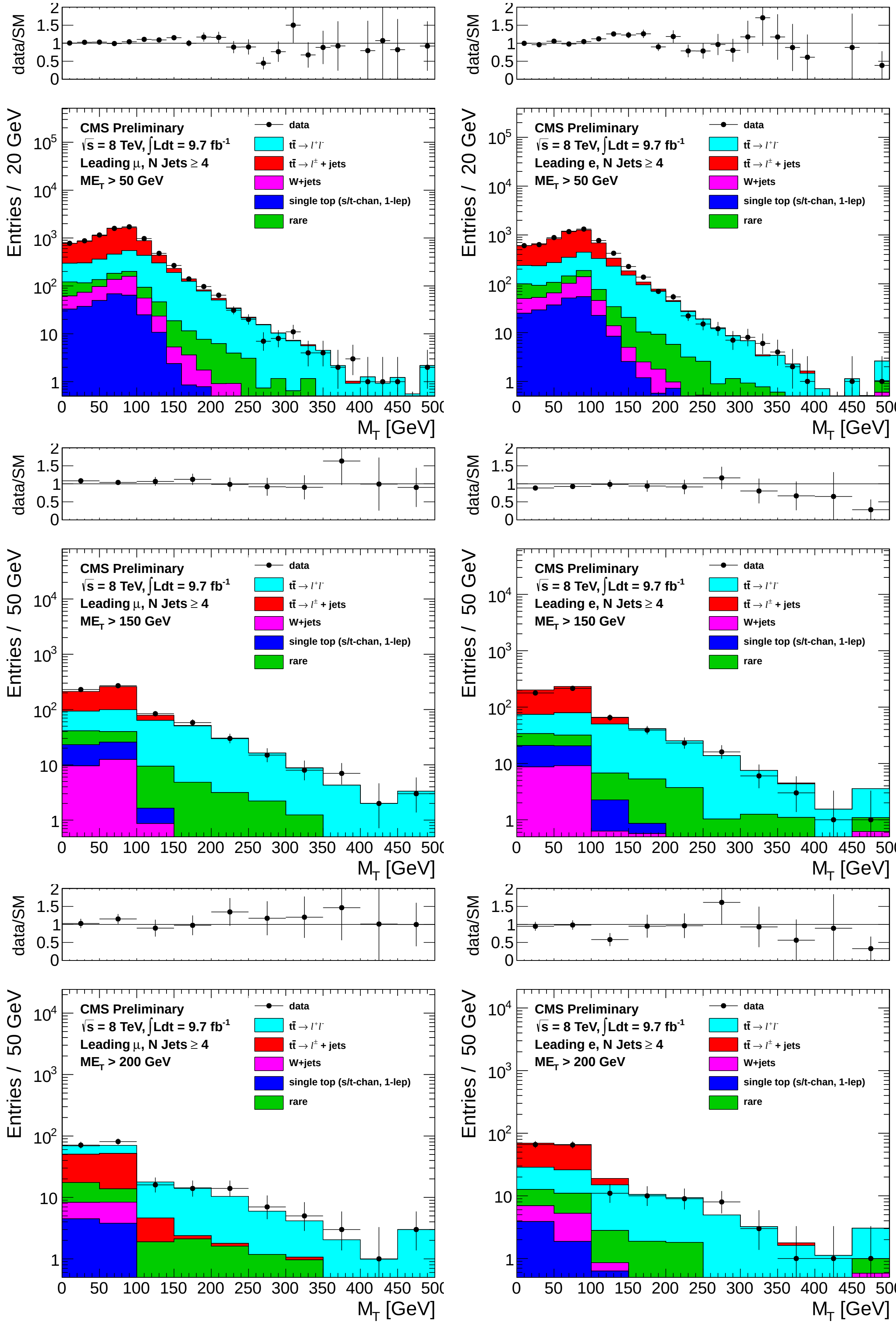

Figure 13: Comparison of the M_{T} distribution in data vs. MC for events with a leading muon (left) and leading electron (right) satisfying the requirements of CR5. The $E_{\mathrm{T}}^{\mathrm{miss}}$ requirements used are 50 GeV (top), 150 GeV (middle) and 200 GeV (bottom).

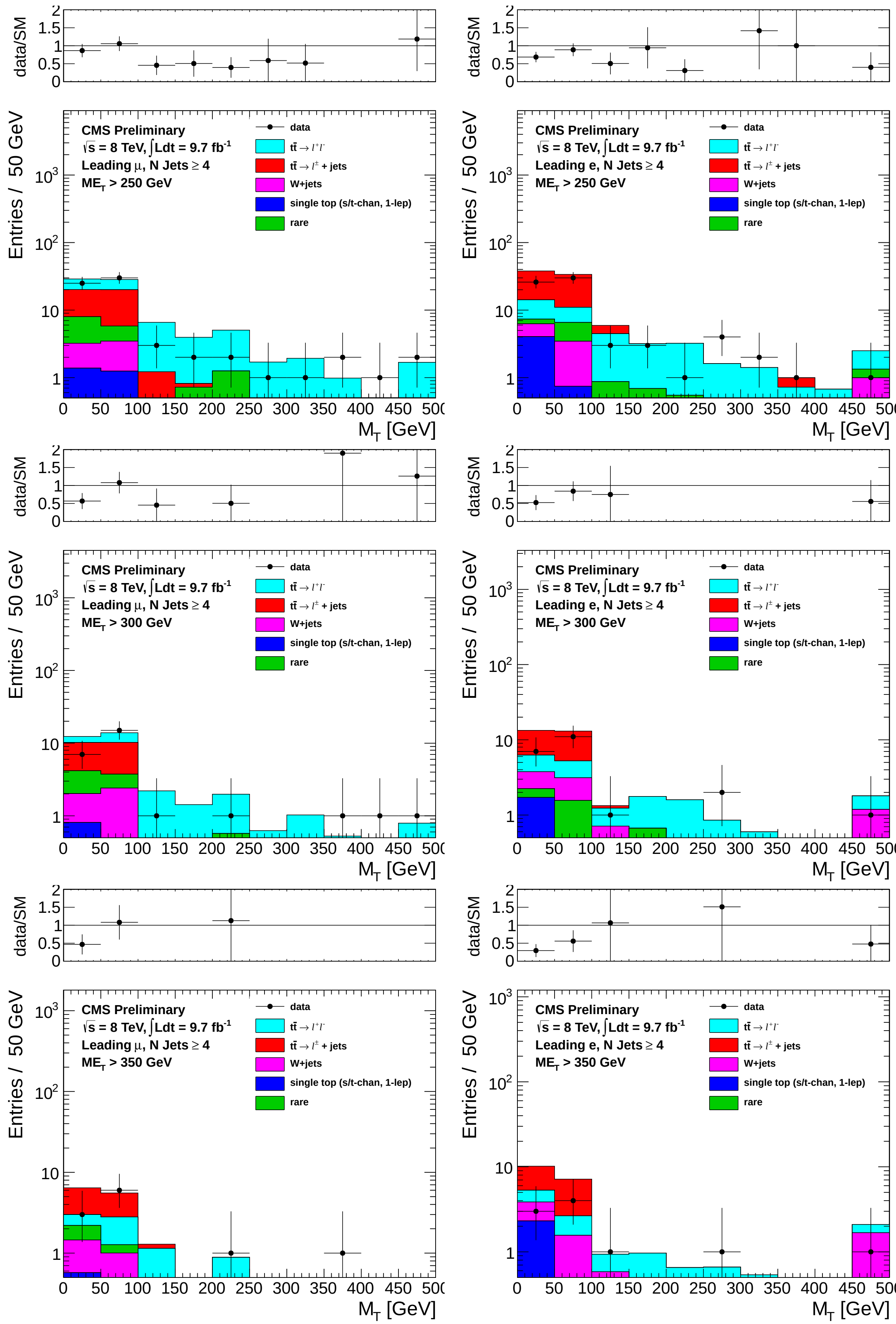

Figure 14: Comparison of the M_{T} distribution in data vs. MC for events with a leading muon (left) and leading electron (right) satisfying the requirements of CR5. The $E_{\mathrm{T}}^{\mathrm{miss}}$ requirements used are 250 GeV (top), 300 GeV (middle) and 350 GeV (bottom).

6 Other Backgrounds

Additional background contributions from rare processes include

- $t\bar{t}$ in association with a boson, $t\bar{t}$ + WZ/γ^*

- Z/γ^*+Jets

- diboson, WW/WZ/ZZ

- triboson, WWW/WWZ/WZZ/ZZZ

- dilepton single top, tW.

These backgrounds are small, contributing at the $\sim 5\%$ level and their predictions are taken from MC, normalized to the corresponding cross sections. A 50% systematic uncertainty is assigned for all these backgrounds. Note that these backgrounds are not double-counted because the contribution to the M_{T} peak region is subtracted off when deriving the M_{T} peak data/MC scale factors.

Backgrounds from QCD are expected to be small in the signal regions with large M_{T} and $E_{\mathrm{T}}^{\mathrm{miss}}$.

7 Tail-to-Peak ratio for lepton + jets top and W events

An important component of the background calculation is the ratio of the number of events with M_T in the signal region to the number of events with $50 < M_T < 80$ GeV. As discussed in Section 2.1, these ratios are different for W+jets and top events.

Sample	SRA	SRB	SRC	SRD	SRE	SRF	SRG
Muons							
R_{top}^{MC}	0.015 ± 0.001	0.035 ± 0.002	0.021 ± 0.002	0.021 ± 0.004	0.025 ± 0.007	0.015 ± 0.009	0.021 ± 0.015
R_{wjet}^{MC}	0.040 ± 0.001	0.071 ± 0.003	0.062 ± 0.004	0.064 ± 0.006	0.065 ± 0.009	0.067 ± 0.012	0.065 ± 0.016
Electrons							
R_{top}^{MC}	0.015 ± 0.001	0.031 ± 0.002	0.026 ± 0.003	0.025 ± 0.005	0.009 ± 0.005	0.021 ± 0.012	0.034 ± 0.024
R_{wjet}^{MC}	0.040 ± 0.002	0.075 ± 0.004	0.067 ± 0.005	0.063 ± 0.007	0.061 ± 0.010	0.067 ± 0.015	0.070 ± 0.021

Table 20: Ratio of MC events in the M_{T}-tail over events in the M_{T}-peak for $t\bar{t} \to \ell +$jets (also used for 1-lepton single top) and W+jets. These are derived before applying the b-tagging requirement.

The MC values of these ratios are shown in Table 20. The e and μ channel results are averaged before corrections are made.

The MC value of R_{wjet}^{MC} is corrected based on the studies of CR1 (Section D.3), which lead to the data/MC scale factor SFR_{wjet} (Table 13). The corrected R_{wjet} is thus given by $R_{wjet}^{MC} \times SFR_{wjet}$.

There is no similar scale factor to correct the MC value of R_{top}^{MC} due to the lack of events in CR2 (Section 5.2). We must therefore use a different procedure to derive a corrected value of R_{top}.

We start by defining optimistic (too small) and pessimistic (too large) predictions for R_{top}.

For the pessimistic prediction, we use the W+jets MC tail-to-peak ratio and data/MC scale factor, R_{wjet}^{MC} and SFR_{wjet} (i.e. the pessimistic prediction is the same as R_{wjet}). This prediction is too large because in W+jets events the M_T tail comes from off-shell Ws and resolution effects, while in top events to first order only resolution effects matter.

For the optimistic prediction, we use the $t\bar{t} \to \ell +$jets MC tail-to-peak ratio R_{top}^{MC}, but take the W+jets data/MC scale factor SFR_{wjet}. This prediction is too small because the true top scale factor is to first order the same as for on-shell Ws, while SFR_{wjet} is a weighted average of the scale factor for on-shell Ws (which is > 1) and the scale factor for off-shell Ws (which is close to 1 as it is well modeled by MC).

The final prediction for R_{top} is given by the average of the optimistic and pessimistic predictions, and the systematic uncertainty is given by half the difference between the two.

The corrected values of R_{wjet} and R_{top} and their uncertainties are given in Table 21.

Sample	SRA	SRB	SRC	SRD	SRE	SRF	SRG
R_{top}	0.045 ± 0.023	0.074 ± 0.031	0.055 ± 0.031	0.042 ± 0.028	0.041 ± 0.036	0.052 ± 0.049	0.053 ± 0.066
R_{wjet}	0.066 ± 0.015	0.101 ± 0.022	0.081 ± 0.025	0.061 ± 0.029	0.064 ± 0.042	0.082 ± 0.062	0.075 ± 0.088

Table 21: Corrected values of R_{wjet} and R_{top}. Both statistical and systematic uncertainties are included.

8 Background Prediction

Here we give the details of how we arrive at the background prediction in a given signal region. We concentrate on the method used to arrive at the central value of the background prediction. The systematic uncertainties will be discussed in Section 9. The actual results for the BG prediction will be given in Section 10.

As mentioned in Section 2, we normalize the main $t\bar{t}$ background to the M_T peak. This is actually a bit tricky because we want to minimize the effect of the isolated track veto on lepton + jets events, which may not be terribly well reproduced. Thus, we define two normaliztion region in the M_T peak ($50 < M_T < 80$ GeV), one before and one after the application of the isolated track veto.

The event counts in pre-veto and post-veto normalization regions are given in Tables 22 and 23. The data-MC agreement in these two tables is quite good, and this is certainly a good thing.

Sample	SRA	SRB	SRC	SRD	SRE	SRF	SRG
			Muon				
$\mathrm{t\bar{t}} \to \ell\ell$	371 ± 6	120 ± 4	43 ± 2	17 ± 1	8 ± 1	4 ± 1	1 ± 0
$\mathrm{t\bar{t}} \to \ell +$jets & single top ($1\ell$)	3666 ± 21	1088 ± 12	355 ± 7	127 ± 4	50 ± 3	22 ± 2	8 ± 1
W+jets	316 ± 8	113 ± 5	46 ± 3	21 ± 2	11 ± 1	5 ± 1	2 ± 1
Rare	117 ± 5	48 ± 3	16 ± 2	6 ± 1	2 ± 1	1 ± 0	1 ± 0
Total	4470 ± 24	1369 ± 13	461 ± 8	171 ± 5	71 ± 3	33 ± 2	13 ± 1
Data	4538	1304	418	168	69	28	12
			Electron				
$\mathrm{t\bar{t}} \to \ell\ell$	290 ± 6	98 ± 3	35 ± 2	13 ± 1	6 ± 1	3 ± 1	1 ± 0
$\mathrm{t\bar{t}} \to \ell +$jets & single top ($1\ell$)	2899 ± 19	861 ± 10	282 ± 6	104 ± 4	42 ± 2	16 ± 2	8 ± 1
W+jets	252 ± 28	87 ± 4	35 ± 3	18 ± 2	8 ± 1	4 ± 1	2 ± 1
Rare	89 ± 5	34 ± 3	15 ± 2	7 ± 1	3 ± 1	0 ± 0	0 ± 0
Total	3530 ± 35	1079 ± 12	367 ± 7	142 ± 5	60 ± 3	24 ± 2	11 ± 1
Data	3358	1022	346	122	51	25	12
			Muon+Electron Combined				
$\mathrm{t\bar{t}} \to \ell\ell$	661 ± 9	218 ± 5	78 ± 3	30 ± 2	14 ± 1	7 ± 1	3 ± 1
$\mathrm{t\bar{t}} \to \ell +$jets & single top ($1\ell$)	6565 ± 28	1949 ± 16	637 ± 9	231 ± 5	92 ± 4	39 ± 2	16 ± 2
W+jets	568 ± 29	199 ± 6	81 ± 4	38 ± 3	19 ± 2	9 ± 1	4 ± 1
Rare	206 ± 7	82 ± 4	31 ± 3	14 ± 2	5 ± 1	2 ± 0	1 ± 0
Total	8000 ± 42	2448 ± 18	828 ± 11	314 ± 7	131 ± 4	56 ± 3	24 ± 2
Data	7896	2326	764	290	120	53	24

Table 22: Preveto MC and data yields in M_{T} peak region. The n-jets k-factors have been applied to the $\mathrm{t\bar{t}} \to \ell\ell$. The uncertainties are statistical only. These MC and data yields are used to derive data/MC SFs, the pre-veto M_{T}-SFs, shown in Table 24.

Sample	SRA	SRB	SRC	SRD	SRE	SRF	SRG
Muon							
$t\bar{t} \to \ell\ell$	139 ± 4	46 ± 2	16 ± 1	7 ± 1	3 ± 1	1 ± 0	1 ± 0
$t\bar{t} \to \ell +$ jets & single top (1ℓ)	3273 ± 20	974 ± 11	321 ± 6	113 ± 4	45 ± 2	21 ± 2	8 ± 1
W+jets	294 ± 8	105 ± 5	42 ± 3	19 ± 2	10 ± 1	5 ± 1	2 ± 1
Rare	83 ± 4	34 ± 3	11 ± 1	4 ± 1	2 ± 1	1 ± 0	1 ± 0
Total	3789 ± 22	1160 ± 12	391 ± 7	143 ± 4	60 ± 3	28 ± 2	11 ± 1
Data	3790	1098	358	143	59	24	11
Electron							
$t\bar{t} \to \ell\ell$	116 ± 4	40 ± 2	14 ± 1	5 ± 1	2 ± 0	1 ± 0	1 ± 0
$t\bar{t} \to \ell +$ jets & single top (1ℓ)	2595 ± 18	774 ± 10	258 ± 6	97 ± 4	40 ± 2	15 ± 1	7 ± 1
W+jets	236 ± 28	82 ± 4	33 ± 3	17 ± 2	8 ± 1	4 ± 1	2 ± 1
Rare	62 ± 4	23 ± 2	9 ± 1	4 ± 1	2 ± 1	0 ± 0	0 ± 0
Total	3009 ± 34	919 ± 11	315 ± 7	123 ± 4	51 ± 3	21 ± 2	10 ± 1
Data	2788	837	288	92	39	19	10
Muon+Electron Combined							
$t\bar{t} \to \ell\ell$	255 ± 5	86 ± 3	30 ± 2	12 ± 1	5 ± 1	2 ± 1	1 ± 0
$t\bar{t} \to \ell +$ jets & single top (1ℓ)	5869 ± 27	1747 ± 15	579 ± 9	209 ± 5	85 ± 3	36 ± 2	15 ± 2
W+jets	529 ± 29	188 ± 6	75 ± 4	36 ± 3	18 ± 2	9 ± 1	4 ± 1
Rare	145 ± 6	58 ± 4	21 ± 2	8 ± 1	3 ± 1	1 ± 0	1 ± 0
Total	6797 ± 40	2079 ± 17	705 ± 10	265 ± 6	111 ± 4	49 ± 3	21 ± 2
Data	6578	1935	646	235	98	43	21

Table 23: MC and data yields in M_T peak region after full selection. The n-jets k-factors have been applied to the $t\bar{t} \to \ell\ell$. The uncertainties are statistical only. These MC and data yields are used to derive data/MC SFs, the post-veto M_T-SFs, shown in Table 24.

The dominant dilepton background is normalized to the pre-veto normalization region. A pre-veto scale factor (SF_{pre}) is defined as a common scale factors that needs to be applied to the $t\bar{t}$, single-top, and $W+$ jets MC to make the data yield in the pre-veto normalization agree with the MC prediction (the small rare MC component is held fixed). Then, the dilepton background prediction is obtained by multiplying the dilepton BG Monte Carlo by SF_{pre}.

The $t\bar{t}$ lepton + jet BG is normalized to post-veto normalization region. A post-veto scale factor (SF_{post}) is defined in (almost) the same way as the pre-veto scale factor. The difference here is that this scale factor applies only to the lepton + jets components and not the dilepton component, since that component is already rescaled by SF_{pre}. This procedure minimizes the reliance on the understanding of the isolated track veto.

The pre-veto and post-veto SF are shown in Table 24.

Sample	SRA	SRB	SRC	SRD	SRE	SRF	SRG
μ pre-veto M_{T}-SF	1.02 ± 0.02	0.95 ± 0.03	0.90 ± 0.05	0.98 ± 0.08	0.97 ± 0.13	0.85 ± 0.18	0.92 ± 0.31
μ post-veto M_{T}-SF	1.00 ± 0.02	0.95 ± 0.03	0.91 ± 0.05	1.00 ± 0.09	0.99 ± 0.13	0.85 ± 0.18	0.96 ± 0.31
μ veto M_{T}-SF	0.98 ± 0.01	0.99 ± 0.01	1.01 ± 0.02	1.02 ± 0.04	1.02 ± 0.06	1.00 ± 0.09	1.04 ± 0.11
e pre-veto M_{T}-SF	0.95 ± 0.02	0.95 ± 0.03	0.94 ± 0.06	0.85 ± 0.09	0.84 ± 0.13	1.05 ± 0.23	1.04 ± 0.33
e post-veto M_{T}-SF	0.92 ± 0.02	0.91 ± 0.03	0.91 ± 0.06	0.74 ± 0.08	0.75 ± 0.13	0.91 ± 0.22	1.01 ± 0.33
e veto M_{T}-SF	0.97 ± 0.01	0.96 ± 0.02	0.97 ± 0.03	0.87 ± 0.05	0.89 ± 0.08	0.86 ± 0.11	0.97 ± 0.14

Table 24: M_{T} peak Data/MC scale factors. The pre-veto SFs are applied to the $\mathrm{t\bar{t}} \to \ell\ell$ sample, while the post-veto SFs are applied to the single lepton samples. The veto SF is shown for comparison across channels. The raw MC is used for backgrounds from rare processes. The uncertainties are statistical only.

Then the $t\bar{t}$ lepton + jet BG is obtained by taking the number of MC-predicted $t\bar{t}$ lepton + jets in the post-veto normalization region, scaling it by SF_{post}, and multiplying it by the corrected tail-to-peak ratio R_{top} of Table 21.

The single top background is obtained in exactly the same way as the $t\bar{t}$ lepton + jet BG, using the same tail-to-peak ratio. The $W+$jets background is done in a similar way, but using a different tail-to-peak ratio (R_{wjets} of Table 21).

Other (small) backgrounds are taken straight from Monte Carlo, as described in Section 6.

Sample	SRA	SRB	SRC	SRD	SRE	SRF	SRG
			Muon				
$t\bar{t} \to \ell\ell$	326 ± 6	193 ± 5	66 ± 3	23 ± 2	9 ± 1	4 ± 1	2 ± 1
$t\bar{t} \to \ell +$ jets & single top (1ℓ)	54 ± 3	38 ± 2	8 ± 1	3 ± 1	1 ± 1	1 ± 0	0 ± 0
W+jets	17 ± 2	8 ± 1	3 ± 1	2 ± 1	0 ± 0	0 ± 0	0 ± 0
Rare	33 ± 2	23 ± 2	9 ± 1	5 ± 1	3 ± 1	1 ± 0	1 ± 0
Total	430 ± 7	262 ± 6	86 ± 3	33 ± 2	14 ± 1	6 ± 1	4 ± 1
			Electron				
$t\bar{t} \to \ell\ell$	261 ± 5	153 ± 4	54 ± 2	19 ± 1	7 ± 1	2 ± 1	1 ± 0
$t\bar{t} \to \ell +$ jets & single top (1ℓ)	41 ± 2	28 ± 2	7 ± 1	3 ± 1	1 ± 0	1 ± 0	1 ± 0
W+jets	11 ± 2	7 ± 1	3 ± 1	2 ± 1	0 ± 0	0 ± 0	0 ± 0
Rare	26 ± 2	16 ± 2	7 ± 1	3 ± 1	1 ± 0	0 ± 0	0 ± 0
Total	340 ± 6	204 ± 5	71 ± 3	26 ± 2	8 ± 1	4 ± 1	2 ± 1
			Muon+Electron Combined				
$t\bar{t} \to \ell\ell$	587 ± 8	346 ± 6	120 ± 4	42 ± 2	16 ± 1	7 ± 1	4 ± 1
$t\bar{t} \to \ell +$ jets & single top (1ℓ)	95 ± 3	67 ± 3	15 ± 1	6 ± 1	2 ± 1	1 ± 1	1 ± 0
W+jets	29 ± 2	15 ± 2	6 ± 1	3 ± 1	1 ± 0	0 ± 0	0 ± 0
Rare	59 ± 3	38 ± 3	16 ± 2	8 ± 1	4 ± 1	2 ± 0	1 ± 0
Total	770 ± 10	466 ± 7	157 ± 4	59 ± 3	22 ± 2	10 ± 1	6 ± 1

Table 25: MC yields in M_{T} tail region after full selection. The n-jets k-factors have been applied to the $t\bar{t} \to \ell\ell$. The uncertainties are statistical only. Note these values are only used for the rare backgrounds prediction.

9 Systematic Uncertainties on the Background

In this Section we discuss the systematic uncertainty on the BG prediction. This prediction is assembled from the event counts in the peak region of the transverse mass distribution as well as Monte Carlo with a number of correction factors, as described previously. The final uncertainty on the prediction is built up from the uncertainties in these individual components. The calculation is done for each signal region, for electrons and muons separately.

The choice to normalize to the peak region of M_T has the advantage that some uncertainties, e.g., luminosity, cancel. It does however introduce complications because it couples some of the uncertainties in non-trivial ways. For example, the primary effect of an uncertainty on the rare MC cross-section is to introduce an uncertainty in the rare MC background estimate which comes entirely from MC. But this uncertainty also affects, for example, the $t\bar{t} \to$ dilepton BG estimate because it changes the $t\bar{t}$ normalization to the peak region (because some of the events in the peak region are from rare processes). These effects are carefully accounted for. The contribution to the overall uncertainty from each background source is tabulated in Section 9.9. Here we discuss the uncertainties one-by-one and comment on their impact on the overall result, at least to first order. Second order effects, such as the one described, are also included.

9.1 Statistical uncertainties on the event counts in the M_T peak regions

These vary between 2% and 20%, depending on the signal region (different signal regions have different $E_{\mathrm{T}}^{\mathrm{miss}}$ requirements, thus they also have different M_T regions used as control). Since the major backgrounds, eg, $t\bar{t}$ are normalized to the peak regions, this fractional uncertainty is pretty much carried through all the way to the end. There is also an uncertainty from the finite MC event counts in the M_T peak regions. This is also included, but it is smaller.

Normalizing to the M_T peak has the distinct advantages that uncertainties on luminosity, cross-sections, trigger efficiency, lepton ID, cancel out. For the low statistics regions with high $E_{\mathrm{T}}^{\mathrm{miss}}$ requirements, the price to pay in terms of event count is that statistical uncertainties start to become significant. In the future we may consider a different normalization startegy in the low statistics regions.

9.2 Uncertainty from the choice of M_T peak region

This choice affects the scale factors of Table 24. If the M_T peak region is not well modelled, this would introduce an uncertainty.

We have tested this possibility by recalculating the post-veto scale factors for a different choice of M_T peak region ($40 < M_T < 100$ GeV instead of the default $50 < M_T < 80$ GeV). This is shown in Table 26. The two results for the scale factors are very compatible. We do not take any systematic uncertainty for this possible effect.

9.3 Uncertainty on the W+jets cross-section and the rare MC cross-sections

These are taken as 50%, uncorrelated. The primary effect is to introduce a 50% uncertainty on the W+ jets and rare BG background predictions, respectively. However they also have an effect on the other BGs via the M_T peak normalization in a way that tends to reduce the uncertainty. This is easy to understand: if the W cross-section is increased by 50%, then the W background goes up. But the number of M_T peak events attributed to $t\bar{t}$ goes down, and since the $t\bar{t}$ BG is scaled to the number of $t\bar{t}$ events in the peak, the $t\bar{t}$ BG goes down.

9.4 Tail-to-peak ratios for lepton + jets top and W events

The tail-to-peak ratios R_{top} and R_{wjet} are described in Section 7. The data/MC scale factors are studied in CR1 and CR2 (Sections D.3 and 5.2). Only the scale factor for W+jets, SFR_{wjet}, is used, and its uncertainty is given in Table 13. This uncertainty affects both R_{wjet} and R_{top}. The additional systematic uncertainty on R_{top} from the variation between optimistic and pessimistic scenarios is given in Section 7.

Sample	SRA	SRB	SRC	SRD	SRE	SRF	SRG
$50 \leq M_T \leq 80$							
μ pre-veto M_T-SF	1.02 ± 0.02	0.95 ± 0.03	0.90 ± 0.05	0.98 ± 0.08	0.97 ± 0.13	0.85 ± 0.18	0.92 ± 0.31
μ post-veto M_T-SF	1.00 ± 0.02	0.95 ± 0.03	0.91 ± 0.05	1.00 ± 0.09	0.99 ± 0.13	0.85 ± 0.18	0.96 ± 0.31
μ veto M_T-SF	0.98 ± 0.01	0.99 ± 0.01	1.01 ± 0.02	1.02 ± 0.04	1.02 ± 0.06	1.00 ± 0.09	1.04 ± 0.11
e pre-veto M_T-SF	0.95 ± 0.02	0.95 ± 0.03	0.94 ± 0.06	0.85 ± 0.09	0.84 ± 0.13	1.05 ± 0.23	1.04 ± 0.33
e post-veto M_T-SF	0.92 ± 0.02	0.91 ± 0.03	0.91 ± 0.06	0.74 ± 0.08	0.75 ± 0.13	0.91 ± 0.22	1.01 ± 0.33
e veto M_T-SF	0.97 ± 0.01	0.96 ± 0.02	0.97 ± 0.03	0.87 ± 0.05	0.89 ± 0.08	0.86 ± 0.11	0.97 ± 0.14
$40 \leq M_T \leq 100$							
μ pre-veto M_T-SF	1.02 ± 0.01	0.97 ± 0.02	0.91 ± 0.05	0.95 ± 0.06	0.97 ± 0.10	0.80 ± 0.14	0.74 ± 0.22
μ post-veto M_T-SF	1.00 ± 0.01	0.96 ± 0.02	0.90 ± 0.04	0.98 ± 0.07	1.00 ± 0.11	0.80 ± 0.15	0.81 ± 0.24
μ veto M_T-SF	0.98 ± 0.01	0.99 ± 0.01	0.99 ± 0.02	1.03 ± 0.03	1.03 ± 0.05	1.01 ± 0.08	1.09 ± 0.09
e pre-veto M_T-SF	0.97 ± 0.01	0.93 ± 0.02	0.94 ± 0.04	0.81 ± 0.06	0.86 ± 0.10	0.95 ± 0.17	1.06 ± 0.26
e post-veto M_T-SF	0.94 ± 0.01	0.91 ± 0.02	0.91 ± 0.04	0.71 ± 0.06	0.82 ± 0.10	0.93 ± 0.17	1.09 ± 0.27
e veto M_T-SF	0.97 ± 0.01	0.98 ± 0.01	0.97 ± 0.02	0.88 ± 0.04	0.95 ± 0.06	0.98 ± 0.08	1.03 ± 0.09

Table 26: M_T peak Data/MC scale factors. The pre-veto SFs are applied to the $t\bar{t} \to \ell\ell$ sample, while the post-veto SFs are applied to the single lepton samples. The veto SF is shown for comparison across channels. The raw MC is used for backgrounds from rare processes. The uncertainties are statistical only.

9.5 Uncertainty on extra jet radiation for dilepton background

As discussed in Section 5.3.1, the jet distribution in $t\bar{t} \to$ dilepton MC is rescaled by the factors K_3 and K_4 to make it agree with the data. The 3% uncertainties on K_3 and K_4 comes from data/MC statistics. This results directly in a 3% uncertainty on the dilepton background, which is by far the most important one.

9.6 Uncertainty from MC statistics

This affects mostly the $t\bar{t} \to \ell\ell$ background estimate, which is taken from Monte Carlo with appropriate correction factors. This uncertainty is negligible in the low E_T^{miss} signal regions, and grows to about 15% in SRG.

9.7 Uncertainty on the $t\bar{t} \to \ell\ell$ Background

The $t\bar{t}$ background prediction is obtained from MC, with corrections derived from control samples in data. The uncertainty associated with the $t\bar{t}$ background is derived from the level of closure of the background prediction in CR4 (Table 17) and CR5 (Table 19). The results from these control region checks are shown in Figure 15. The uncertainties assigned to the $t\bar{t} \to \ell\ell$ background prediction based on these tests are 5% (SRA), 10% (SRB), 15% (SRC), 25% (SRD), 40% (SRE-G).

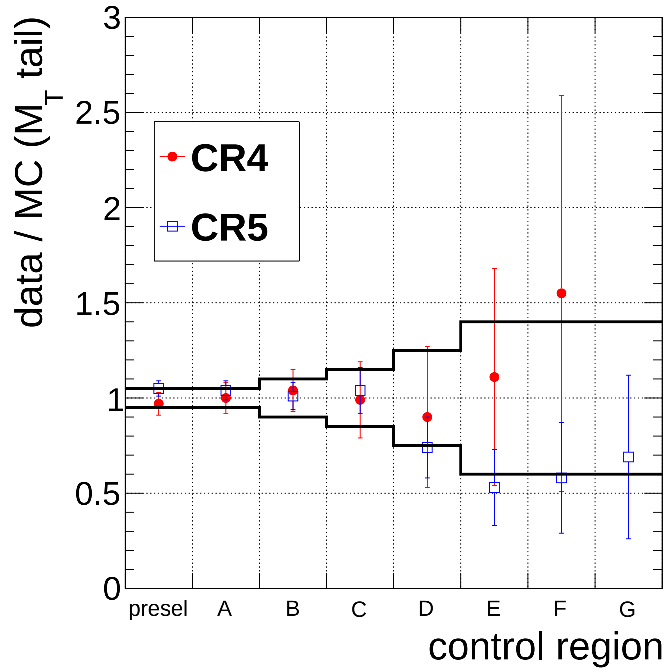

Figure 15: Results of the comparison of yields in the M_{T} tail comparing the MC prediction (after applying SFs) to data for CR4 and CR5 for all the signal region requirements considered (A-G). The bands indicate the systematic uncertainties assigned based on these tests, ranging from 5% for SRA to 40% for SRE-G.

9.7.1 Check of the impact of Signal Contamination

We examine the contribution of possible signal events in the $t\bar{t} \to \ell\ell$ control regions (CR4 and CR5). It should be emphasized that these regions are not used to apply data/MC SFs. They are used only to quantify the level of data/MC agreement and assign a corresponding uncertainty. As a result, if signal events were to populate these control regions this would not lead to an increase in the predicted background.

To illustrate how much signal is expected to populate these control regions, we examine signal points near the edge of the analysis sensitivity (m(stop) = 450 m(χ^0) = 0 for T2tt, m(stop) = 450 m(χ^0) = 0, x=0.75 for T2bw). Table 27 compares the expected signal yields and the raw total MC background prediction in the control regions with the $E_{\mathrm{T}}^{\mathrm{miss}}$ and M_{T} requirements corresponding to SRB, SRC and SRD (these are the signal regions that dominate the sensitivity). The signal contamination is smaller than the uncertainty on the dilepton background (10%, 15%, and 25% for SRB, SRC, SRD, respectively) and smaller than the signal/background in the signal regions. Based on the fact that the CR4 and CR5 are not used to extract data/MC scale factors and that we do not observe evidence for signal contamination in these control regions (CR5, the control region with larger statistical precision, actually shows a slight deficit of data w.r.t. MC), we do not assign a correction for signal contamination in these control regions.

Sample		CR B	CR C	CR D
CR4	Raw MC	168.2 ± 4.5	51.5 ± 2.5	19.6 ± 1.5
	T2tt m(stop) = 450 m(χ^0) = 0	2.6 ± 0.3 (2%)	2.0 ± 0.2 (4%)	1.4 ± 0.2 (7%)
	T2bw x=0.75 m(stop) = 450 m(χ^0) = 0	10.5 ± 0.4 (6%)	6.1 ± 0.3 (12%)	3.1 ± 0.2 (16%)
CR5	Raw MC	306.5 ± 6.2	101.8 ± 3.6	38.0 ± 2.2
	T2tt m(stop) = 450 m(χ^0) = 0	10.6 ± 0.6 (3%)	7.8 ± 0.5 (8%)	5.4 ± 0.4 (14%)
	T2bw x=0.75 m(stop) = 450 m(χ^0) = 0	17.3 ± 0.5 (6%)	11.3 ± 0.4 (11%)	6.2 ± 0.3 (16%)
SIGNAL	Raw MC	486.3 ± 7.8	164.3 ± 4.5	61.5 ± 2.8
	T2tt m(stop) = 450 m(χ^0) = 0	65.3 ± 1.4 (13%)	48.8 ± 1.2 (30%)	32.9 ± 1.0 (53%)
	T2bw x=0.75 m(stop) = 450 m(χ^0) = 0	69.3 ± 1.0 (14%)	47.3 ± 0.8 (29%)	27.3 ± 0.6 (44%)

Table 27: Yields in M_{T} tail comparing the raw SM MC prediction to the yields for a few signal points on the edge of our sensitivity in the $t\bar{t} \to \ell\ell$ control regions CR4, CR5 and in the corresponding signal region. The numbers in parenthesis are the expected signal yield divided by the total background. The uncertainties are statistical only.

9.7.2 Check of the uncertainty on the $t\bar{t} \to \ell\ell$ Background

We check that the systematic uncertainty assigned to the $t\bar{t} \to \ell\ell$ background prediction covers the uncertainty associated with the theoretical modeling of the $t\bar{t}$ production and decay by comparing the background predictions obtained using alternative MC samples. It should be noted that the full analysis is performed with the alternative samples under consideration, including the derivation of the various data-to-MC scale factors. The variations considered are

- Top mass: The alternative values for the top mass differ from the central value by 6 GeV: $m_{\mathrm{top}} =$ 178.5 GeV and $m_{\mathrm{top}} = 166.5$ GeV.
- Jet-parton matching scale: This corresponds to variations in the scale at which the Matrix Element partons from Madgraph are matched to Parton Shower partons from Pythia. The nominal value is $x_q > 20$ GeV. The alternative values used are $x_q > 10$ GeV and $x_q > 40$ GeV.
- Renormalization and factorization scale: The alternative samples correspond to variations in the scale $\times 2$ and $\times 0.5$. The nominal value for the scale used is $Q^2 = m_{\mathrm{top}}^2 + \sum_{\mathrm{jets}} p_{\mathrm{T}}^2$.
- Alternative generators: Samples produced with different generators, Powheg (our default) and Madgraph.
- Modeling of taus: The alternative sample does not include Tauola and is otherwise identical to the Powheg sample. This effect was studied earlier using 7 TeV samples and found to be negligible.

- The PDF uncertainty is estimated following the PDF4LHC recommendations. The events are reweighted using alternative PDF sets for CT10 and MSTW2008 and the uncertainties for each are derived using the alternative eigenvector variations and the “master equation”. The NNPDF2.1 set with 100 replicas is also used. The central value is determined from the mean and the uncertainty is derived from the 1σ range. The overall uncertainty is derived from the envelope of the alternative predictions and their uncertainties. This effect was studied earlier using 7 TeV samples and found to be negligible.

Δ/N [%]	Madgraph	Mass Up	Mass Down	Scale Up	Scale Down	Match Up	Match Down
SRA	2	2	5	12	7	0	2
SRB	6	0	6	5	12	5	6

Table 28: Relative difference in $t\bar{t} \to \ell\ell$ predictions for alternative MC samples in the higher statistics regions SRA and SRB. These differences are based on the central values of the predictions. For a fuller picture of the situation, including statistical uncertainites, see Fig. 16.

In Fig. 16 we compare the alternate MC $t\bar{t} \to \ell\ell$ background predictions for regions A through E. We can make the following observations based on this Figure.

- In the tighter signal regions we are running out of statistics.
- Within the limited statistics, there is no evidence that the situation changes as we go from signal region A to signal region E.
- In signal regions B and above, the uncertainties assigned in Section 9.7 fully cover the alternative MC variations.
- In order to fully (as opposed as 1σ) cover the alternative MC variations in region A we would have to take a systematic uncertainty of $\approx 10\%$ instead of 5%. This would be driven by the scale up/scale down variations, see Table 28.

Sample	K3	K4
Powheg	1.01 ± 0.03	0.93 ± 0.04
Madgraph	1.01 ± 0.04	0.92 ± 0.04
Mass Up	1.00 ± 0.04	0.92 ± 0.04
Mass Down	1.06 ± 0.04	0.99 ± 0.05
Scale Up	1.14 ± 0.04	1.23 ± 0.06
Scale Down	0.89 ± 0.03	0.74 ± 0.03
Match Up	1.02 ± 0.04	0.97 ± 0.04
Match Down	1.02 ± 0.04	0.91 ± 0.04

Table 29: $E_{\mathrm{T}}^{\mathrm{miss}} > 100$ GeV: Data/MC scale factors used to account for differences in the fraction of events with additional hard jets from radiation in $t\bar{t} \to \ell\ell$ events.

However, we have two pieces of information indicating that the scale up/scale down variations are inconsistent with the data. These are described below.

The first piece of information is that the jet multiplicity in the scale up/scale down sample is the most inconsistent with the data. This is shown in Table 29, where we tabulate the K_3 and K_4 factors of Section 5.3.1 for different $t\bar{t}$ MC samples. The data/MC disagreement in the N_{jets} distribution for the scale up/scale down samples is also shown in Fig. 17 and 18. This should be compared with the equivalent N_{jets} plots for the default Powheg MC, see Fig. 9, which agrees much better with data.

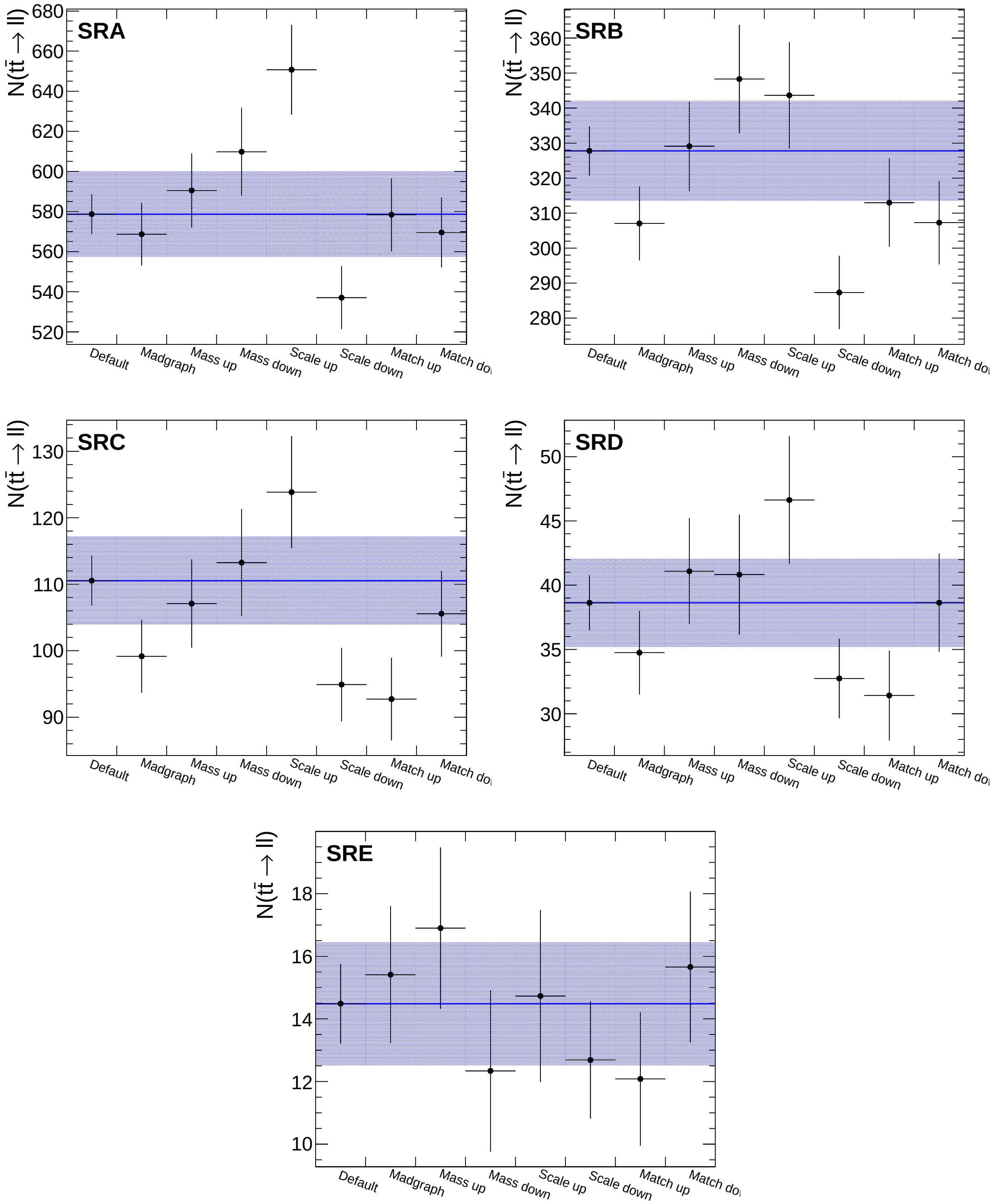

Figure 16: Comparison of the $t\bar{t} \to \ell\ell$ central prediction with those using alternative MC samples. The blue band corresponds to the total statistical error for all data and MC samples. The alternative sample predictions are indicated by the datapoints. The uncertainties on the alternative predictions correspond to the uncorrelated statistical uncertainty from the size of the alternative sample only. Note the suppressed vertical scales.

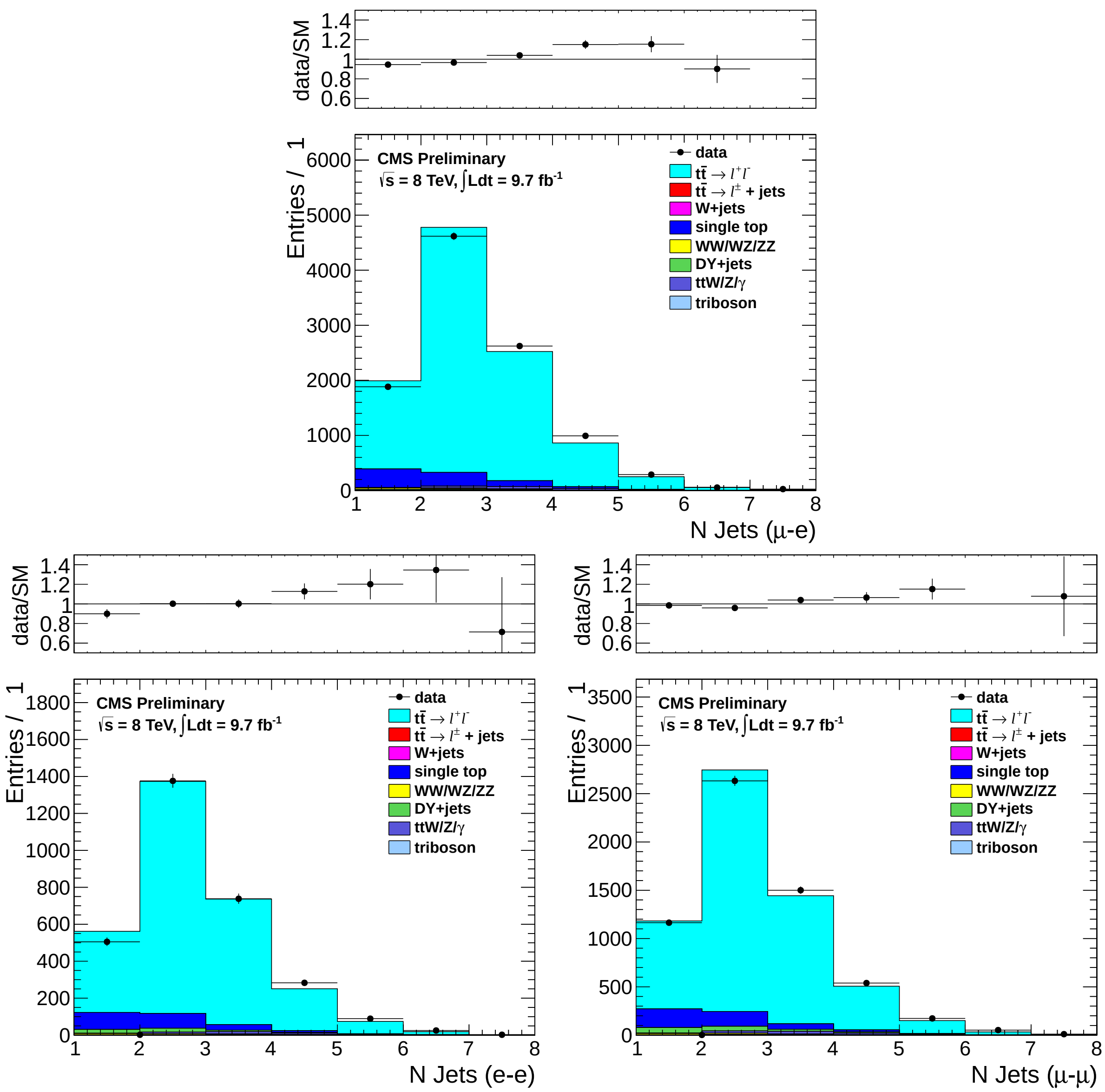

Figure 17: SCALE UP: Comparison of the jet multiplicity distribution in data and MC for dilepton events in the e-μ (top), e-e (bottom left) and μ-μ (bottom right) channels.

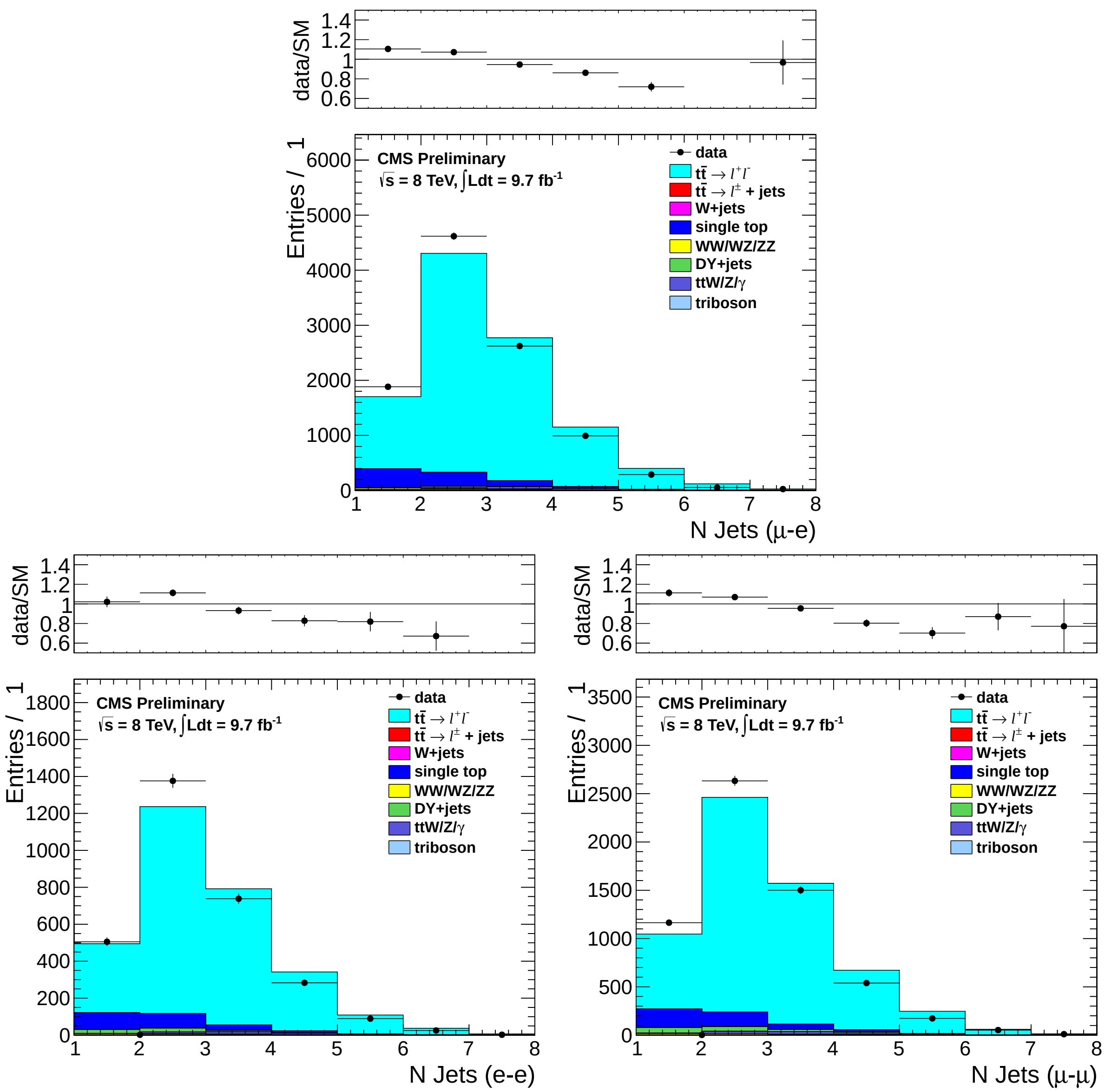

Figure 18: SCALE DOWN: Comparison of the jet multiplicity distribution in data and MC for dilepton events in the e-μ (top), e-e (bottom left) and μ-μ (bottom right) channels.

The second piece of information is that we have performed closure tests in CR5 using the alternative MC samples. These are exactly the same tests as the one performed in Section D.2 on the Powheg sample. As we argued previously, this is a very powerful test of the background calculation. The results of this test are summarized in Table 30. Concentrating on the relatively high statistics CR5A region, we see for all $t\bar{t}$ MC samples except scale up/scale down we obtain closure within 1σ. The scale up/scale down tests closes worse, only within 2σ. This again is evidence that the scale up/scale down variations are in disagreement with the data.

Sample	CR5PRESEL	CR5A	CR5B	CR5C	CR5D	CR5E
POWHEG						
μ Data/MC SF	1.05 ± 0.05	1.04 ± 0.06	1.08 ± 0.09	1.17 ± 0.17	0.64 ± 0.20	0.54 ± 0.29
e Data/MC SF	1.06 ± 0.06	1.04 ± 0.07	0.93 ± 0.09	0.89 ± 0.16	0.86 ± 0.25	0.52 ± 0.28
μ+e Data/MC SF	1.05 ± 0.04	1.04 ± 0.05	1.01 ± 0.07	1.04 ± 0.12	0.74 ± 0.16	0.53 ± 0.20
MADGRAPH						
μ Data/MC SF	1.05 ± 0.05	1.06 ± 0.07	1.08 ± 0.10	1.21 ± 0.19	0.64 ± 0.21	0.43 ± 0.24
e Data/MC SF	1.06 ± 0.06	1.04 ± 0.08	0.97 ± 0.10	0.97 ± 0.18	1.10 ± 0.34	0.68 ± 0.38
μ+e Data/MC SF	1.06 ± 0.04	1.05 ± 0.05	1.03 ± 0.07	1.10 ± 0.13	0.83 ± 0.18	0.53 ± 0.21
MASS UP						
μ Data/MC SF	1.04 ± 0.06	1.04 ± 0.07	1.07 ± 0.10	1.20 ± 0.19	0.57 ± 0.18	0.56 ± 0.31
e Data/MC SF	1.04 ± 0.06	1.05 ± 0.08	1.01 ± 0.11	1.12 ± 0.22	1.02 ± 0.33	0.61 ± 0.34
μ+e Data/MC SF	1.04 ± 0.04	1.04 ± 0.05	1.04 ± 0.07	1.17 ± 0.15	0.74 ± 0.17	0.58 ± 0.23
MASS DOWN						
μ Data/MC SF	1.02 ± 0.06	1.02 ± 0.07	1.04 ± 0.10	1.25 ± 0.21	0.82 ± 0.28	0.94 ± 0.56
e Data/MC SF	1.06 ± 0.06	1.02 ± 0.08	0.95 ± 0.11	0.91 ± 0.18	1.07 ± 0.35	0.59 ± 0.33
μ+e Data/MC SF	1.04 ± 0.04	1.02 ± 0.05	1.00 ± 0.07	1.09 ± 0.14	0.94 ± 0.22	0.72 ± 0.30
SCALE UP						
μ Data/MC SF	0.94 ± 0.05	0.94 ± 0.07	0.99 ± 0.10	1.24 ± 0.21	0.71 ± 0.24	0.69 ± 0.39
e Data/MC SF	0.94 ± 0.06	0.89 ± 0.07	0.81 ± 0.09	0.77 ± 0.15	0.84 ± 0.27	0.49 ± 0.28
μ+e Data/MC SF	0.94 ± 0.04	0.91 ± 0.05	0.91 ± 0.07	1.00 ± 0.13	0.77 ± 0.18	0.57 ± 0.23
SCALE DOWN						
μ Data/MC SF	1.11 ± 0.06	1.10 ± 0.07	1.24 ± 0.12	1.26 ± 0.20	0.64 ± 0.21	0.70 ± 0.39
e Data/MC SF	1.16 ± 0.07	1.20 ± 0.09	1.00 ± 0.11	1.02 ± 0.19	1.02 ± 0.32	0.53 ± 0.29
μ+e Data/MC SF	1.13 ± 0.04	1.14 ± 0.06	1.13 ± 0.08	1.15 ± 0.14	0.80 ± 0.18	0.60 ± 0.23
MATCH UP						
μ Data/MC SF	1.06 ± 0.06	1.06 ± 0.07	1.20 ± 0.11	1.42 ± 0.23	0.70 ± 0.23	0.63 ± 0.35
e Data/MC SF	1.06 ± 0.06	1.04 ± 0.08	0.97 ± 0.11	0.93 ± 0.18	1.25 ± 0.41	0.63 ± 0.36
μ+e Data/MC SF	1.06 ± 0.04	1.06 ± 0.05	1.09 ± 0.08	1.18 ± 0.15	0.92 ± 0.21	0.63 ± 0.25
MATCH DOWN						
μ Data/MC SF	1.08 ± 0.06	1.06 ± 0.07	1.14 ± 0.11	1.17 ± 0.19	0.59 ± 0.19	0.45 ± 0.25
e Data/MC SF	1.05 ± 0.06	0.99 ± 0.08	0.86 ± 0.09	0.78 ± 0.15	0.79 ± 0.25	0.50 ± 0.28
μ+e Data/MC SF	1.07 ± 0.04	1.03 ± 0.05	1.00 ± 0.07	0.98 ± 0.12	0.68 ± 0.15	0.48 ± 0.18

Table 30: Ratio of yields in M_{T} tail comparing the MC prediction (after applying SFs) to data. The uncertainties are statistical only.

Based on the two observations above, we argue that the MC scale up/scale down variations are too extreme. We feel that a reasonable choice would be to take one-half of the scale up/scale down variations in our MC. This factor of 1/2 would then bring the discrepancy in the closure test of Table 30 for the scale up/scale down variations from about 2σ to about 1σ.

Then, going back to Table 28, and reducing the scale up/scale down variations by a factor 2, we can see that a systematic uncertainty of 5% covers the range of reasonable variations from different MC models in SRA and SRB. Note that this 5% is also consistent with the level at which we are able to test the closure of the method with alternative samples in CR5 for the high statistics regions (Table 30). The range of reasonable variations obtained with the alternative samples are consistent with the uncertainties assigned for the $t\bar{t} \to \ell\ell$ background based on the closure of the background predictions and data in CR4 and CR5.

9.8 Uncertainty from the isolated track veto

This is the uncertainty associated with how well the isolated track veto performance is modeled by the Monte Carlo. This uncertainty only applies to the fraction of dilepton BG events that have a second e/μ or a one prong $\tau \rightarrow h$, with $P_T > 10$ GeV in $|\eta| < 2.4$. This fraction is about 1/3, see Table 31. The uncertainty for these events is 6% and is obtained from tag-and-probe studies, see Section 9.8.1.

Sample	SRA	SRB	SRC	SRD	SRE	SRF	SRG
μ Frac. $t\bar{t} \rightarrow \ell\ell$ with true iso. trk.	0.32 ± 0.03	0.30 ± 0.03	0.32 ± 0.06	0.34 ± 0.10	0.35 ± 0.16	0.40 ± 0.24	0.50 ± 0.32
e Frac. $t\bar{t} \rightarrow \ell\ell$ with true iso. trk.	0.32 ± 0.03	0.31 ± 0.04	0.33 ± 0.06	0.38 ± 0.11	0.38 ± 0.19	0.60 ± 0.31	0.61 ± 0.45

Table 31: Fraction of $t\bar{t} \rightarrow \ell\ell$ events with a true isolated track.

9.8.1 Isolated Track Veto: Tag and Probe Studies

In this section we compare the performance of the isolated track veto in data and MC using tag-and-probe studies with samples of Z$\rightarrow$ee and Z$\rightarrow$ $\mu\mu$. The purpose of these studies is to demonstrate that the efficiency to satisfy the isolated track veto requirements is well-reproduced in the MC, since if this were not the case we would need to apply a data-to-MC scale factor in order to correctly predict the $t\bar{t} \rightarrow \ell\ell$ background.

This study addresses possible data vs. MC discrepancies for the **efficiency** to identify (and reject) events with a second **genuine** lepton (e, μ, or τ $\rightarrow$1-prong). It does not address possible data vs. MC discrepancies in the fake rate for rejecting events without a second genuine lepton; this is handled separately in the top normalization procedure by scaling the $t\bar{t} \rightarrow \ell+$jets contribution to match the data in the $M_{\rm T}$ peak after applying the isolated track veto.

Furthermore, we test the data and MC isolated track veto efficiencies for electrons and muons since we are using a Z tag-and-probe technique, but we do not directly test the performance for hadronic tracks from τ decays. The performance for hadronic τ decay products may differ from that of electrons and muons for two reasons. First, the τ may decay to a hadronic track plus one or two π^0's, which may decay to $\gamma\gamma$ followed by a photon conversion. As shown in Figure 37, the isolation distribution for charged tracks from τ decays that are not produced in association with π^0s are consistent with that from es and μs. Since events from single prong τ decays produced in association with π^0s comprise a small fraction of the total sample, and since the kinematics of τ, π^0 and $\gamma \rightarrow e^+e^-$ decays are well-understood, we currently demonstrate that the isolation is well-reproduced for electrons and muons only. Second, hadronic tracks may undergo nuclear interactions and hence their tracks may not be reconstructed. As discussed above, independent studies show that the MC reproduces the hadronic tracking efficiency within 4%, leading to a total background uncertainty of less than 0.5% (after taking into account the fraction of the total background due to hadronic τ decays with $p_{\rm T} > 10$ GeV tracks), and we hence regard this effect as negligible.

The tag-and-probe studies are performed in the full data sample, and compared with the DYJets madgraph sample. All events must contain a tag-probe pair (details below) with opposite-sign and satisfying the Z mass requirement 76–106 GeV. We compare the distributions of absolute track isolation for probe electrons/muons in data vs. MC. The contributions to this isolation sum are from ambient energy in the event from underlying event, pile-up and jet activitiy, and hence do not depend on the $p_{\rm T}$ of the probe lepton. We therefore restrict the probe $p_{\rm T}$ to be > 30 GeV in order to suppress fake backgrounds with steeply-falling $p_{\rm T}$ spectra. To suppress non-Z backgrounds (in particular $t\bar{t}$) we require $E_{\rm T}^{\rm miss} < 30$ GeV and 0 b-tagged events. The specific criteria for tags and probes for electrons and muons are:

- Electrons
  - Tag criteria
    - Electron passes full analysis ID/iso selection
    - $p_{\rm T} > 30$ GeV, $|\eta| < 2.1$
    - Matched to the single electron trigger `HLT_Ele27_WP80_v*`
  - Probe criteria

        * Electron passes full analysis ID selection
        * $p_{\mathrm{T}} > 30$ GeV

- Muons
    - Tag criteria
        * Muon passes full analysis ID/iso selection
        * $p_{\mathrm{T}} > 30$ GeV, $|\eta| < 2.1$
        * Matched to 1 of the 2 single muon triggers
            · `HLT_IsoMu30_v*`
            · `HLT_IsoMu30_eta2p1_v*`
    - Probe criteria
        * Muon passes full analysis ID selection
        * $p_{\mathrm{T}} > 30$ GeV

The absolute track isolation distributions for passing probes are displayed in Fig. 19. In general we observe good agreement between data and MC. To be more quantitative, we compare the data vs. MC efficiencies to satisfy absolute track isolation requirements varying from > 1 GeV to > 5 GeV, as summarized in Table 32. In the ≥ 0 and ≥ 1 jet bins where the efficiencies can be tested with statistical precision, the data and MC efficiencies agree within 6%, and we apply this as a systematic uncertainty on the isolated track veto efficiency. For the higher jet multiplicity bins the statistical precision decreases, but we do not observe any evidence for a data vs. MC discrepancy in the isolated track veto efficiency.

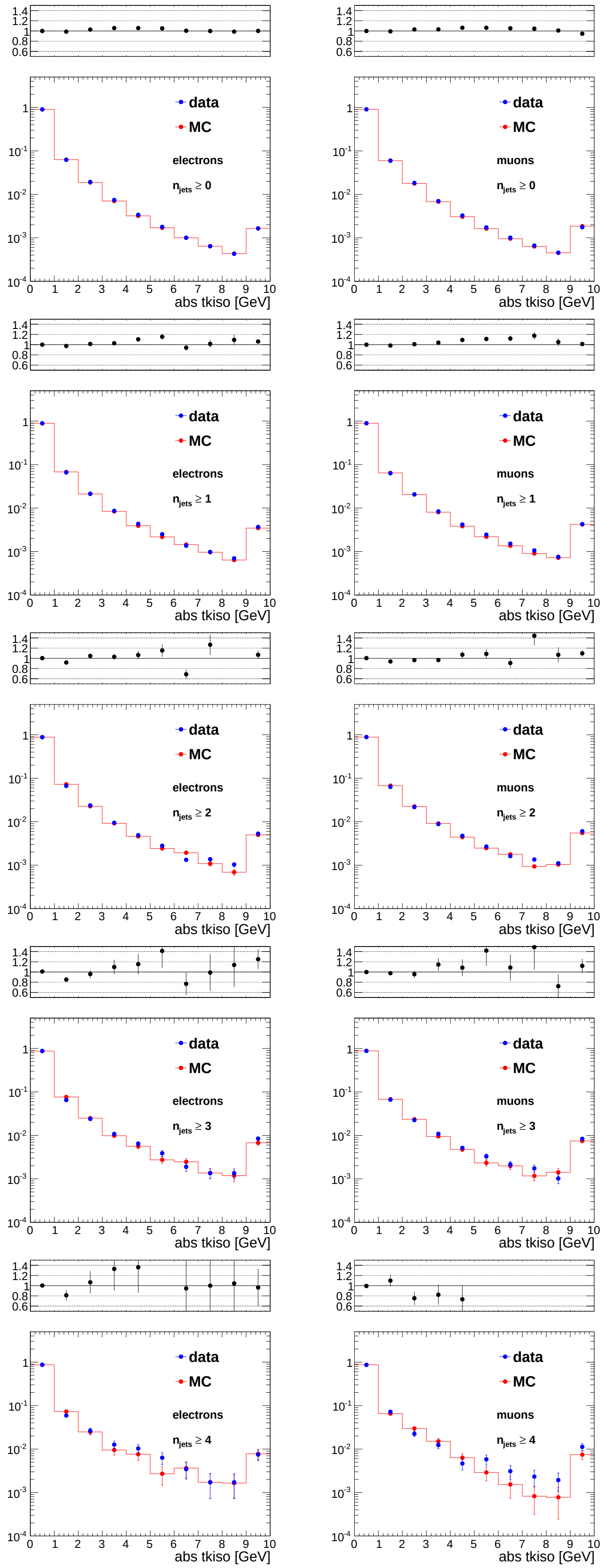

Figure 19: Comparison of the absolute track isolation in data vs. MC for electrons (left) and muons (right) for events with the $N_{\rm jets}$ requirement varied from $N_{\rm jets} \geq 0$ to $N_{\rm jets} \geq 4$.

e + ≥0 jets	> 1 GeV	> 2 GeV	> 3 GeV	> 4 GeV	> 5 GeV
data	0.098 ± 0.0002	0.036 ± 0.0001	0.016 ± 0.0001	0.009 ± 0.0001	0.006 ± 0.0000
mc	0.097 ± 0.0002	0.034 ± 0.0001	0.016 ± 0.0001	0.009 ± 0.0001	0.005 ± 0.0000
data/mc	1.00 ± 0.00	1.04 ± 0.00	1.04 ± 0.01	1.03 ± 0.01	1.02 ± 0.01
μ + ≥0 jets	> 1 GeV	> 2 GeV	> 3 GeV	> 4 GeV	> 5 GeV
data	0.094 ± 0.0001	0.034 ± 0.0001	0.016 ± 0.0001	0.009 ± 0.0000	0.006 ± 0.0000
mc	0.093 ± 0.0001	0.033 ± 0.0001	0.015 ± 0.0001	0.009 ± 0.0000	0.006 ± 0.0000
data/mc	1.01 ± 0.00	1.03 ± 0.00	1.03 ± 0.01	1.03 ± 0.01	1.02 ± 0.01
e + ≥1 jets	> 1 GeV	> 2 GeV	> 3 GeV	> 4 GeV	> 5 GeV
data	0.110 ± 0.0005	0.044 ± 0.0003	0.022 ± 0.0002	0.014 ± 0.0002	0.009 ± 0.0002
mc	0.110 ± 0.0005	0.042 ± 0.0003	0.021 ± 0.0002	0.013 ± 0.0002	0.009 ± 0.0001
data/mc	1.00 ± 0.01	1.04 ± 0.01	1.06 ± 0.02	1.08 ± 0.02	1.06 ± 0.03
μ + ≥1 jets	> 1 GeV	> 2 GeV	> 3 GeV	> 4 GeV	> 5 GeV
data	0.106 ± 0.0004	0.043 ± 0.0003	0.023 ± 0.0002	0.014 ± 0.0002	0.010 ± 0.0001
mc	0.106 ± 0.0004	0.042 ± 0.0003	0.021 ± 0.0002	0.013 ± 0.0002	0.009 ± 0.0001
data/mc	1.00 ± 0.01	1.04 ± 0.01	1.06 ± 0.01	1.08 ± 0.02	1.07 ± 0.02
e + ≥2 jets	> 1 GeV	> 2 GeV	> 3 GeV	> 4 GeV	> 5 GeV
data	0.117 ± 0.0012	0.050 ± 0.0008	0.026 ± 0.0006	0.017 ± 0.0005	0.012 ± 0.0004
mc	0.120 ± 0.0012	0.048 ± 0.0008	0.025 ± 0.0006	0.016 ± 0.0005	0.011 ± 0.0004
data/mc	0.97 ± 0.01	1.05 ± 0.02	1.05 ± 0.03	1.07 ± 0.04	1.07 ± 0.05
μ + ≥2 jets	> 1 GeV	> 2 GeV	> 3 GeV	> 4 GeV	> 5 GeV
data	0.111 ± 0.0010	0.048 ± 0.0007	0.026 ± 0.0005	0.018 ± 0.0004	0.013 ± 0.0004
mc	0.115 ± 0.0010	0.048 ± 0.0006	0.025 ± 0.0005	0.016 ± 0.0004	0.012 ± 0.0003
data/mc	0.97 ± 0.01	1.01 ± 0.02	1.04 ± 0.03	1.09 ± 0.04	1.09 ± 0.04
e + ≥3 jets	> 1 GeV	> 2 GeV	> 3 GeV	> 4 GeV	> 5 GeV
data	0.123 ± 0.0031	0.058 ± 0.0022	0.034 ± 0.0017	0.023 ± 0.0014	0.017 ± 0.0012
mc	0.131 ± 0.0030	0.055 ± 0.0020	0.030 ± 0.0015	0.020 ± 0.0013	0.015 ± 0.0011
data/mc	0.94 ± 0.03	1.06 ± 0.06	1.14 ± 0.08	1.16 ± 0.10	1.17 ± 0.12
μ + ≥3 jets	> 1 GeV	> 2 GeV	> 3 GeV	> 4 GeV	> 5 GeV
data	0.121 ± 0.0025	0.055 ± 0.0018	0.033 ± 0.0014	0.022 ± 0.0011	0.017 ± 0.0010
mc	0.120 ± 0.0024	0.052 ± 0.0016	0.029 ± 0.0012	0.019 ± 0.0010	0.014 ± 0.0009
data/mc	1.01 ± 0.03	1.06 ± 0.05	1.14 ± 0.07	1.14 ± 0.08	1.16 ± 0.10
e + ≥4 jets	> 1 GeV	> 2 GeV	> 3 GeV	> 4 GeV	> 5 GeV
data	0.129 ± 0.0080	0.070 ± 0.0061	0.044 ± 0.0049	0.031 ± 0.0042	0.021 ± 0.0034
mc	0.132 ± 0.0075	0.059 ± 0.0053	0.035 ± 0.0041	0.025 ± 0.0035	0.017 ± 0.0029
data/mc	0.98 ± 0.08	1.18 ± 0.15	1.26 ± 0.20	1.24 ± 0.24	1.18 ± 0.28
μ + ≥4 jets	> 1 GeV	> 2 GeV	> 3 GeV	> 4 GeV	> 5 GeV
data	0.136 ± 0.0067	0.064 ± 0.0048	0.041 ± 0.0039	0.029 ± 0.0033	0.024 ± 0.0030
mc	0.130 ± 0.0063	0.065 ± 0.0046	0.035 ± 0.0034	0.020 ± 0.0026	0.013 ± 0.0022
data/mc	1.04 ± 0.07	0.99 ± 0.10	1.19 ± 0.16	1.47 ± 0.25	1.81 ± 0.37

Table 32: Comparison of the data vs. MC efficiencies to satisfy the indicated requirements on the absolute track isolation, and the ratio of these two efficiencies. Results are indicated separately for electrons and muons and for various jet multiplicity requirements.

9.9 Summary of uncertainties

The contribution from each source to the total uncertainty on the background yield is given in Tables 33 and 34 for the relative and absolute uncertainties, respectively. In the low-$E_{\mathrm{T}}^{\mathrm{miss}}$ regions the dominant uncertainty comes from the top tail-to-peak ratio, R_{top} (Section 7), while in the high-$E_{\mathrm{T}}^{\mathrm{miss}}$ regions the $\mathrm{t\bar{t}} \to \ell\ell$ systematic uncertainty dominates (Section 9.7).

Sample	SRA	SRB	SRC	SRD	SRE	SRF	SRG
Muon							
W+jets cross-section	1.7%	2.3%	3.0%	3.7%	4.2%	4.2%	5.3%
rare cross-sections	2.0%	2.3%	3.4%	5.6%	8.8%	8.0%	10.4%
top tail-to-peak ratio	12.6%	8.7%	8.6%	6.7%	7.1%	8.6%	4.6%
W+jets tail-to-peak ratio	6.5%	5.3%	5.8%	6.9%	8.9%	12.0%	13.6%
$\mathrm{t\bar{t}} \to \ell\ell$ (stat)	1.1%	1.5%	2.8%	4.7%	6.7%	9.7%	12.2%
K_3 and K_4	1.9%	1.9%	2.0%	2.0%	1.9%	1.8%	1.8%
2nd lepton veto	1.2%	1.3%	1.3%	1.3%	1.2%	1.2%	1.2%
$\mathrm{t\bar{t}} \to \ell\ell$ (CR4 and CR5 closure tests)	3.1%	6.5%	10.2%	16.9%	25.1%	23.8%	23.4%
M_T peak data and MC (stat)	1.1%	2.1%	3.8%	6.0%	8.6%	13.1%	20.0%
total	15.0%	13.0%	16.1%	22.1%	31.3%	33.7%	37.9%
Electron							
W+jets cross-section	1.7%	2.3%	2.9%	4.2%	4.4%	4.5%	4.6%
rare cross-sections	2.1%	2.1%	2.9%	3.7%	1.9%	3.2%	1.9%
top tail-to-peak ratio	12.4%	8.6%	8.3%	6.1%	8.7%	11.0%	8.8%
W+jets tail-to-peak ratio	6.4%	5.2%	5.5%	6.3%	10.8%	15.4%	25.7%
$\mathrm{t\bar{t}} \to \ell\ell$ (stat)	1.3%	1.8%	3.2%	5.6%	8.7%	13.6%	16.6%
K_3 and K_4	1.9%	2.0%	2.1%	2.1%	2.1%	2.0%	2.0%
2nd lepton veto	1.2%	1.3%	1.4%	1.4%	1.4%	1.3%	1.3%
$\mathrm{t\bar{t}} \to \ell\ell$ (CR4 and CR5 closure tests)	3.1%	6.6%	10.4%	17.7%	28.1%	26.1%	26.6%
M_T peak data and MC (stat)	1.4%	2.5%	4.3%	7.4%	11.5%	15.2%	22.5%
total	14.8%	13.0%	16.1%	22.7%	34.9%	38.7%	47.5%
Muon+Electron Combined							
W+jets cross-section	1.7%	2.3%	3.0%	3.9%	4.3%	4.3%	5.1%
rare cross-sections	2.0%	2.2%	3.2%	4.9%	6.4%	6.2%	7.6%
top tail-to-peak ratio	12.5%	8.7%	8.5%	6.5%	7.7%	9.5%	6.0%
W+jets tail-to-peak ratio	6.4%	5.2%	5.7%	6.6%	9.6%	13.3%	17.6%
$\mathrm{t\bar{t}} \to \ell\ell$ (stat)	1.2%	1.6%	3.0%	5.1%	7.4%	11.1%	13.6%
K_3 and K_4	1.9%	2.0%	2.1%	2.1%	2.0%	1.9%	1.8%
2nd lepton veto	1.2%	1.3%	1.4%	1.4%	1.3%	1.2%	1.2%
$\mathrm{t\bar{t}} \to \ell\ell$ (CR4 and CR5 closure tests)	3.1%	6.5%	10.3%	17.3%	26.1%	24.7%	24.5%
M_T peak data and MC (stat)	0.9%	1.7%	2.9%	4.7%	7.0%	10.1%	15.4%
total	14.9%	12.9%	15.9%	21.8%	31.7%	34.2%	38.2%

Table 33: Contributions to the total relative uncertainties.

Sample	SRA	SRB	SRC	SRD	SRE	SRF	SRG
Muon							
W+jets cross-section	9.0	6.5	2.6	1.2	0.6	0.3	0.2
rare cross-sections	10.4	6.6	3.0	1.9	1.3	0.5	0.4
top tail-to-peak ratio	67.1	24.8	7.6	2.2	1.0	0.5	0.2
W+jets tail-to-peak ratio	34.5	14.9	5.1	2.3	1.3	0.7	0.5
$\mathrm{t\bar{t}} \to \ell\ell$ (stat)	6.0	4.4	2.4	1.6	1.0	0.6	0.5
K_3 and K_4	9.9	5.5	1.8	0.7	0.3	0.1	0.1
2nd lepton veto	6.5	3.6	1.2	0.4	0.2	0.1	0.0
$\mathrm{t\bar{t}} \to \ell\ell$ (CR4 and CR5 closure tests)	16.5	18.3	8.9	5.6	3.6	1.5	0.9
M_T peak data and MC (stat)	6.0	6.1	3.4	2.0	1.2	0.8	0.8
total	79.8	36.8	14.2	7.3	4.5	2.1	1.4
Electron							
W+jets cross-section	6.8	5.0	2.2	1.0	0.3	0.2	0.1
rare cross-sections	8.1	4.6	2.2	0.9	0.1	0.1	0.0
top tail-to-peak ratio	49.2	18.9	6.1	1.4	0.7	0.4	0.2
W+jets tail-to-peak ratio	25.3	11.4	4.1	1.4	0.8	0.6	0.5
$\mathrm{t\bar{t}} \to \ell\ell$ (stat)	5.2	3.9	2.4	1.3	0.7	0.5	0.3
K_3 and K_4	7.4	4.3	1.5	0.5	0.2	0.1	0.0
2nd lepton veto	4.9	2.9	1.0	0.3	0.1	0.0	0.0
$\mathrm{t\bar{t}} \to \ell\ell$ (CR4 and CR5 closure tests)	12.4	14.4	7.7	4.0	2.2	1.0	0.5
M_T peak data and MC (stat)	5.7	5.4	3.2	1.7	0.9	0.6	0.4
total	58.8	28.5	11.9	5.2	2.7	1.5	0.9
Muon+Electron Combined							
W+jets cross-section	15.9	11.5	4.8	2.2	0.9	0.4	0.3
rare cross-sections	18.5	11.1	5.1	2.7	1.4	0.6	0.4
top tail-to-peak ratio	116.3	43.6	13.7	3.6	1.7	1.0	0.3
W+jets tail-to-peak ratio	59.8	26.3	9.1	3.7	2.1	1.3	1.0
$\mathrm{t\bar{t}} \to \ell\ell$ (stat)	11.2	8.3	4.8	2.9	1.7	1.1	0.8
K_3 and K_4	17.4	9.8	3.3	1.2	0.4	0.2	0.1
2nd lepton veto	11.5	6.5	2.2	0.8	0.3	0.1	0.1
$\mathrm{t\bar{t}} \to \ell\ell$ (CR4 and CR5 closure tests)	28.9	32.8	16.6	9.7	5.8	2.5	1.4
M_T peak data and MC (stat)	8.7	8.4	4.7	2.6	1.5	1.0	0.9
total	138.4	64.8	25.6	12.2	7.0	3.4	2.2

Table 34: Contributions to the total uncertainties.

10 Results

The results of the search are shown in Table 35, including both statistical and systematic uncertainties. Agreement is observed between the data and the predicted background for all signal regions. The predicted and observed $E_{\mathrm{T}}^{\mathrm{miss}}$ distribution for $E_{\mathrm{T}}^{\mathrm{miss}} > 150$ GeV and $M_{\mathrm{T}} > 120$ GeV are shown in Figure 20, obtained from the yields for SRB to SRG. Two signal points are shown for comparison, corresponding to the low and high stop mass sensitivity boundaries for this search. This shows that the lower $E_{\mathrm{T}}^{\mathrm{miss}}$ region is more sensitive to lighter stop signals, while the higher $E_{\mathrm{T}}^{\mathrm{miss}}$ region is more sensitive to heavier stops, for the T2tt signal model shown. The M_T distributions for increasing values of $E_{\mathrm{T}}^{\mathrm{miss}}$ are shown in Fig 21 and 22.

Sample	SRA	SRB	SRC	SRD	SRE	SRF	SRG
Muon							
$t\bar{t} \to \ell\ell$	331 ± 22	183 ± 21	59.5 ± 10.0	23 ± 6	9.0 ± 3.9	3.7 ± 1.8	2.2 ± 1.2
$t\bar{t} \to \ell +$ jets & single top (1ℓ)	148 ± 75	67.9 ± 28.9	16.1 ± 9.1	4.7 ± 3.2	1.8 ± 1.6	0.9 ± 0.9	0.4 ± 0.5
W+jets	19.2 ± 4.5	10.0 ± 2.2	3.11 ± 0.98	1.2 ± 0.6	0.6 ± 0.4	0.4 ± 0.3	0.2 ± 0.2
Rare	33.2 ± 16.6	22.7 ± 11.4	9.00 ± 4.50	4.8 ± 2.4	2.9 ± 1.5	1.2 ± 0.6	1.0 ± 0.5
Total	531 ± 80	284 ± 37	87.7 ± 14.2	33 ± 7	14 ± 5	6.1 ± 2.1	3.8 ± 1.4
Data	494	254	76	31	8	2	1
Electron							
$t\bar{t} \to \ell\ell$	248 ± 17	144 ± 17	51.1 ± 8.8	16 ± 5	5.5 ± 2.5	2.5 ± 1.3	1.3 ± 0.7
$t\bar{t} \to \ell +$ jets & single top (1ℓ)	108 ± 55	51.8 ± 22.1	12.9 ± 7.3	3.0 ± 2.0	1.2 ± 1.1	0.7 ± 0.7	0.4 ± 0.5
W+jets	14.3 ± 3.3	7.50 ± 1.66	2.43 ± 0.77	0.8 ± 0.4	0.4 ± 0.3	0.3 ± 0.2	0.1 ± 0.2
Rare	25.8 ± 12.9	15.8 ± 7.9	7.10 ± 3.55	2.9 ± 1.5	0.7 ± 0.4	0.3 ± 0.2	0.1 ± 0.1
Total	396 ± 59	219 ± 29	73.5 ± 11.9	23 ± 5	7.8 ± 2.7	3.9 ± 1.5	1.9 ± 0.9
Data	367	202	74	30	15	7	2
Muon+Electron Combined							
$t\bar{t} \to \ell\ell$	579 ± 38	328 ± 37	111 ± 18	39 ± 10	14 ± 6	6.2 ± 2.9	3.5 ± 1.8
$t\bar{t} \to \ell +$ jets & single top (1ℓ)	256 ± 131	120 ± 51	29.0 ± 16.4	7.7 ± 5.1	3.1 ± 2.7	1.7 ± 1.6	0.8 ± 1.0
W+jets	33.5 ± 8.2	17.5 ± 4.5	5.54 ± 1.98	2.0 ± 1.0	1.0 ± 0.7	0.7 ± 0.6	0.3 ± 0.4
Rare	59.0 ± 29.5	38.5 ± 19.3	16.1 ± 8.1	7.7 ± 3.9	3.6 ± 1.8	1.5 ± 0.8	1.1 ± 0.6
Total	927 ± 138	504 ± 65	161 ± 26	56 ± 12	22 ± 7	10 ± 3	5.7 ± 2.2
Data	861	456	150	61	23	9	3

Table 35: The result of the search.

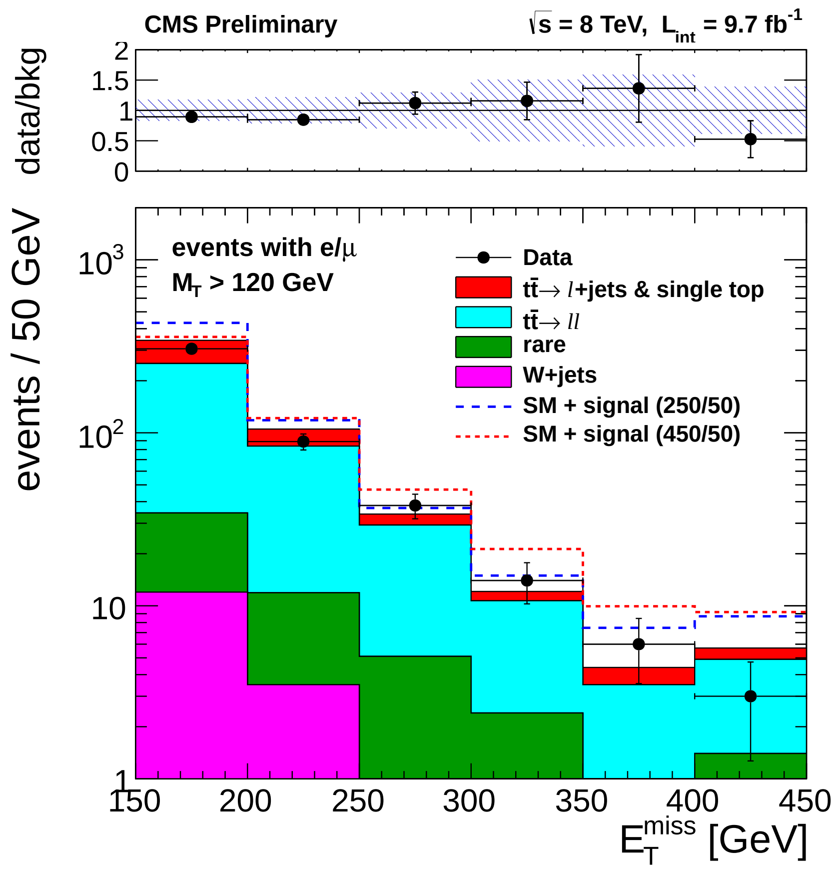

Figure 20: Predicted and observed E_T^{miss} for $M_T > 120$ GeV, obtained from the yields for SRB to SRG. Note SRB corresponds to the integral of the distribution, while subsequent signal regions SRC to SRG correspond to integrals from subsequent bins. The band on the ratio (above) corresponds to the full relative background uncertainty.

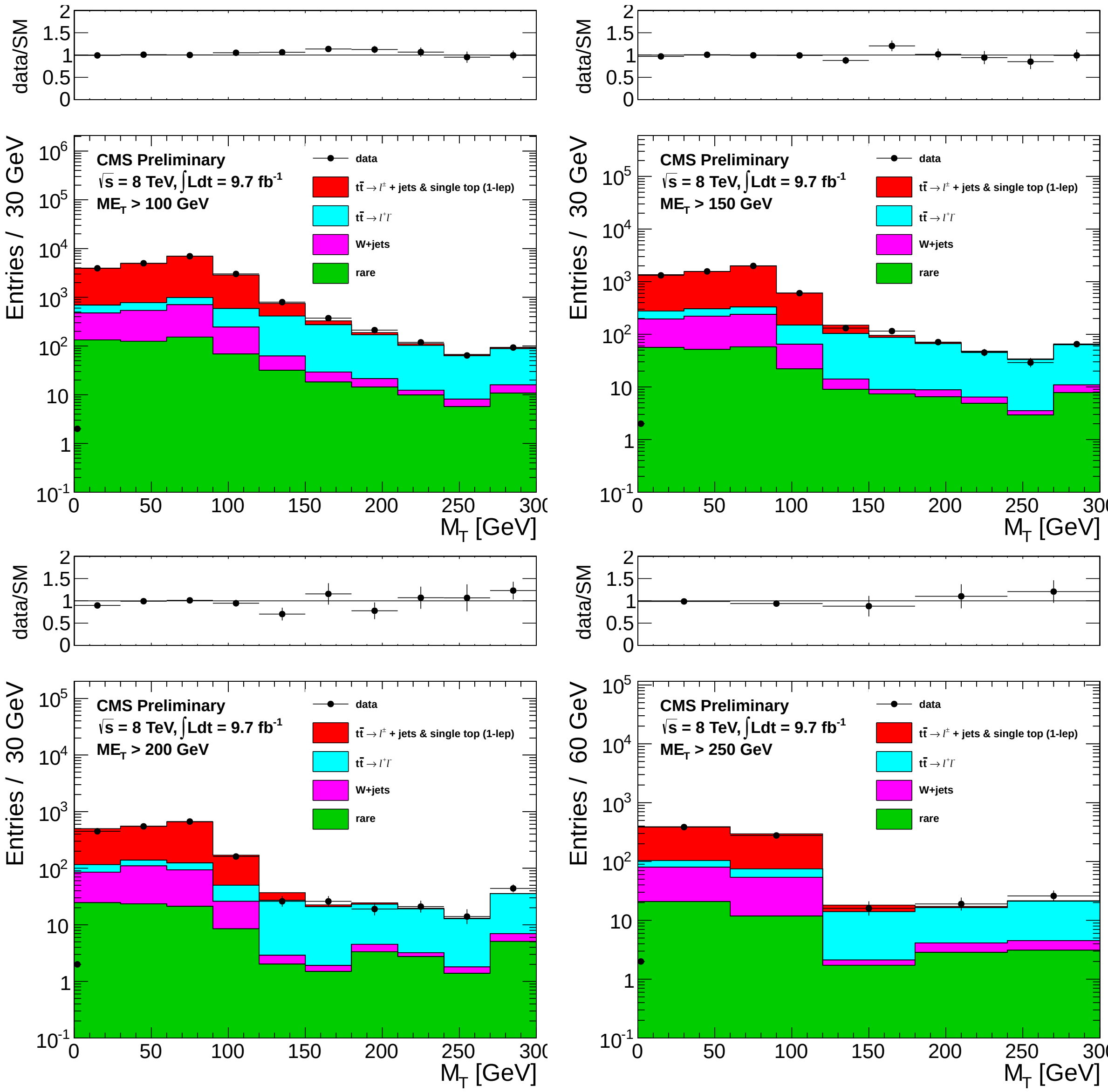

Figure 21: M_T in the data compared to SM Monte Carlo, for increasing values of $E_{\mathrm{T}}^{\mathrm{miss}}$. Only statistical uncertainties are shown. Note that the MC tails have not been rescaled at this point.

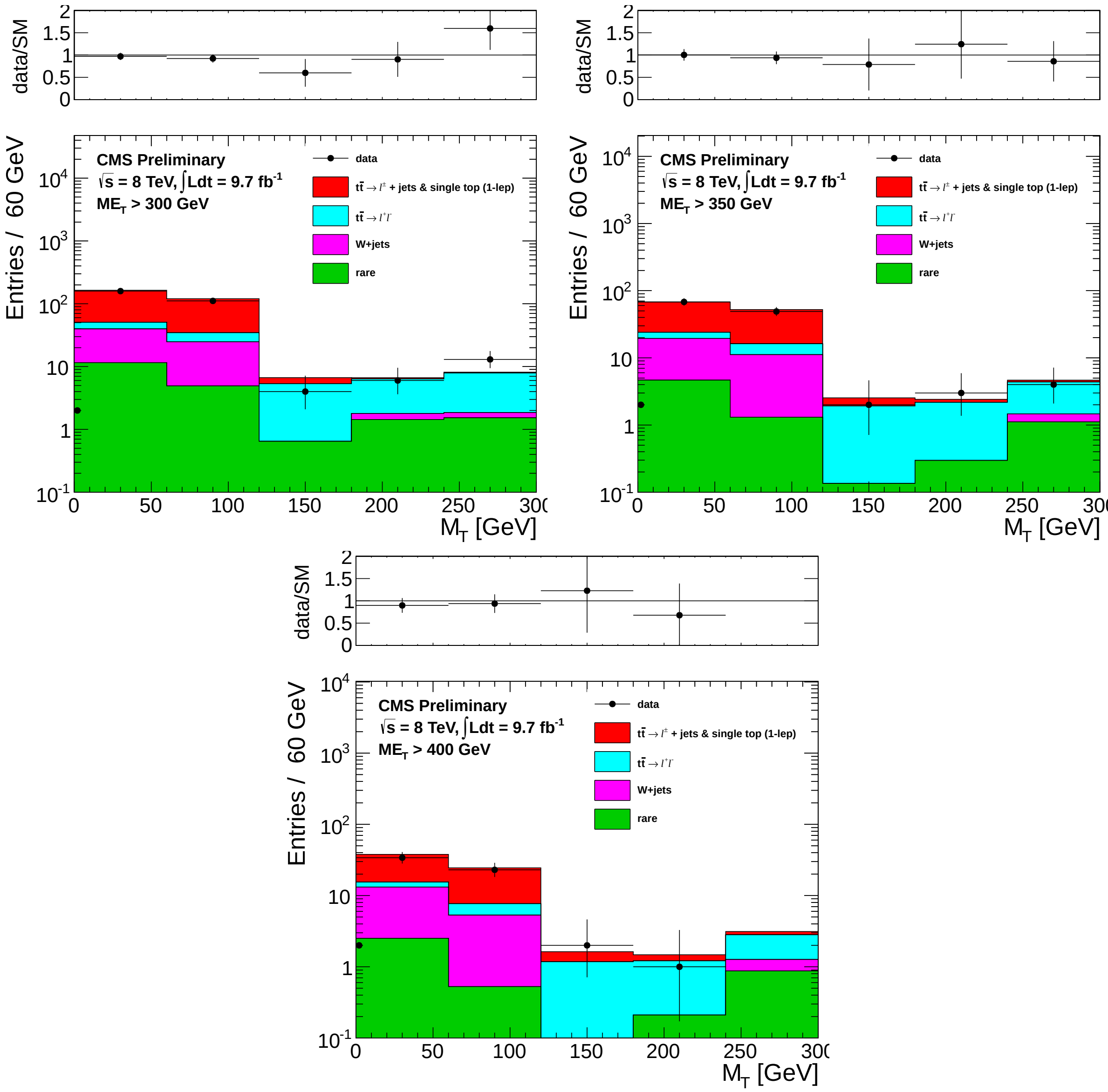

Figure 22: M_T in the data compared to SM Monte Carlo, for increasing values of $E_{\mathrm{T}}^{\mathrm{miss}}$. Only statistical uncertainties are shown. Note that the MC tails have not been rescaled at this point.

11 Limits

In this Section, we interpret the results of this search in terms of the T2tt and T2bw simplified models, see Figure 23. The branching fractions for the stop decay are assumed to be 100% for each model. The signal samples are normalized to cross sections calculated at NLO in α_S, including the resummation of soft gluon emission at next-to-leading-logarithmic accuracy (NLO+NLL).

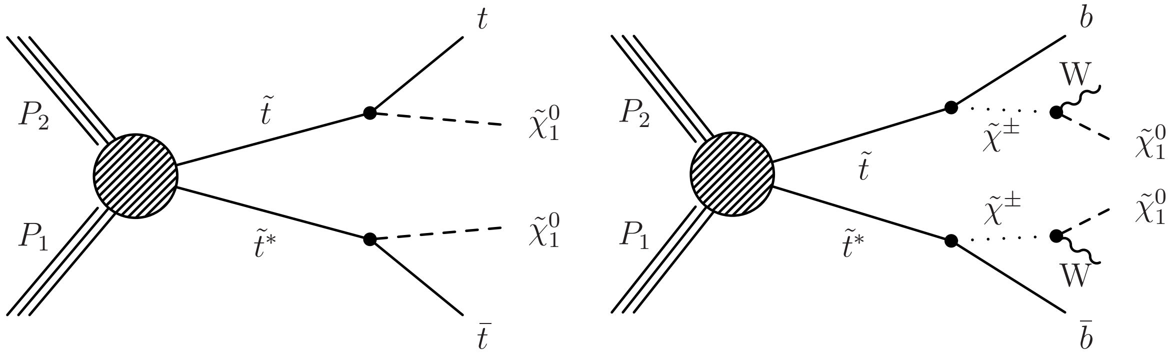

Figure 23: Diagram for the T2tt (left) and T2bw (right) simplified models.

The exclusion is performed using the results from the counting experiments in the signal regions defined by $E_{\mathrm{T}}^{\mathrm{miss}}$ and M_{T} and listed in Table 4. The cross section upper limit calculation is performed with the LandS software using the LHC-type CLs criterion.

The signal efficiency uncertainties include the luminosity (4.4%), lepton ID and isolation efficiency (2%), and trigger efficiency (3%). The uncertainty from JES is assessed for each scan point following the POG-recommended procedure, by varying the jet energies by the p_{T}- and η- dependent uncertainties, and propagating this to the jet multiplicity, $E_{\mathrm{T}}^{\mathrm{miss}}$ and M_{T}. The official b-tagging scale-factors for CSVM are used to compute scale factors for the signal. The results are nearly constant across the model parameter space, and an overall scale factor of $(98 \pm 2)\%$ is used.

The signal efficiency in the stop vs LSP mass plane for T2tt is shown for each signal region in Figures 24, 25 and 26 (left). The corresponding distributions for T2bw are shown in Figures 27, 28 and 29 for x=0.75 and in Figure 30, 31 and 32 for x=0.5 (left). The current analysis is not sensitive to the x=0.25 scenario (Figure 34, bottom).

These distributions show how challenging it is to have sensitivity near the kinematical boundaries. The cross section upper limits, along with the observed and expected exclusion contours, are also shown in Figures 24, 25 and 26 for T2tt, in Figures 27, 28 and 29 for T2bw with x=0.75, and in Figure 30, 31 and 32 for T2bw with x=0.5 (right). The complementarity of the different signal regions is readily apparent. The sensitivity to low (high) stop masses comes from the low (high) $E_{\mathrm{T}}^{\mathrm{miss}}$ signal regions.

A combined result is obtained using the observed limit from the signal region with the best expected limit for each scan point. The combined cross section upper limits, with the observed and expected exclusion contours, are shown in Figure 33 for T2tt and Figure 34 for T2bw (left). The signal region with the best expected limit for each scan point is also shown in Figure 33 for T2tt and Figure 34 for T2bw (right). For the T2tt scenario, these results exclude stops with masses in the range of approximately $230 - 460$ GeV, for LSP masses up to about 130 GeV. In the T2bw scenario with x=0.75, this search excludes stops with masses in the range of approximately $150 - 430$ GeV, for LSP masses up to about 140 GeV. The sensitivity is reduced in the x=0.5 scenario, where the results exclude stops with masses in the range of approximately $250 - 360$ GeV, for LSP masses less than approximately 100 GeV.

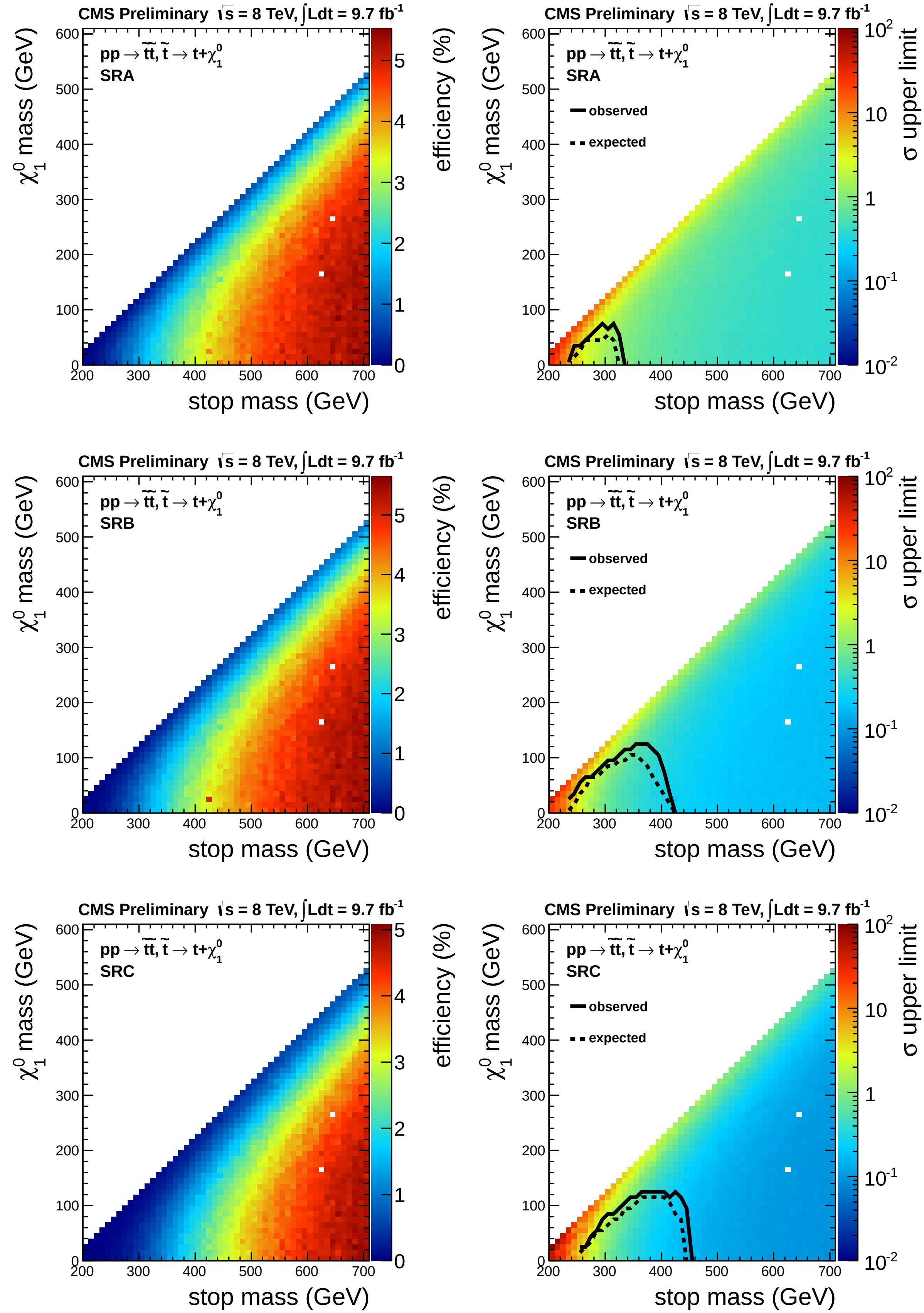

Figure 24: Signal efficiency (left) and cross section upper limit (right) for the T2tt model, showing both the expected and observed exclusion contours. The results for signal regions SRA (top), SRB (middle) and SRC (bottom) are shown separately.

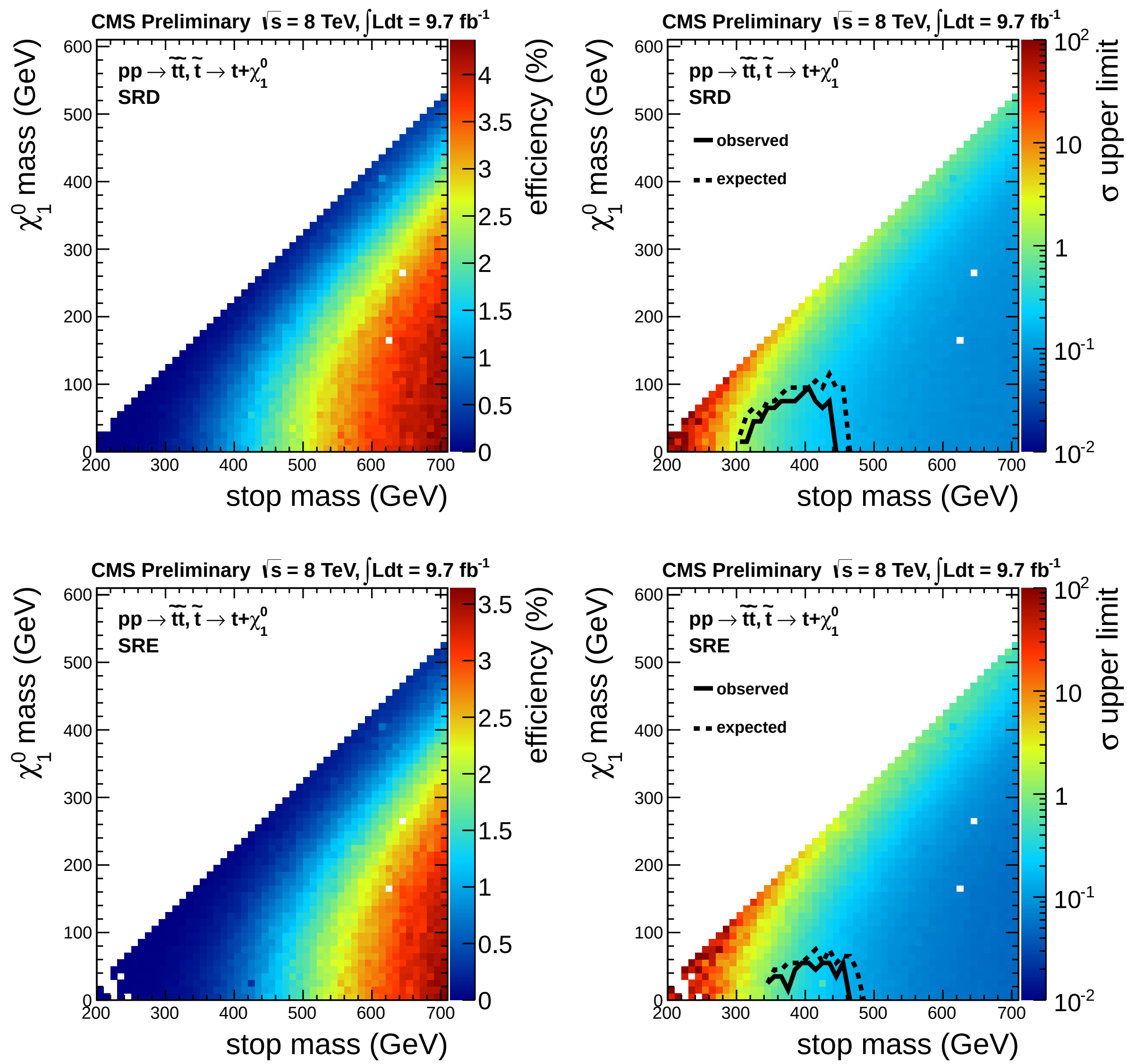

Figure 25: Signal efficiency (left) and cross section upper limit (right) for the T2tt model, showing both the expected and observed exclusion contours. The results for signal regions SRD (top), and SRE (bottom) are shown separately.

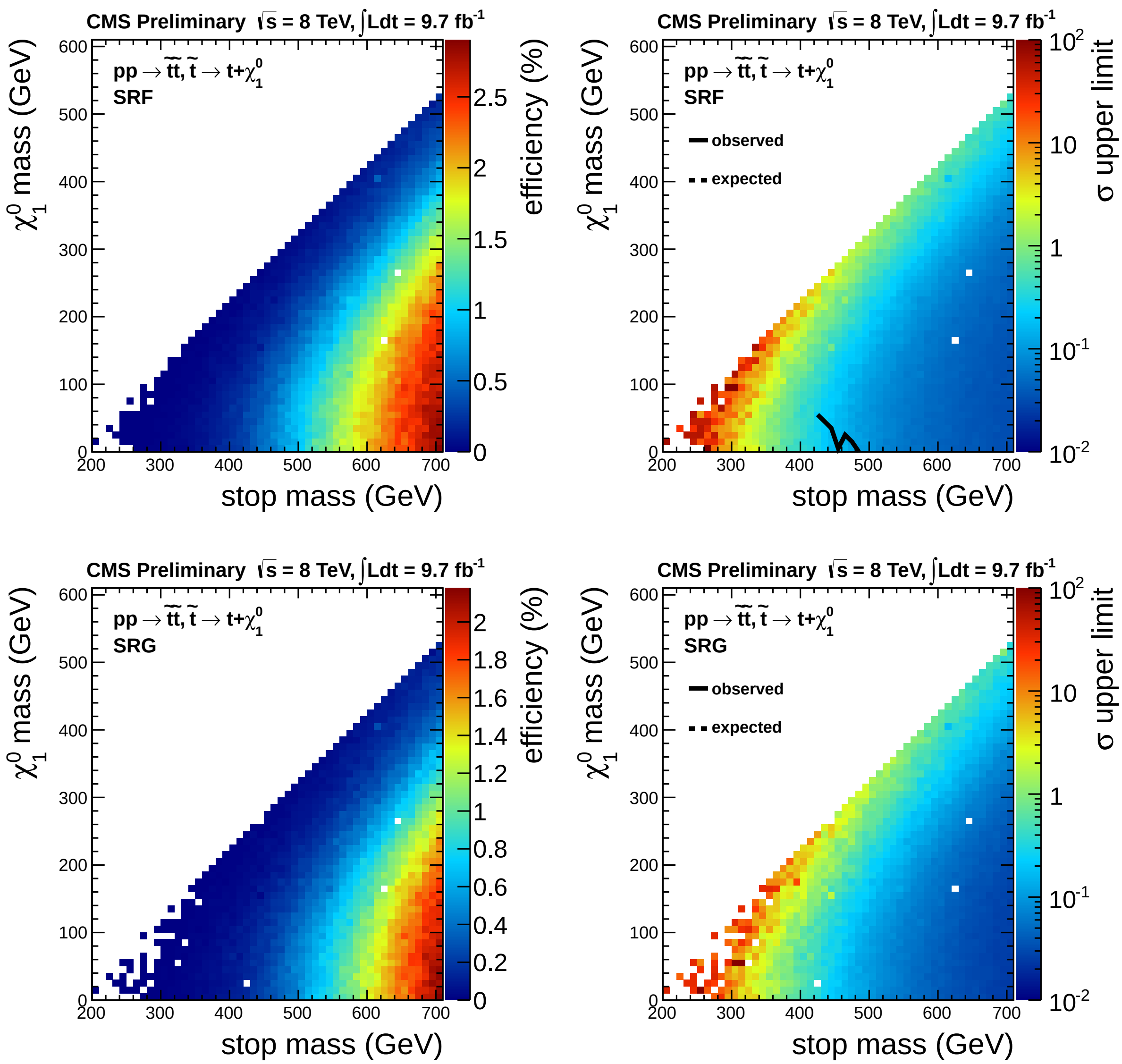

Figure 26: Signal efficiency (left) and cross section upper limit (right) for the T2tt model, showing both the expected and observed exclusion contours. The results for signal regions SRF (top), and SRG (bottom) are shown separately.

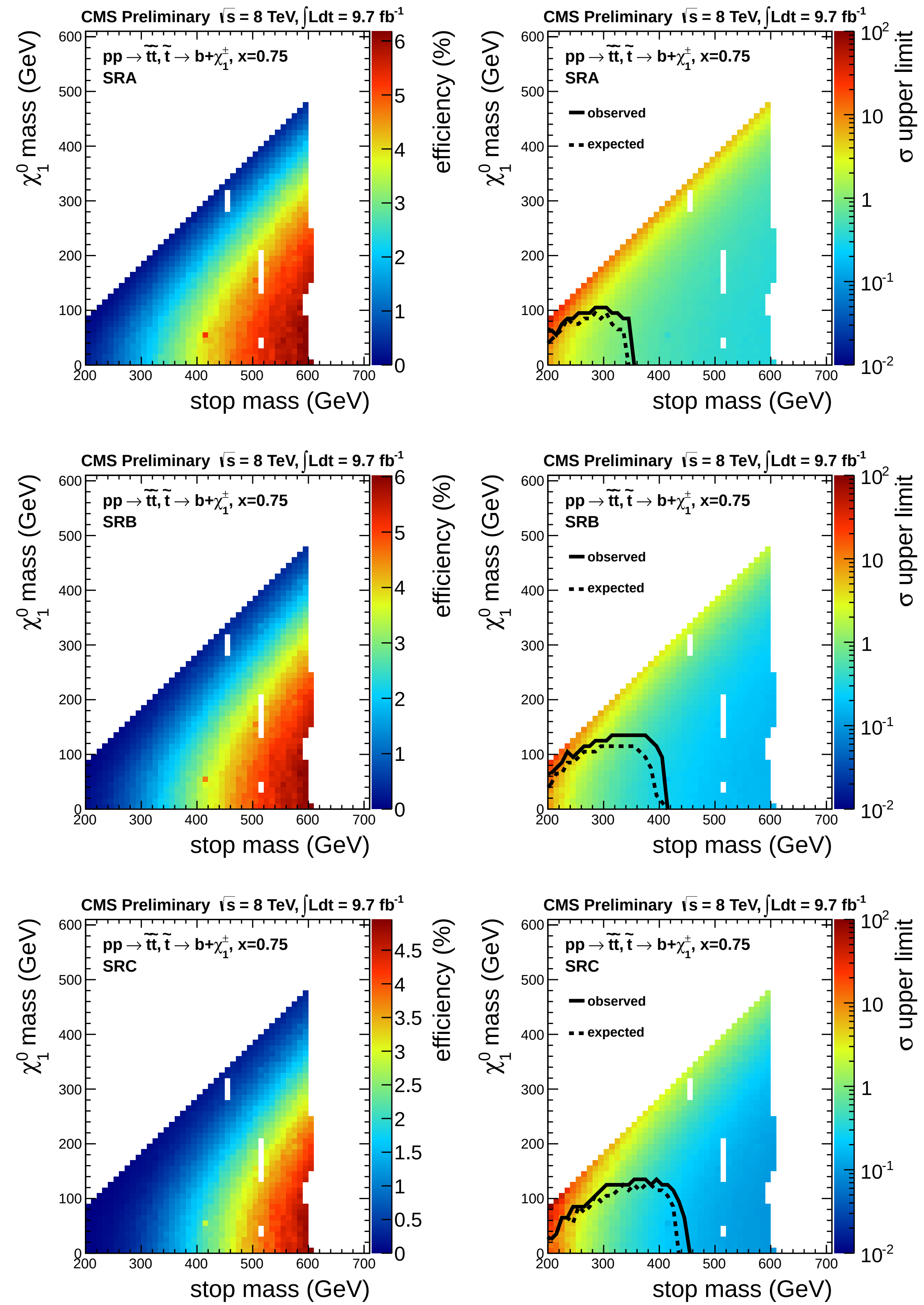

Figure 27: Signal efficiency (left) and cross section upper limit (right) for the T2bw model with x=0.75, showing both the expected and observed exclusion contours. The results for signal regions SRA (top), SRB (middle) and SRC (bottom) are shown separately.

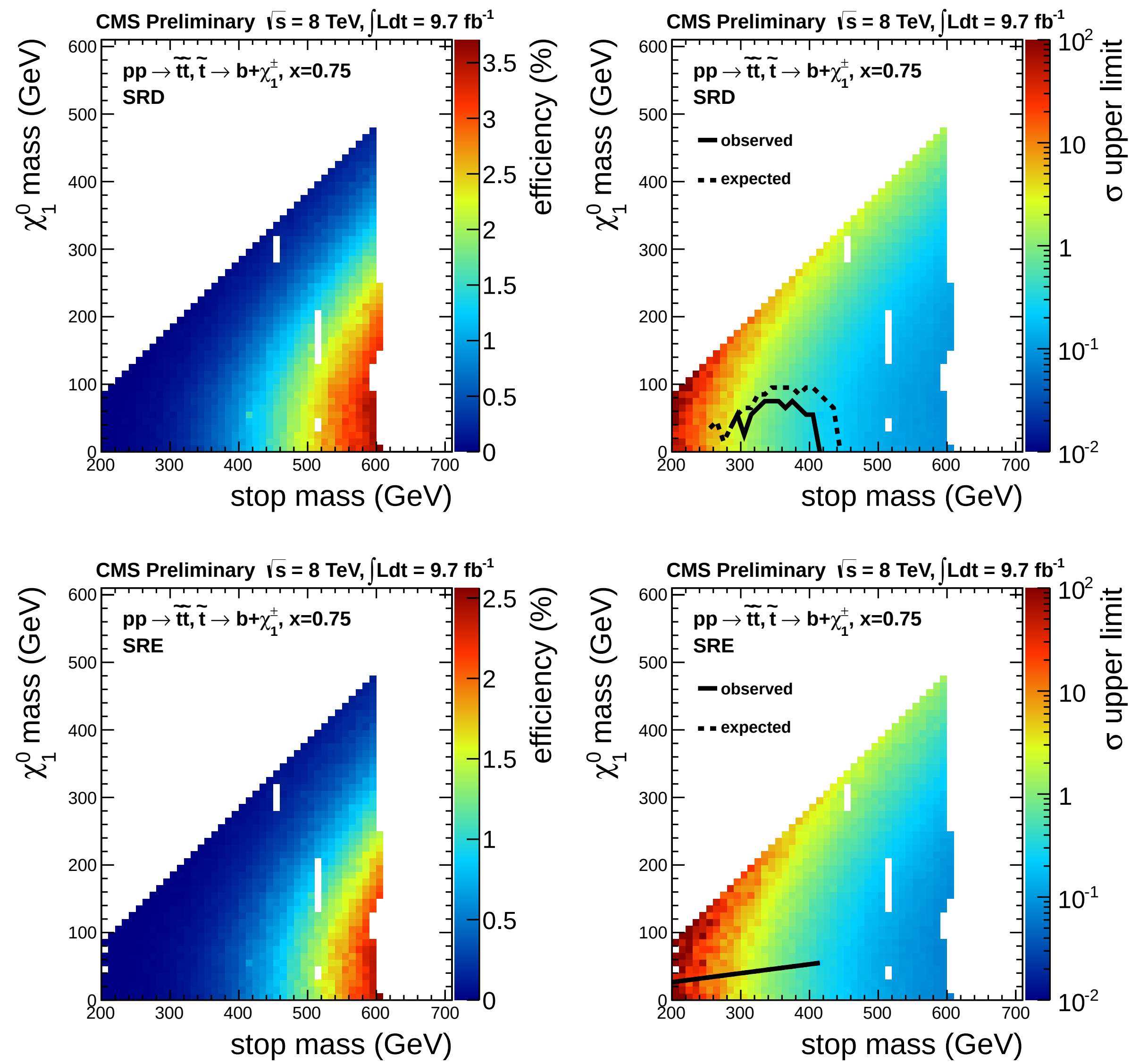

Figure 28: Signal efficiency (left) and cross section upper limit (right) for the T2bw model with x=0.75, showing both the expected and observed exclusion contours. The results for signal regions SRD (top), and SRE (bottom) are shown separately.

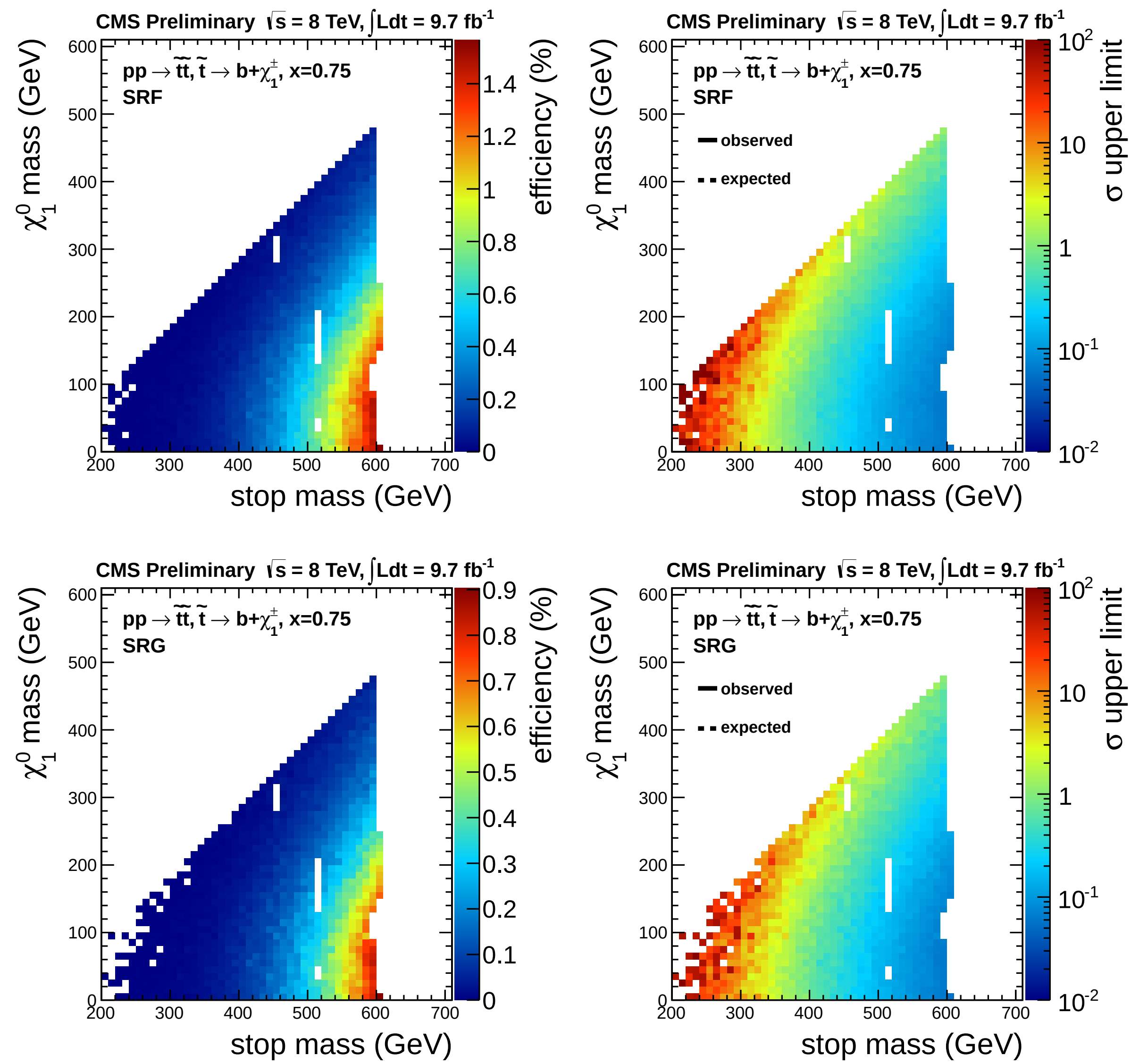

Figure 29: Signal efficiency (left) and cross section upper limit (right) for the T2bw model with x=0.75, showing both the expected and observed exclusion contours. The results for signal regions SRF (top), and SRG (bottom) are shown separately.

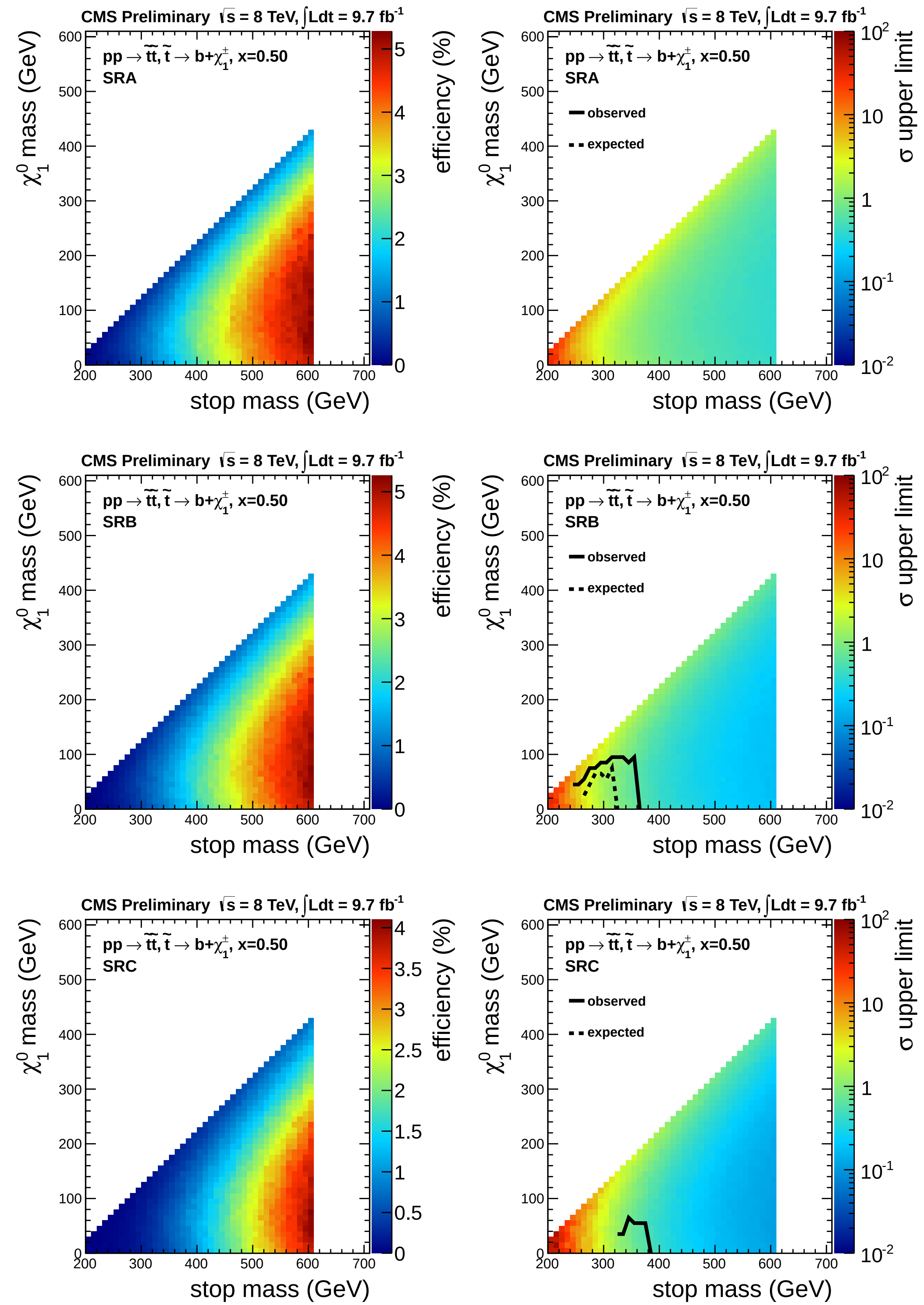

Figure 30: Signal efficiency (left) and cross section upper limit (right) for the T2bw model with x=0.5, showing both the expected and observed exclusion contours. The results for signal regions SRA (top), SRB (middle) and SRC (bottom) are shown separately.

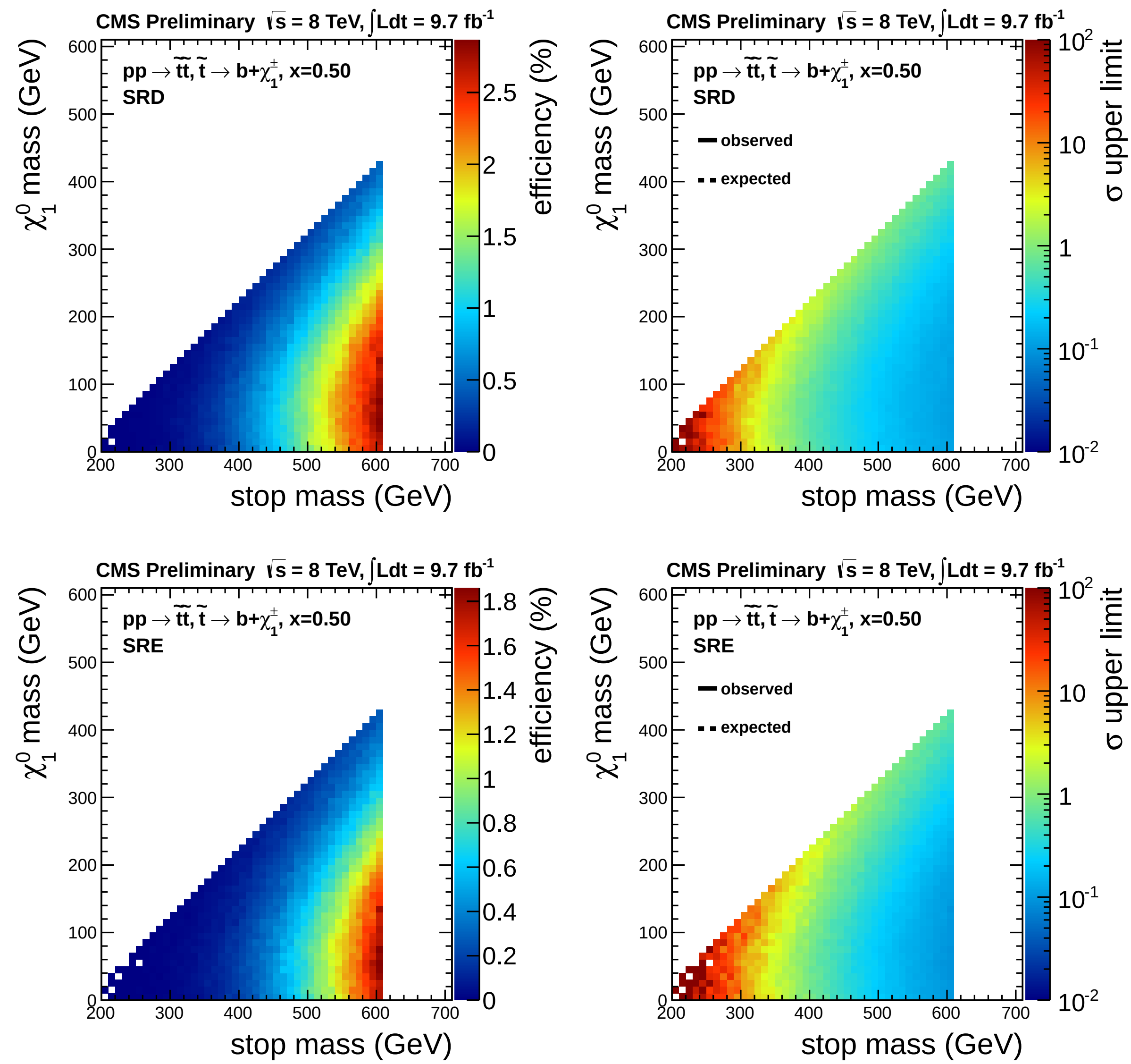

Figure 31: Signal efficiency (left) and cross section upper limit (right) for the T2bw model with x=0.5, showing both the expected and observed exclusion contours. The results for signal regions SRD (top), and SRE (bottom) are shown separately.

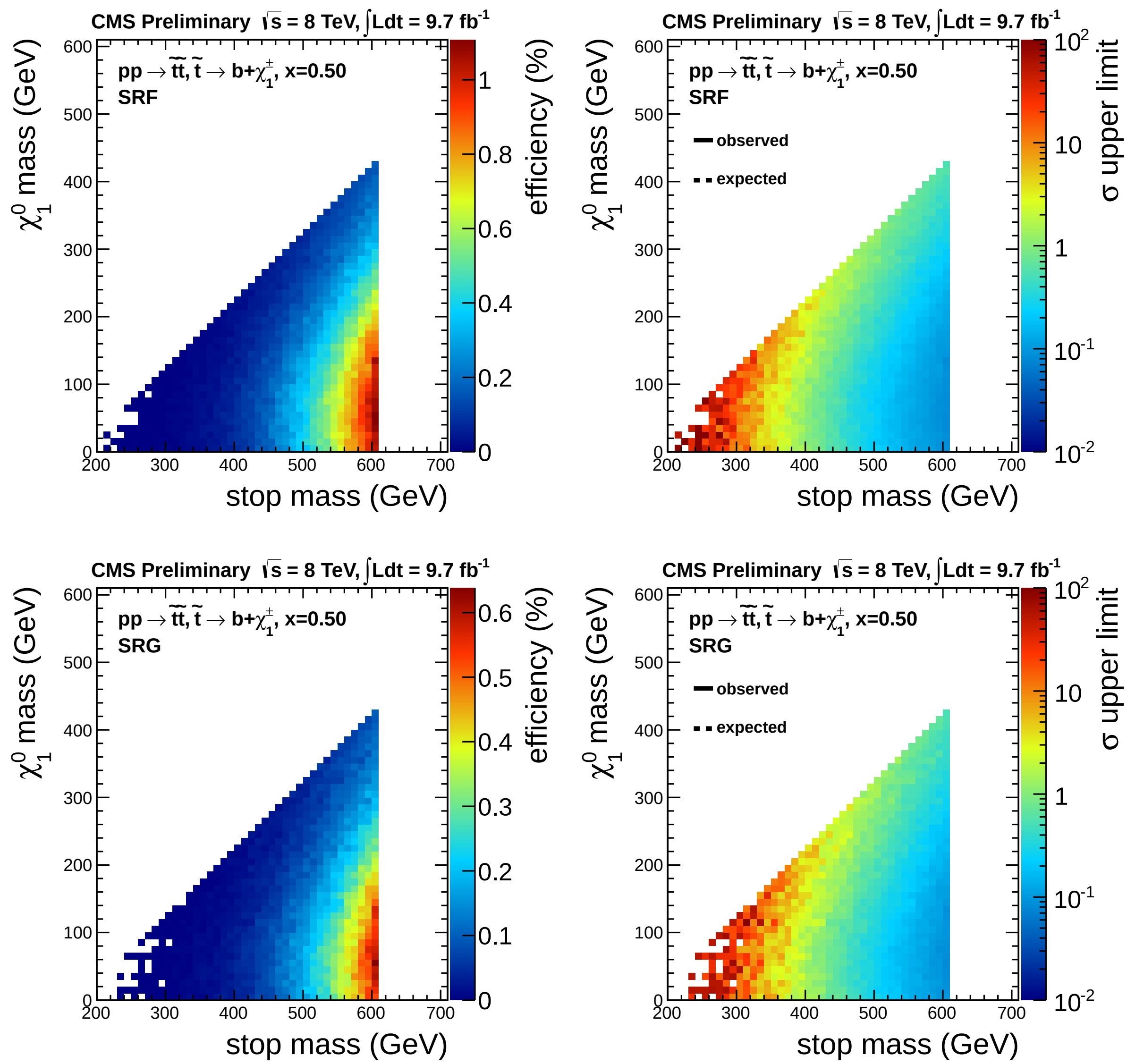

Figure 32: Signal efficiency (left) and cross section upper limit (right) for the T2bw model with x=0.5, showing both the expected and observed exclusion contours. The results for signal regions SRF (top), and SRG (bottom) are shown separately.

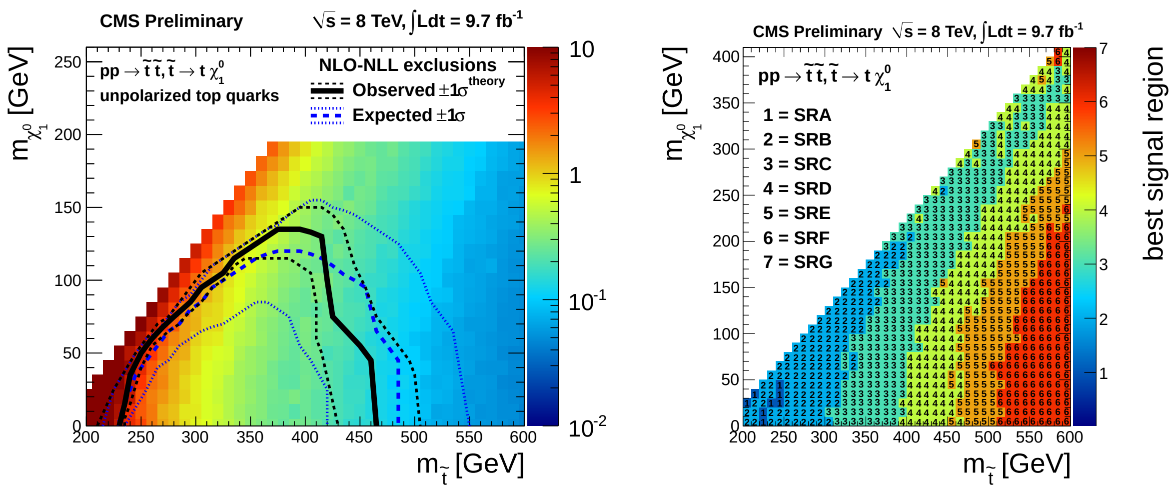

Figure 33: Upper limit on the cross section for the T2tt model in the plane of stop vs. LSP mass, showing both the expected (dashed) and observed (solid curve) exclusion contours (left). The observed limit is selected from the signal region with the best expected limit (shown on right). All uncertainties are included and the dotted contours around the dashed expected limit correspond to the $\pm 1\sigma$ result.

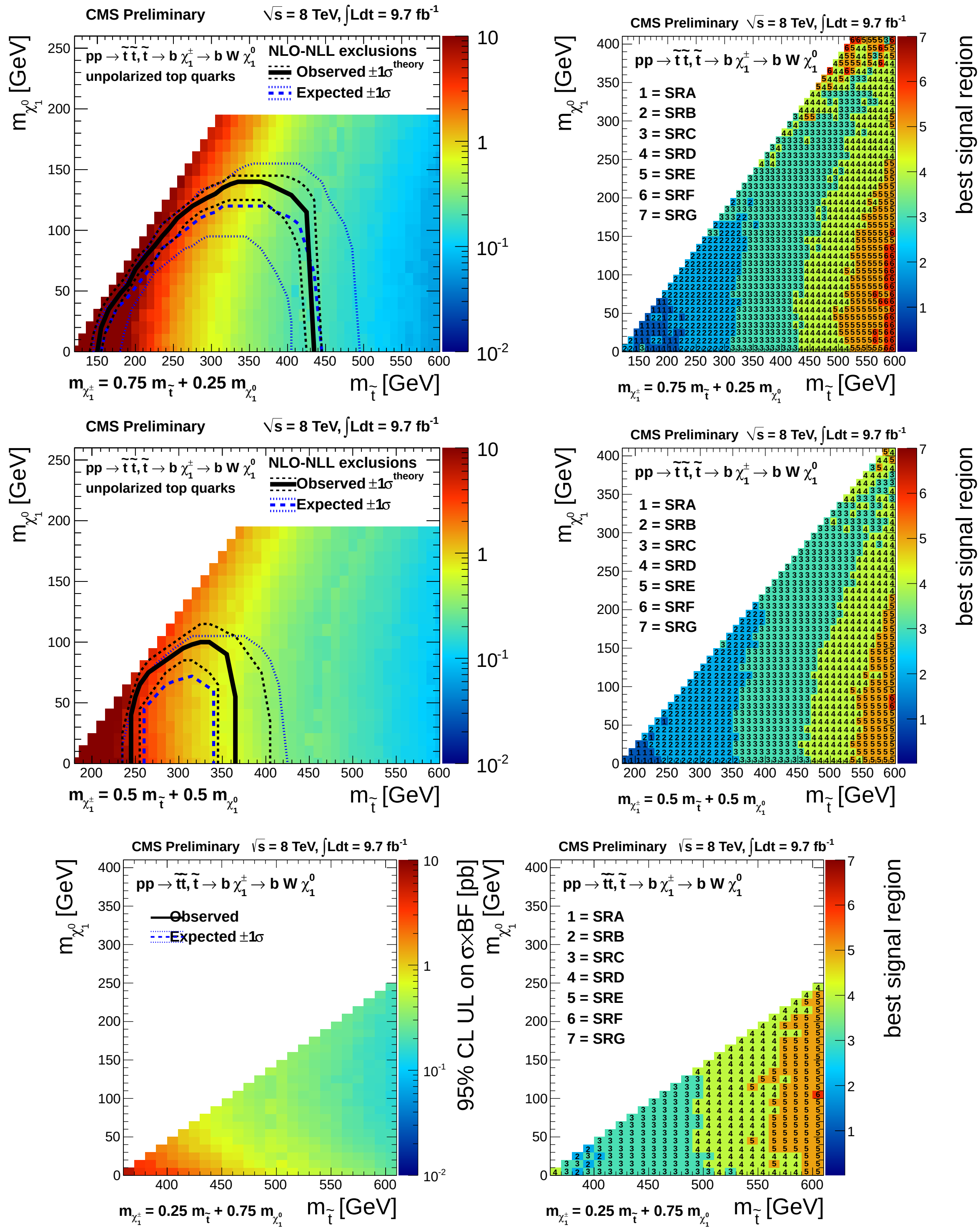

Figure 34: Upper limit on the cross section for the T2bw model for x=0.7 (top), x=0.5 (middle) and x=0.25 (bottom) in the plane of stop vs. LSP mass, showing both the expected (dashed) and observed (solid curve) exclusion contours (left). The observed limit is selected from the signal region with the best expected limit (shown on right). All uncertainties are included and the dotted contours around the dashed expected limit correspond to the $\pm 1\sigma$ result.

11.1 Model dependence of the signal acceptance

The signal acceptance for T2tt events has a significant dependence on the model parameters, particularly the mixing angle of left- and right-handed stops. Depending on the choice of mixing angle, the top quarks produced in the decay can have a polarization anywhere between $+p_{\chi_1^0}/E_{\chi_1^0}$ and $-p_{\chi_1^0}/E_{\chi_1^0}$ [4], which for a massless χ_1^0 becomes ± 1. For right-handed top quarks, the charged lepton is emitted preferentially in the direction parallel to the top velocity, resulting in larger lepton p_{T} and M_{T}.

The default signal MC used in this analysis has unpolarized top quarks. We estimate the impact of the top polarization on our signal acceptance by reweighting our signal MC events to match the expected distribution of the charged lepton decay angle (θ^*) corresponding to the choice of top polarizations of ± 1. The default and reweighted $\cos\theta^*$ distributions are shown in Figure 35, for the signal sample with $M(\tilde{t}) = 450$ GeV and $M(\chi_1^0) = 0$ GeV. Note that this is only an approximate study, because the angular distribution is in fact triply differential. We attempt to account for the dominant effect.

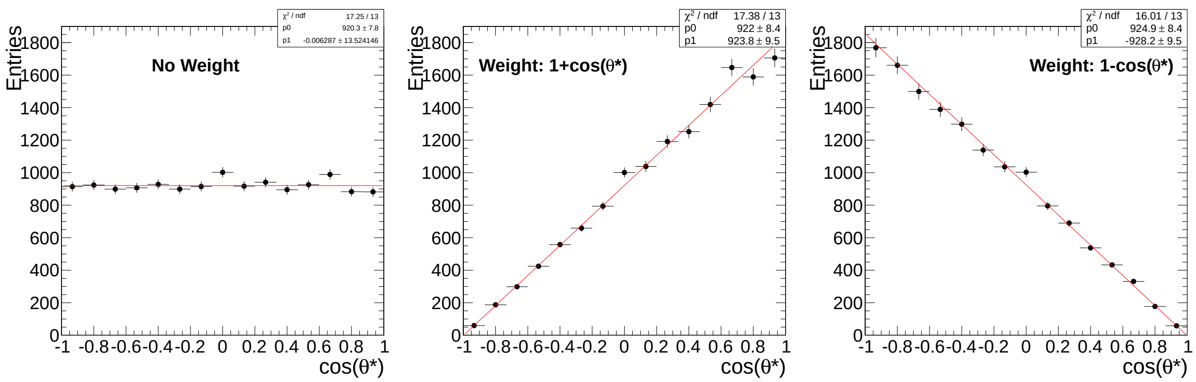

Figure 35: The default and reweighted $\cos\theta^*$ distributions for the signal sample with $M(\tilde{t}) = 450$ GeV and $M(\chi_1^0) = 0$ GeV. The $1 \pm \cos\theta^*$ weightings correspond to top polarizations of ± 1.

We find that reweighting to simulate a top polarization of +1 increases the signal acceptance by 16-24% relative to the default MC, while simulating a top polarization of -1 decreases the signal acceptance by a similar amount. The results for the individual signal regions are given in Table 36.

Sample	SRA	SRB	SRC	SRD	SRE	SRF	SRG
$P = +1$	+22%	+17%	+16%	+19%	+22%	+21%	+24%
$P = -1$	−22%	−17%	−16%	−19%	−22%	−21%	−24%

Table 36: Change in signal acceptance after reweighing the events to simulate a top quark polarization (P) of ± 1, for the signal sample with $M(\tilde{t}) = 450$ GeV and $M(\chi_1^0) = 0$ GeV.

12 Conclusion

This note presents a search for the production of stop quark pairs in events with a single isolated lepton, several jets, missing transverse energy, and large transverse mass. The dataset used corresponds to an integrated luminosity of 9.7 fb^{-1} at center-of-mass energy of 8 TeV. Seven signal regions are defined, based on $E_{\mathrm{T}}^{\mathrm{miss}}$ and M_{T} requirements. Agreement is observed between the data and the predicted backgrounds for all signal regions. The results are interpreted in the context of simplified SUSY models where the stops decay to top-neutralino or b-chargino and are used to place constraints on the stop mass.

References

[1] https://twiki.cern.ch/twiki/bin/view/LHCPhysics/SUSYCrossSections8TeVstopsbottom

[2] T. Plenh *et al.*, JHEP 1208(2012) 091.

[3] These are measured by the Florida group in the context of the same sign and ewk-ino analyses.

[4] M. Perelstein, A. Weiler, arXiv:0811.1024v2 [hep-ph]

A Performance of the Isolation Requirement

The last requirement used in the analysis is an isolated track veto. This selection criteria rejects events containing a track of $p_{\mathrm{T}} > 10$ GeV with relative track isolation $\sum p_{\mathrm{T}}/p_{\mathrm{T}}(trk)$ in a cone of size $R = 0.3 < 0.1$. It may be noted that only tracks consistent with the vertex with highest $\sum p_{\mathrm{T}}^2$ are considered in order to reduce the impact of spurious tracks, for example from pileup interactions. This requirement has very good performance. Figure 36 shows the efficiency for rejecting dilepton events compared to the efficiency for selecting single lepton events for various cone sizes and cut values. The chosen working point provides a signal efficiency of $\epsilon(sig) = 92\%$ for a background rejection of $\epsilon(bkg) = 53\%$ in MC. With "signal" ("background") we are referring to $\mathrm{t\bar{t}} \to \ell + \mathrm{jets}$ ($\mathrm{t\bar{t}} \to \ell\ell$).

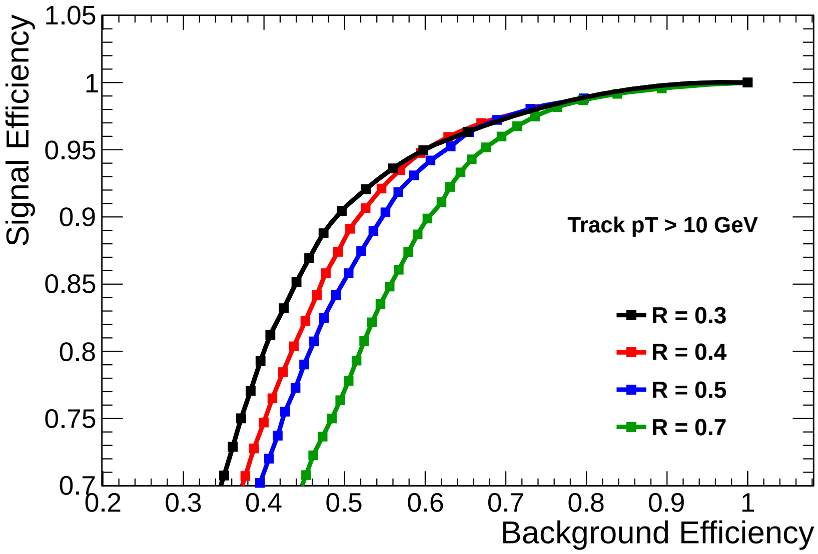

Figure 36: Comparison of the performance in terms of signal (single lepton events) efficiency and background (dilepton events) rejection for various cone sizes and cut values. The current isolation requirement uses a cone of size $\Delta R = 0.3$ and a cut value of 0.1, corresponding to $\epsilon(sig) = 92\%$ for $\epsilon(bkg) = 53\%$.

It should be emphasized that the isolated track veto has a different impact on the samples with a single lepton (mainly $\mathrm{t\bar{t}} \to \ell + \mathrm{jets}$ and W+jets) and that with two leptons (mainly $\mathrm{t\bar{t}} \to \ell\ell$). For the dilepton background, the veto rejects events which have a genuine second lepton. Thus the performance may be understood as an efficiency $\epsilon_{iso\ trk}$ to identify the isolated track. In the case of the single lepton background, the veto rejects events which do not have a genuine second lepton, but rather which contain a "fake" isolated track. The isolated track veto thus effectively scales the single lepton sample by (1-ϵ_{fake}), where ϵ_{fake} is the probability to identify an isolated track with p_{T}> 10 GeVin events which contain no genuine second lepton. It is thus necessary to study the isolated track efficiency $\epsilon(trk)$ and ϵ_{fake} in order to fully characterize the veto performance.

The veto efficiency for dilepton events is calculated using the tag and probe method in Z events. A good lepton satisfying the full ID and isolation criteria and matched to a trigger object serves as the tag. The probe is defined as a track with $p_{\mathrm{T}} > 10$ GeV that has opposite charge to the tag and has an invariant mass with the probe consistent with the Z mass.

The variable used to study the performance of the veto is the absolute track isolation, since it removes the dependence of the isolation variable on the p_{T} of the object under consideration. This is particularly useful because the underlying p_{T} distribution is different for second leptons in $\mathrm{t\bar{t}} \to \ell\ell$ events compared to Z events, particularly due to the presence of τs that have softer decay products. As shown in Figure 37, the absolute isolation is consistent between $\mathrm{Z}+4$ jet events and $\mathrm{t\bar{t}} \to \ell\ell$ events, including leptons from W and τ decays. This supports the notion that the isolation, defined as the energy surrounding the object under consideration, depends only on the environment of the object and not on the object itself. The isolation is thus sensitive to the ambient pileup and jet activity in the event, which is uncorrelated with the lepton p_{T}. It is thus justified to use tag and probe in $\mathrm{Z}+4$ jet events, where the jet activity is similar to $\mathrm{t\bar{t}} \to \ell\ell$ events in our $N_{\mathrm{jets}} > 4$ signal region, in order to estimate the performance of the isolation requirement for the various leptonic categories of $\mathrm{t\bar{t}} \to \ell\ell$ events.

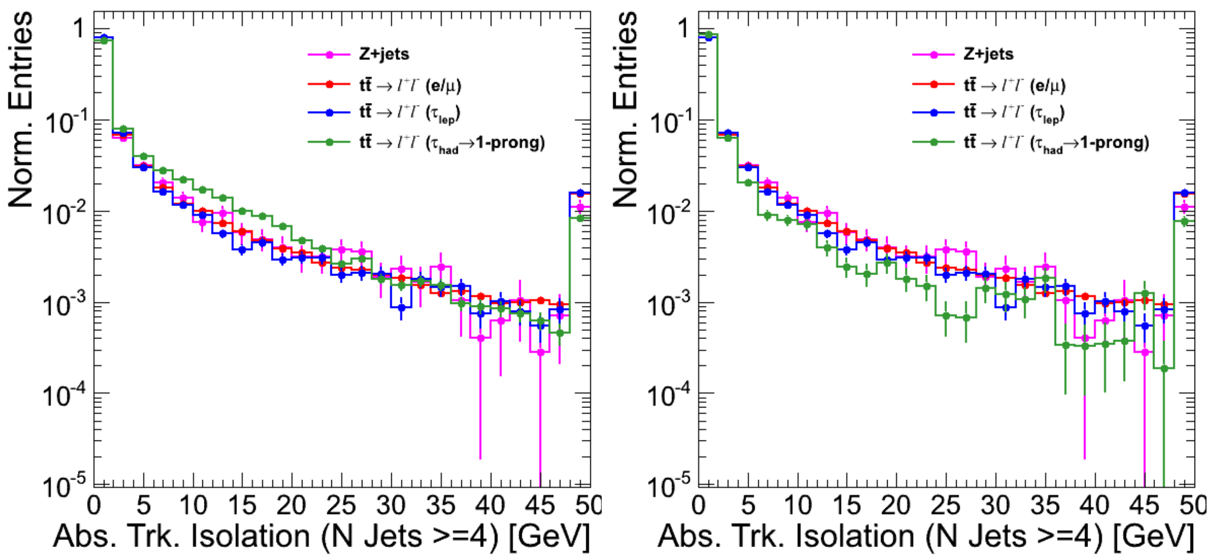

Figure 37: Comparison of absolute track isolation for track probes in $\mathrm{Z}+4$ jet and $\mathrm{t\bar{t}} \to \ell\ell$ events for different lepton types. The isolation variables agree across samples, except for single prong τs, that tend to be slightly less isolated (left). The agreement across isolation distributions is recovered after removing single prong τ events produced in association with π^0s from the sample (right).

B Example BG prediction calculation

The calculation of the background prediction is a bit complicated. Here we walk the reader through a concrete example.

NB: the numbers in this section corresponded to the numbers in V3 of the analysis note. They will not be updated, because this is meant as an illustration only..

The main background is $t\bar{t}$. The main idea is to normalize to the M_T peak region ($50 < M_T < 80$ GeV). This eliminates dependence on $\mathrm{t\bar{t}}$ cross-section, luminosity, trigger efficiency, JES, lepton ID, etc. This gets a bit complicated because the M_T peak region, while dominantly $\mathrm{t\bar{t}}$ lepton + jets, also includes some W+jets, $\mathrm{t\bar{t}} \to \ell\ell$, rare processes, etc. Also, we want to minimize our need to understand the effect of the isolated track veto on $\mathrm{t\bar{t}} \to \ell +$ jets. As a result we actually define two M_T peak regions: one before and one after applying the isolated track veto. Then the $\mathrm{t\bar{t}} \to \ell\ell$ background is normalized the the "before veto" region, and the $\mathrm{t\bar{t}} \to \ell +$ jets and W+jets background are normalized to the "post veto" region.

This complex procedure is important for the high statistics signal regions with relatively low $E_{\mathrm{T}}^{\mathrm{miss}}$ requirements, eg, SRA. For these SRs we want to keep the systematics low in order to be sensitive to low mass stop; for the signal regions with hard cuts on $E_{\mathrm{T}}^{\mathrm{miss}}$ this is less important. However, we apply the same procedure to all SRs.

For concreteness, we show the calculation for SRA, electron channel. The MC and data event counts used in the background calculation are collected in Table 37. Note that the background uncertainties have already been described in Section 9. The one tricky point to keep in mind is that when the W+jets and rare cross-sections are changed by their assumed uncertainties (50% each), the whole calculation describe below is repeated in order to take care of all the correlations properly.

Sample	M_T peak, before trk veto	M_T peak, after trk veto	Signal Region A
$\mathrm{t\bar{t}} \to \ell\ell$	290 ± 6	116 ± 4	261 ± 6
$\mathrm{t\bar{t}} \to \ell +$ jets (1ℓ)	2899 ± 19	2595 ± 18	not used
W+jets	252 ± 28	236 ± 28	not used
Rare	89 ± 5	62 ± 4	26 ± 2
Total	3530 ± 35	3009 ± 34	not used
Data	3358	2787	not used

Table 37: Data and MC event counts used to predict the background in SRA, for electron events. Uncertainties are statistical only. The trigger efficiency has been applied to the MC samples. In the case of $\mathrm{t\bar{t}} \to \ell\ell$ the K_3 and K_4 factors of Section 5.3.1 have also been applied.

B.1 Central value of dilepton background

A "before veto" scale factor is defined from the second column in Table 37 as the factor by which all MC except the "rare" need to be scaled up in order to have data/MC agreement. This is

$SF_{pre} = (3358 - 89)/(2899 + 252 + 290) = 0.950.$

Then the $\mathrm{t\bar{t}} \to \ell\ell$ background prediction is the number of events predicted by the MC in SRA (261 from the last column of SRA), rescaled by SF_{pre}. The result for the central value is 248 events.

B.2 Central value of the $\mathrm{t\bar{t}} \to \ell +$ jets background

A "post veto" scale factor is defined from the third column in Table 37 as the factor by which the $\mathrm{t\bar{t}} \to \ell +$ jets and the W+jets backgrounds need to be scaled to have data/MC agreement.

$SF_{post} = (2787 - 62 - SF_{pre} \cdot 116)/(2595 + 236) = 0.924.$

Then the $\mathrm{t\bar{t}} \to \ell +$ jets background is obtained as the product of the following three factors

- $SF_{post} = 0.924$ as obtained above
- 2595, from the third column of Table 37

- The tail-to-peak ratio $R_{top} = 0.045$ from Table 21

The result for the central value is 108 events.

B.3 Central value for the W+jets background

It is calculated as the product of

- $SF_{post} = 0.924$ from Section B.2
- 236, from the third column of Table 37
- The tail-to-peak ratio $R_{wjet} = 0.066$ from Table 21

The result for the central value is 14.3 events.

B.4 Central value for the rare backgrounds

This is 26 events from Table 37

C Additional CR Data and MC Comparisons

This appendix shows some additional comparisons of the data and MC background samples for various CRs. Figure 38 shows some additional components of the M_{T}, the lepton p_{T} and the azimuthal angle between the lepton and the $E_{\mathrm{T}}^{\mathrm{miss}}$ for CR1 (Section D.3). Figure 39 shows the equivalent distributions for CR2 (Section 5.2), the positive lepton p_{T} and the angle between this lepton and the pseudo-$E_{\mathrm{T}}^{\mathrm{miss}}$. Similarly, figure 42 shows the lepton p_{T} and and the azimuthal angle between the lepton and the $E_{\mathrm{T}}^{\mathrm{miss}}$ for CR5 (Section D.2). Figures 40 and 41 provide some data and MC comparisons of the $t\bar{t} \to \ell\ell$ control sample CR4 (Section 5.3) for various kinematic distributions: leading lepton p_{T} and eta, as well as the angles between the two leptons and between the leading lepton and the $E_{\mathrm{T}}^{\mathrm{miss}}$. These distributions show quite good agreement between data and MC. More quantitative information is included in the section discussing each control region.

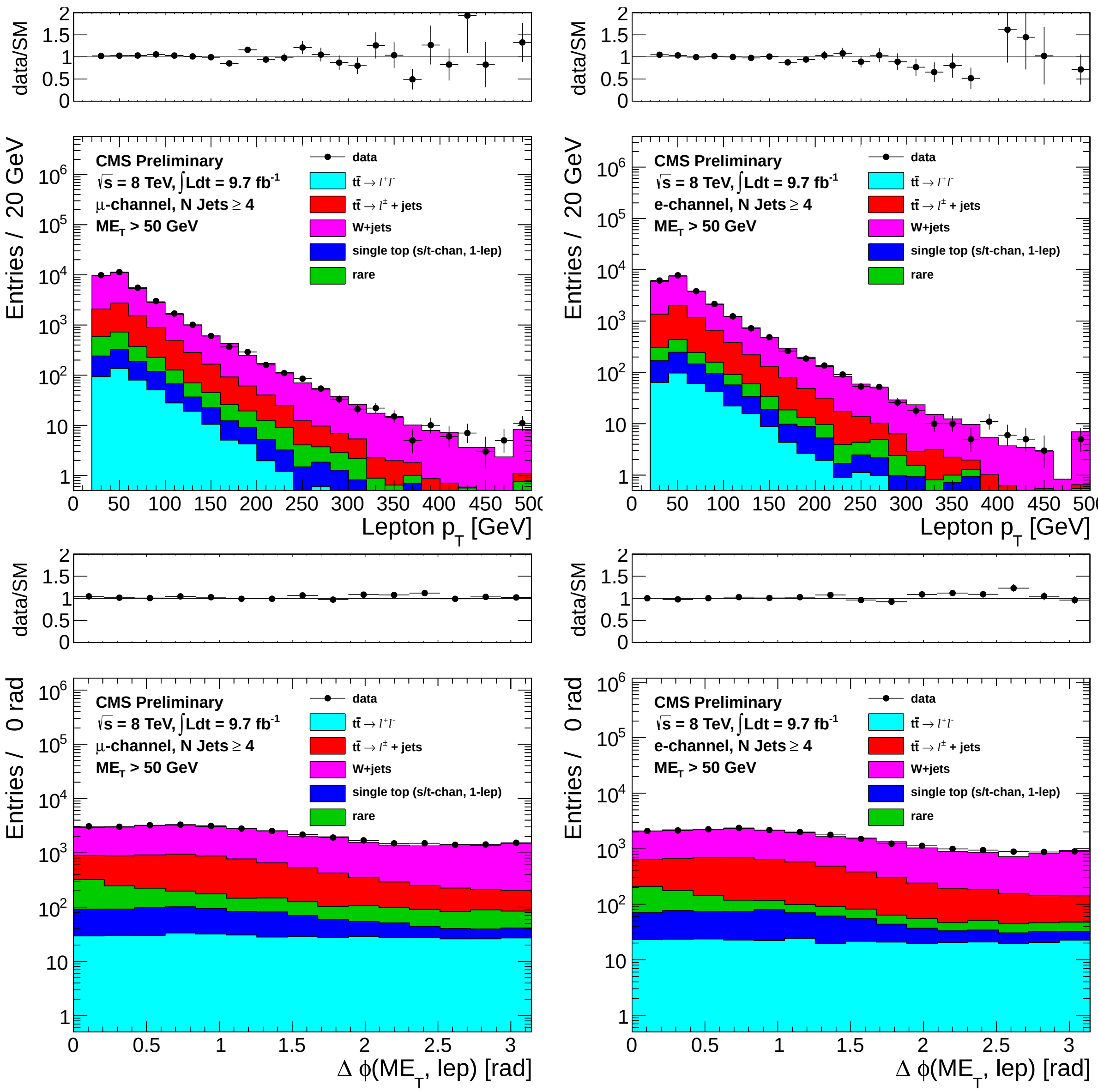

Figure 38: Comparison of the lepton p_{T} (top) and azimuthal angle between the $E_{\mathrm{T}}^{\mathrm{miss}}$ and the lepton (bottom) for data vs. MC for events with a leading muon (left) and leading electron (right) satisfying the requirements of CR1.

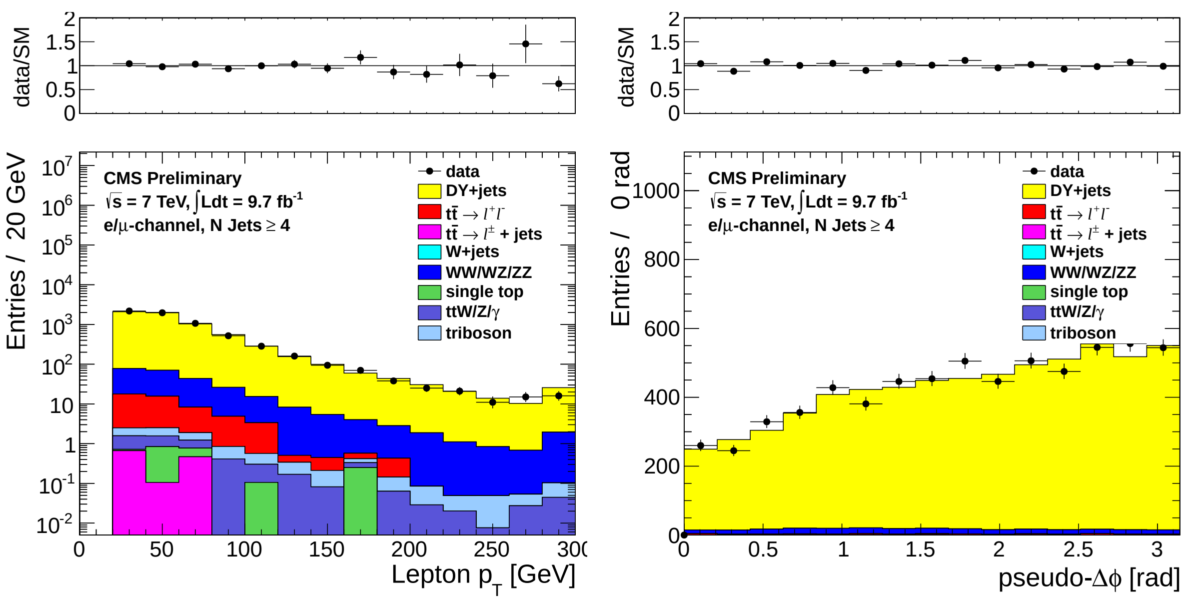

Figure 39: Comparison of the positive lepton p_{T} (left) and the azimuthal angle between this lepton and the pseudo-$E_{\mathrm{T}}^{\mathrm{miss}}$ (right) distributions in data vs. MC for events satisfying the requirements of CR2, combining both the muon and electron channels.

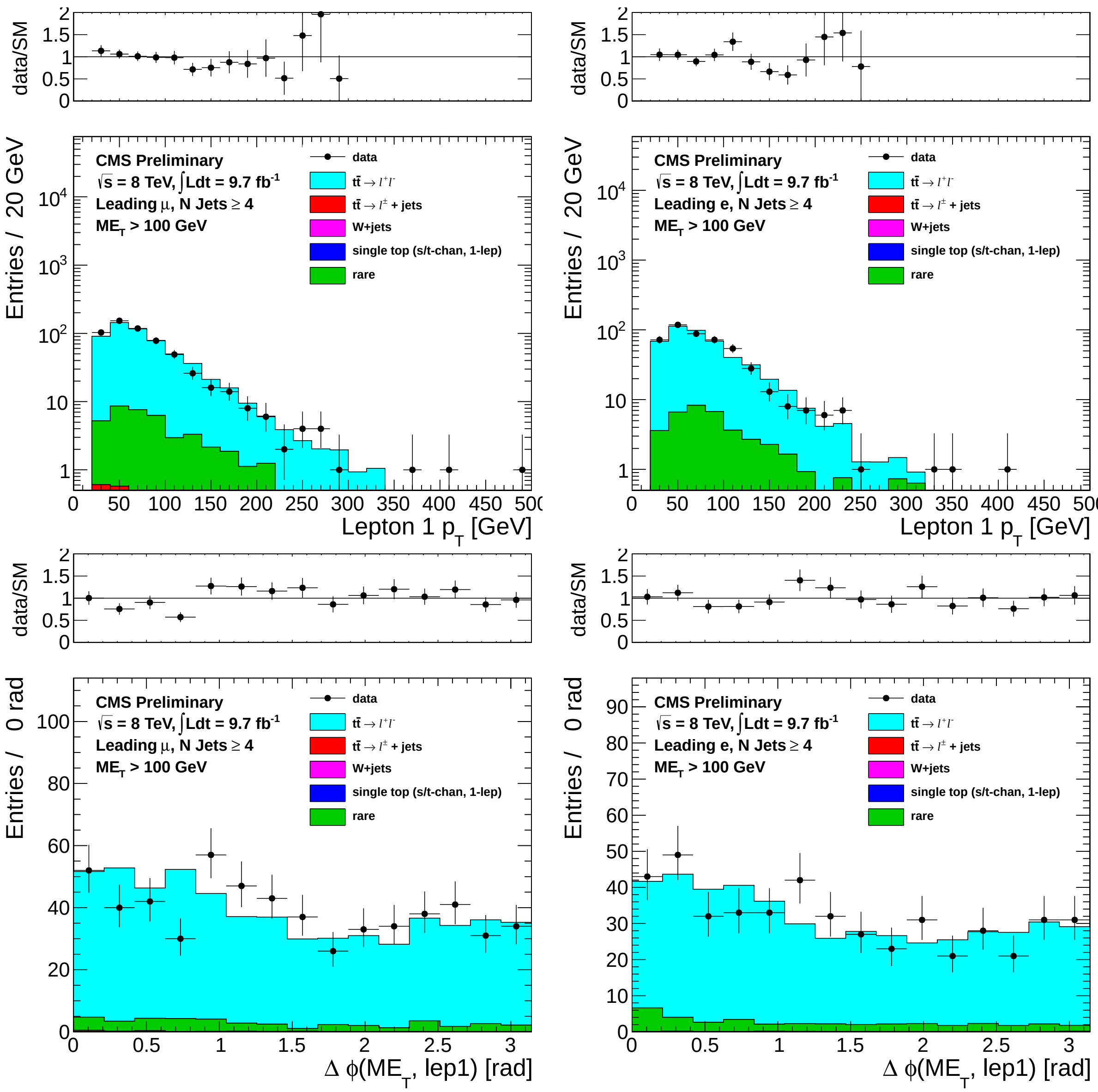

Figure 40: Comparison of the leading lepton p_{T} (top) and azimuthal angle between the leading lepton and the $E_{\mathrm{T}}^{\mathrm{miss}}$ for $E_{\mathrm{T}}^{\mathrm{miss}} > 100$ GeV distributions in data vs. MC for events with a leading muon (left) and leading electron (right) satisfying the requirements of CR4.

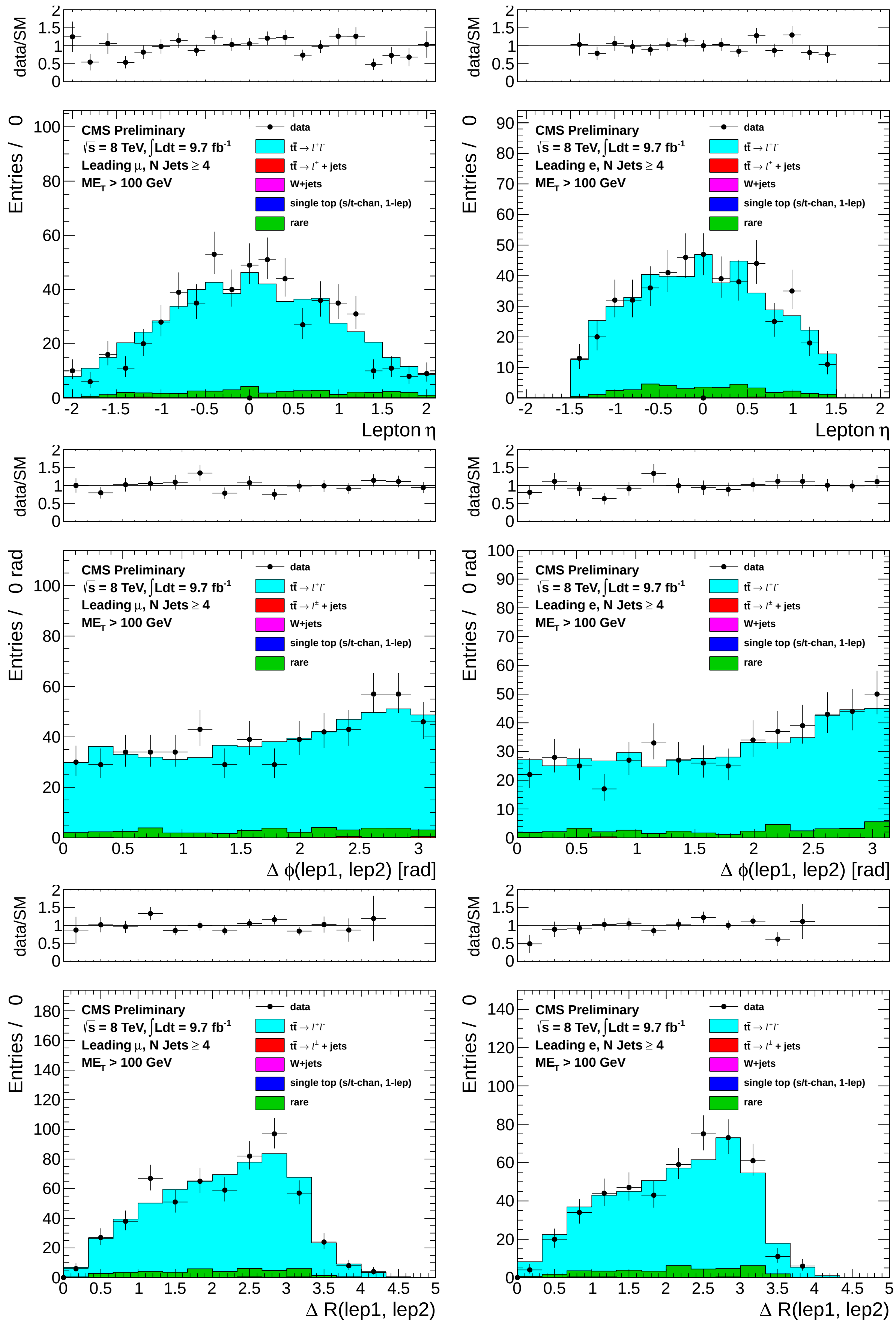

Figure 41: Comparison of the leading lepton eta (top), difference in the azimuthal angle (center) and ΔR separation (bottom) between the two leptons for $E_{\mathrm{T}}^{\mathrm{miss}} > 100$ GeV distributions in data vs. MC for events with a leading muon (left) and leading electron (right) satisfying the requirements of CR4.

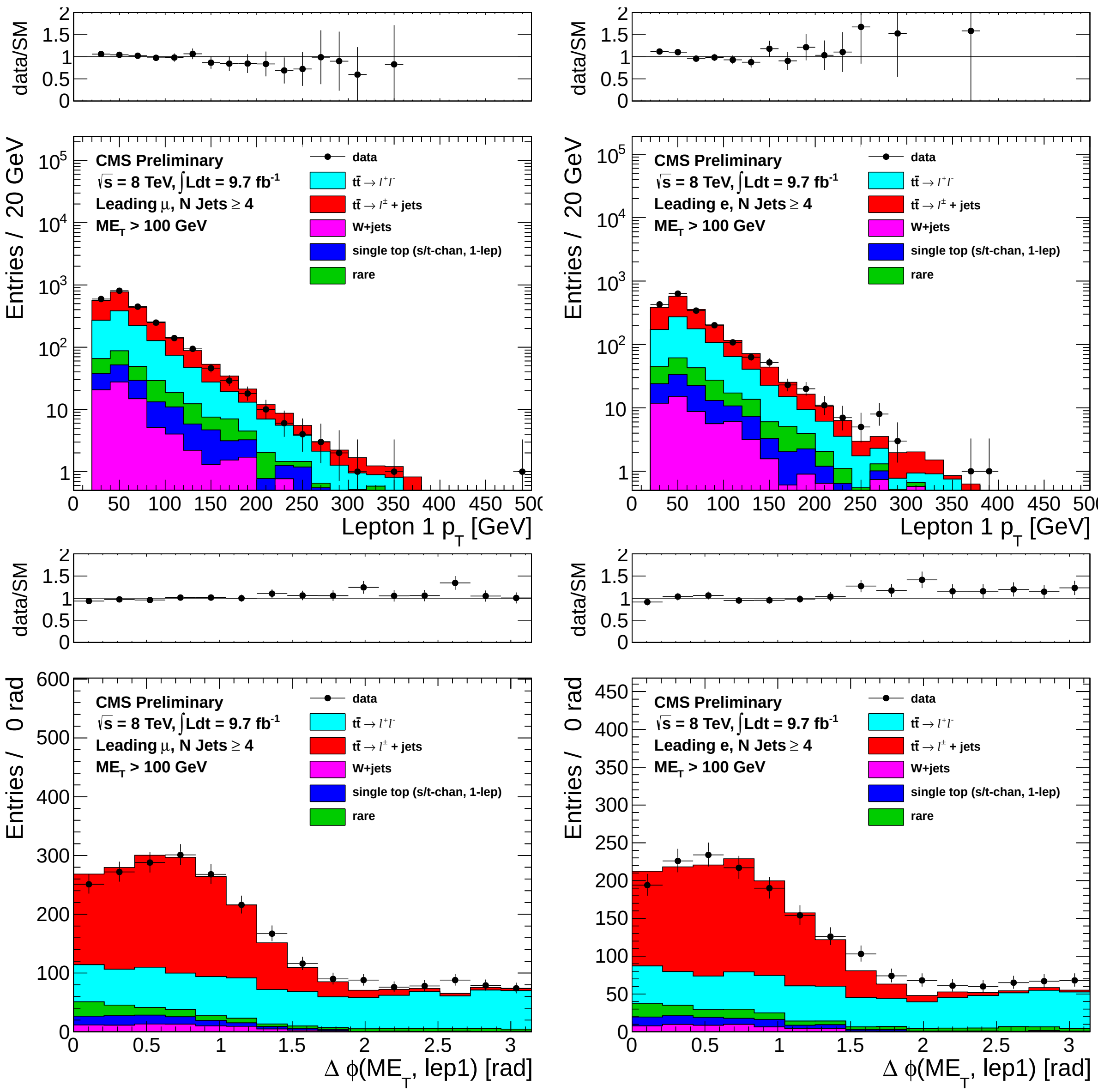

Figure 42: Comparison of the lepton p_{T} (top) and azimuthal angle between the $E_{\mathrm{T}}^{\mathrm{miss}}$ and the lepton (bottom) for data vs. MC for $E_{\mathrm{T}}^{\mathrm{miss}} > 100$ GeV for events with a leading muon (left) and leading electron (right) satisfying the requirements of CR5.

D Control Region Plots Summary

This appendix includes distributions from the various control regions used in the analysis used to validate the MC modeling of the $E_{\mathrm{T}}^{\mathrm{miss}}$ and M_{T} distributions in data and derive systematic uncertainties on the background predictions. The distributions are shown in both log and linear scale.

D.1 CR4: $\geq$1 b-tag, exactly 2 leptons

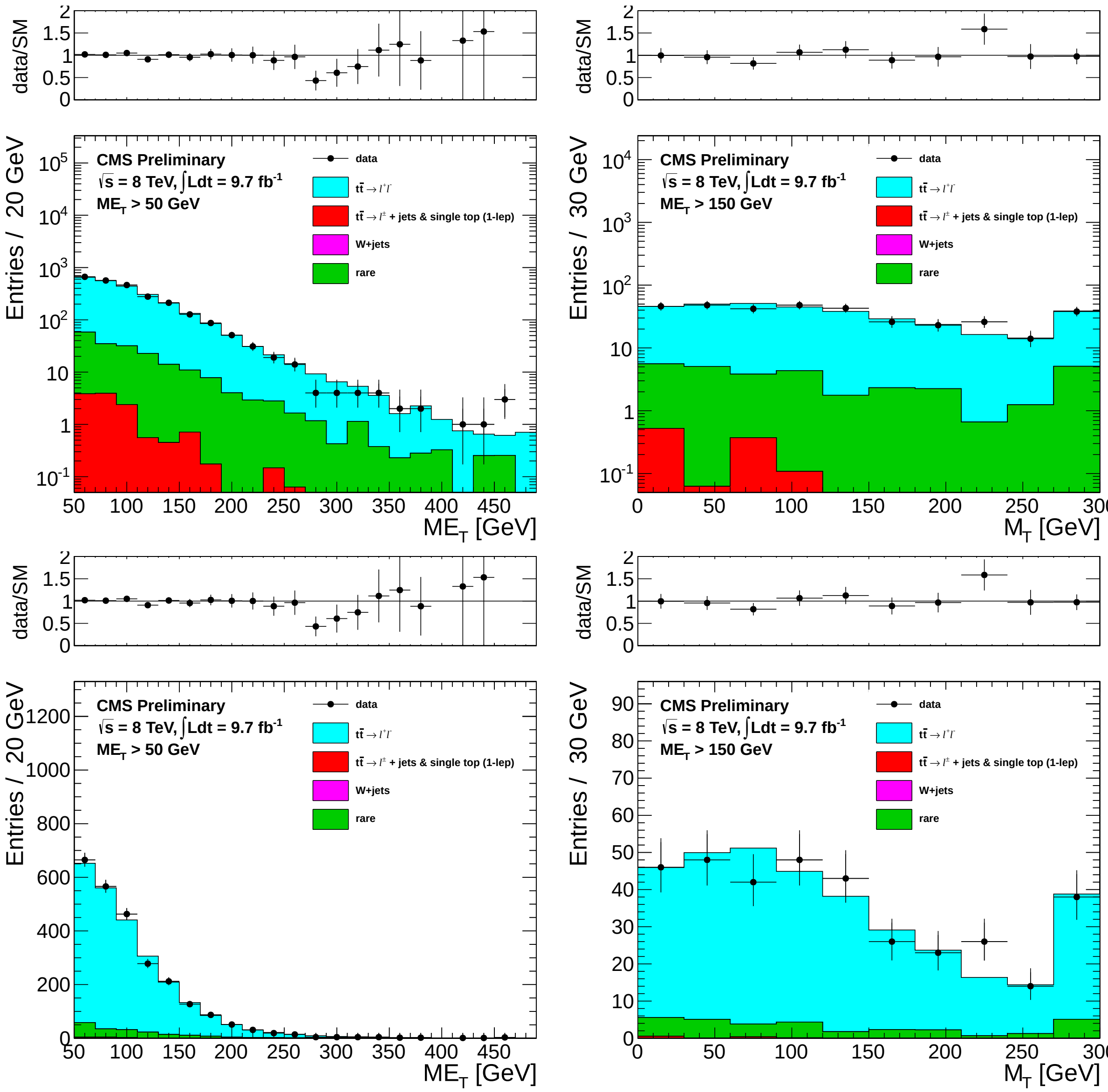

Figure 43: Comparison of the $E_{\mathrm{T}}^{\mathrm{miss}}$ distribution (left) and M_{T} distribution for events satisfying $E_{\mathrm{T}}^{\mathrm{miss}}$ $>$ 150 GeV (right) in data vs. MC for CR4.

D.2 CR5: $\geq$ 1 b-tag, 1 lepton + 1 isolated track

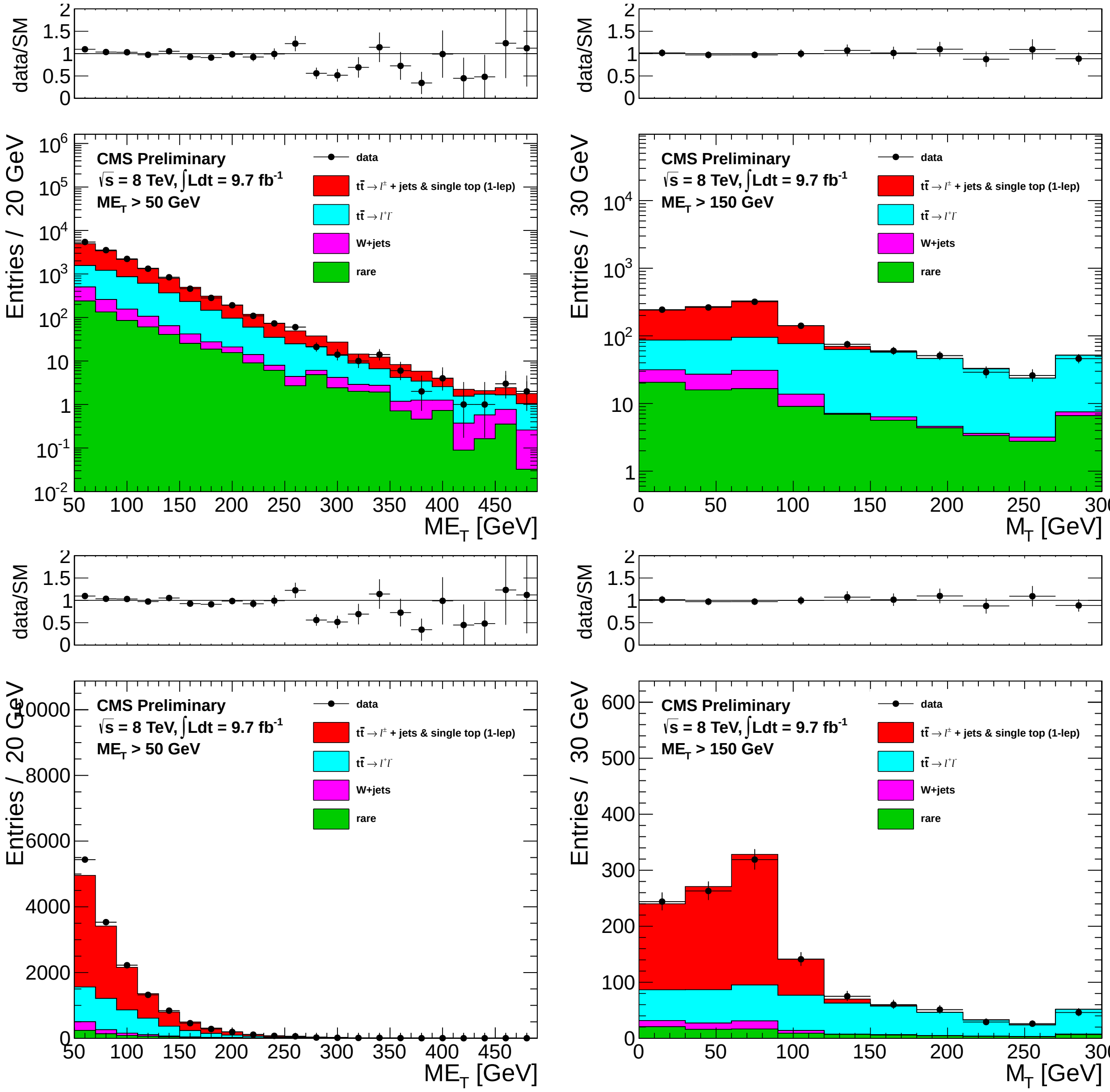

Figure 44: Comparison of the $E_{\mathrm{T}}^{\mathrm{miss}}$ distribution (left) and M_{T} distribution for events satisfying $E_{\mathrm{T}}^{\mathrm{miss}}$ > 150 GeV (right) in data vs. MC for CR5.

818 ## D.3 CR1: 0 b-tags, exactly 1 lepton

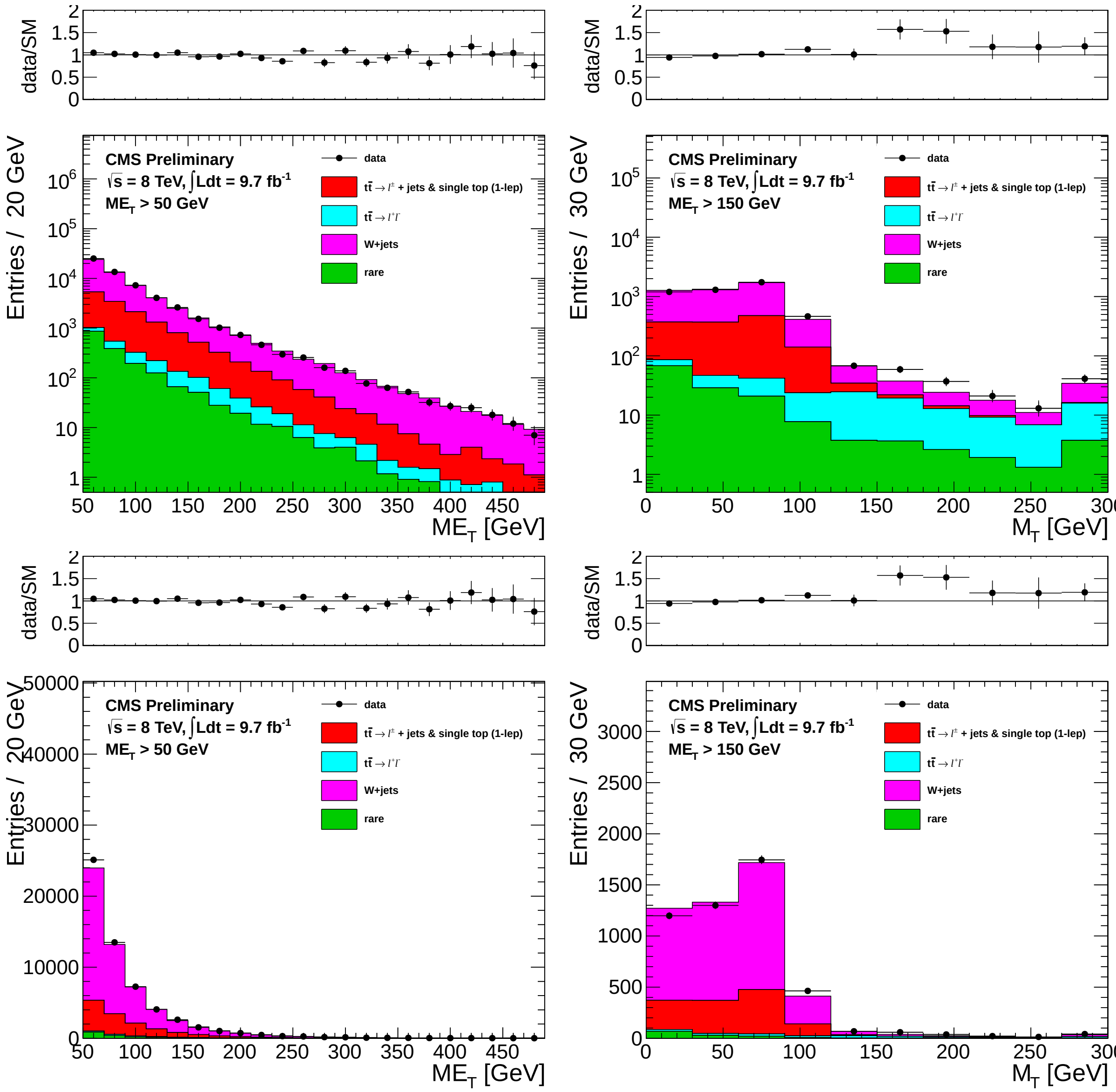

Figure 45: Comparison of the $E_{\mathrm{T}}^{\mathrm{miss}}$ distribution (left) and the M_{T} distribution after a $E_{\mathrm{T}}^{\mathrm{miss}} > 150$ GeV requirement (right) in data vs. MC for events satisfying the requirements of CR1.

D.4 CR2: 0 b-tags, exactly 2 leptons

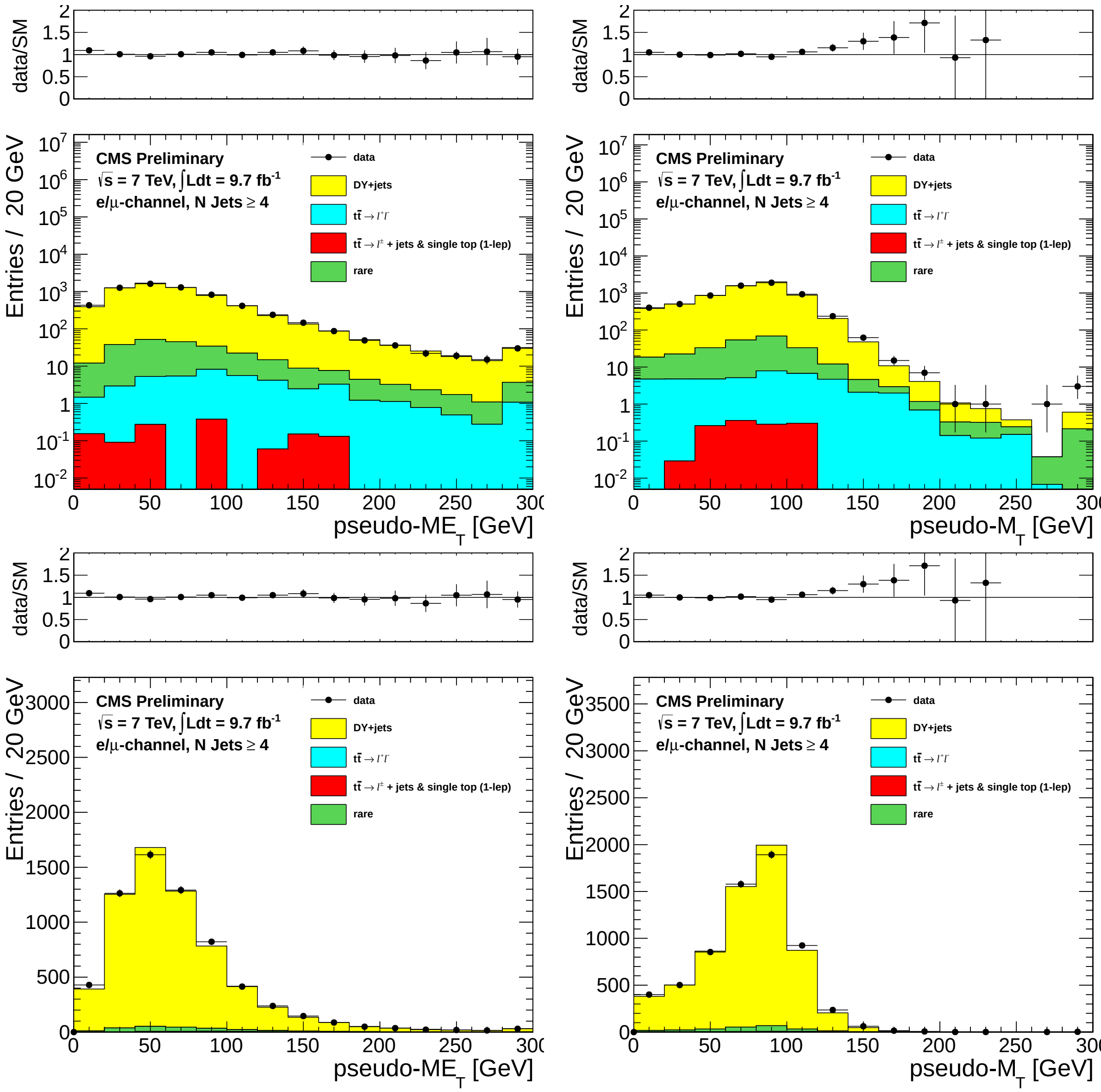

Figure 46: Comparison of the pseudo-$E_{\mathrm{T}}^{\mathrm{miss}}$ distribution (left) and the pseudo-M_{T} distribution (right) in data vs. MC for CR2.

E Signal Kinematics

This appendix includes some kinematic distributions for a few signal points in the T2tt (Figure 47) and T2bw (Figure 48) models. The parameter values shown correspond to the edge of the sensitivity of the analysis and reflect the range of kinematics of the signal. The lower M($\tilde{t}$) samples have softer $E_{\mathrm{T}}^{\mathrm{miss}}$ and M_{T} distributions and are thus better targetted by the signal regions with looser requirements. The higher M($\tilde{t}$) samples are harder in $E_{\mathrm{T}}^{\mathrm{miss}}$ and M_{T} and the signal regions with tighter requirements provide higher sensitivity to these models.

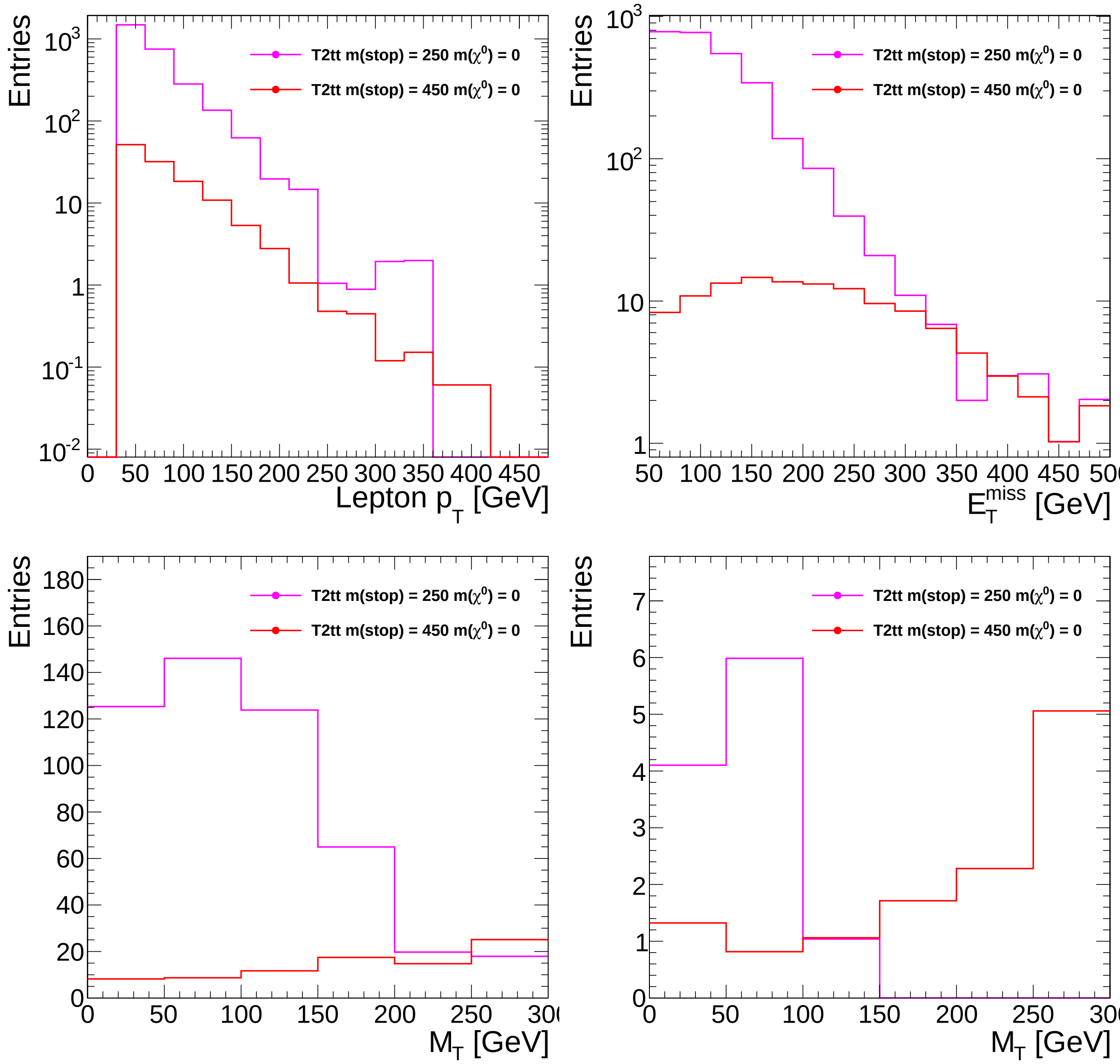

Figure 47: Signal kinematics for two signal points in the T2tt model: the lepton p_{T} (top, left), the $E_{\mathrm{T}}^{\mathrm{miss}}$ (top, right) and the M_{T} for two values of the $E_{\mathrm{T}}^{\mathrm{miss}}$ requirement, $E_{\mathrm{T}}^{\mathrm{miss}} > 150$ GeV (bottom, left) and $E_{\mathrm{T}}^{\mathrm{miss}} > 350$ GeV (bottom, right).

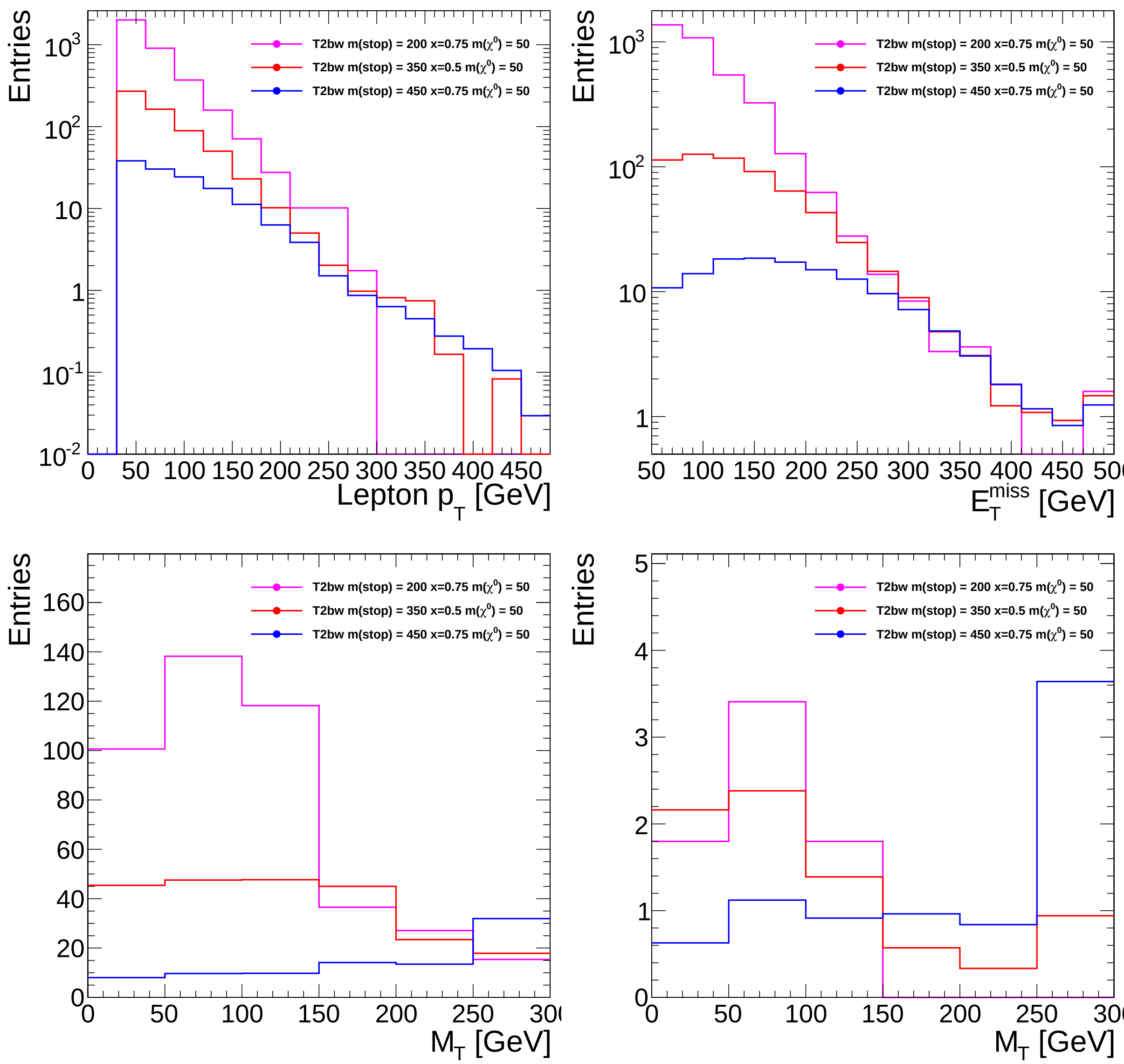

Figure 48: Signal kinematics for three signal points in the T2bw model: the lepton p_{T} (top, left), the $E_{\mathrm{T}}^{\mathrm{miss}}$ (top, right) and the M_{T} for two values of the $E_{\mathrm{T}}^{\mathrm{miss}}$ requirement, $E_{\mathrm{T}}^{\mathrm{miss}} > 150$ GeV (bottom, left) and $E_{\mathrm{T}}^{\mathrm{miss}} > 350$ GeV (bottom, right).

F Glossary of abbreviations

R_{wjet}^{MC}, R_{wjet}
Monte Carlo and corrected ratios of W+jets events in the M_T tail to the M_T peak.

R_{top}^{MC}, R_{top}
Monte Carlo and corrected ratios of $t\bar{t}$ or single-top $\ell+$ jets events in the M_T tail to the M_T peak.

SFR_{wjet}
Data/MC scale factor for R_{wjet}^{MC}

SFR_{top}
Data/MC scale factor for R_{top}^{MC} (not used)

K_3 and K_4
Scale factors for $\mathrm{t\bar{t}} \to \ell\ell$ events with one or two extra jets from radiation

SF_{pre} and SF_{post}
Scale factors to be applied to MC to normalize to the yields in the M_T control region before and after the application of the isolated track veto.